LOGIC TREE FOR GROUND MOTION CHARACTERIZATION OF THE VERTICAL COMPONENT: A CASE STUDY BASED ON UPDATED TURKISH GROUND MOTION DATABASE

A THESIS SUBMITTED TO
THE GRADUATE SCHOOL OF NATURAL AND APPLIED SCIENCES
OF
MIDDLE EAST TECHNICAL UNIVERSITY

BY

NIMA AGHA ALIPOUR

IN PARTIAL FULFILLMENT OF THE REQUIREMENTS
FOR
THE DEGREE OF MASTER OF SCIENCE
IN
EARTHQUAKE STUDIES

SEPTEMBER 2019

Approval of the thesis:

LOGIC TREE FOR GROUND MOTION CHARACTERIZATION OF THE VERTICAL COMPONENT: A CASE STUDY BASED ON UPDATED TURKISH GROUND MOTION DATABASE

submitted by **NIMA AGHA ALIPOUR** in partial fulfillment of the requirements for the degree of **Master of Science in Earthquake Studies Department, Middle East Technical University** by,

Prof. Dr. Halil Kalıpçılar
Dean, Graduate School of **Natural and Applied Sciences** _____

Prof. Dr. Ayşegül Askan Gündoğan
Head of Department, **Earthquake Studies** _____

Assoc. Prof. Dr. Zeynep Gülerce
Supervisor, **Earthquake Studies, METU** _____

Assist. Prof. Dr. Mustafa Abdullah Sandıkkaya
Co-Supervisor, **Civil Engineering, Hacettepe Uni.** _____

Examining Committee Members:

Prof. Dr. Kemal Önder Çetin
Civil Engineering, METU _____

Assoc. Prof. Dr. Zeynep Gülerce
Earthquake Studies, METU _____

Prof. Dr. Ayşegül Askan Gündoğan
Civil Engineering, METU _____

Assist. Prof. Dr. Atilla Arda Özacar
Geological Engineering, METU _____

Assist. Prof. Dr. Mustafa Abdullah Sandıkkaya
Civil Engineering, Hacettepe Uni. _____

Date: 20.09.2019

I hereby declare that all information in this document has been obtained and presented in accordance with academic rules and ethical conduct. I also declare that, as required by these rules and conduct, I have fully cited and referenced all material and results that are not original to this work.

Name, Surname: Nima Agha Alipour

Signature:

ABSTRACT

LOGIC TREE FOR GROUND MOTION CHARACTERIZATION OF THE VERTICAL COMPONENT: A CASE STUDY BASED ON UPDATED TURKISH GROUND MOTION DATABASE

Agha Alipour, Nima
Master of Science, Earthquake Studies
Supervisor: Assoc. Prof. Dr. Zeynep Gülerce
Co-Supervisor: Assist. Prof. Dr. Mustafa Abdullah Sandıkkaya

September 2019, 81 pages

Two approaches are used to develop the vertical design spectra in Probabilistic Seismic Hazard Assessment (PSHA): performing the PSHA for the vertical component using vertical ground motion models (GMMs) and utilizing the V/H ratio GMMs to scale the horizontal spectrum during or after the hazard calculations for the horizontal component. This study intends to develop a new framework for building the vertical ground motion logic tree that combines both vertical and V/H ratio GMMs in the PSHA analysis. The main objectives of this study are: (i) to compile a reliable and up-to-date strong ground motion database for Turkey (TSMD), (ii) to choose the V/H ratio and vertical GMMs that are consistent with the magnitude, distance, depth, and site amplification scaling of the updated TSMD, and (iii) to combine the selected vertical GMMs with the V/H ratio models to provide the ground motion characterization logic tree for vertical ground motion component in Turkey. For this purpose, the TSMD is updated with the recordings from the earthquakes occurred between 2008 and 2015, including the Mw=6.1 Elazığ and Mw=7.2 Van earthquakes. Updated TSMD contains 2698 recordings with the earthquake metadata, source-to-site distance metrics for the recordings, measured shear wave velocity profiles for the recording stations, and spectral accelerations for horizontal and vertical components.

Four candidate V/H ratio GMMs (Gulerce and Abrahamson, 2011; Gulerce and Akyuz, 2013; Akkar et al., 2014; Bozorgnia and Campbell, 2016) together with four candidate vertical GMMs (Bozorgnia and Campbell, 2016; Stewart et al., 2016; and Gulerce et al., 2017 and Çagnan et al., 2017 model) are selected and the model predictions are compared with the actual data in the updated TSMD using the analysis of the residuals and data-driven techniques. Analysis results of V/H ratio GMMs showed that the median predictions of the V/H ratio GMMs proposed by Gulerce and Akyuz (2013), Akkar et al. (2014), and Bozorgnia and Campbell (2016) are compatible with the V/H ratios in the updated TSMD. Analysis results of vertical GMMs depicted that the magnitude scaling of Çagnan et al. (2017) model and the depth scaling of the Bozorgnia and Campbell (2016) model are inconsistent with the updated TSMD. Additionally, small magnitude (SM) scaling of Stewart et al. (2016) and Gulerce et al. (2017) GMMs should be modified for a better fit with the Turkish dataset. Trellis plots of SM-modified Stewart et al. (2016) and SM-modified Gulerce et al. (2017) vertical GMMs and selected V/H ratio models multiplied by NGA-West 2 and TR-adjusted NGA-W1 horizontal models are used to determine the logic tree weights for the proposed vertical ground motion characterization logic tree for Turkey.

Keywords: Updated Turkish Strong Motion Database, V/H Ratio Ground Motion Models, Vertical Ground Motion Models, Compatibility Analysis, Logic Tree Weight Factors

ÖZ

DÜŞEY BİLEŞEN İÇİN YER HAREKETİ KARAKTERİZASYONU MANTIK AĞACI: GÜNCELLENMİŞ TÜRK YER HAREKETİ VERİTABANINA DAYALI BİR VAKA İNCELEMESİ

Agha Alipour, Nima
Yüksek Lisans, Deprem Çalışmaları
Tez Danışmanı: Doç. Dr. Zeynep Gülerce
Ortak Tez Danışmanı: Dr. Öğr. Üyesi Mustafa Abdullah Sandıkkaya

Eylül 2019, 81 sayfa

Olasılıksal Sismik Tehlike Analizi (OSTA)'da dikey tasarım spektrumunu geliştirmek için iki yaklaşım kullanılmaktadır: ilk yaklaşımda dikey yer hareketi tahmin modelleri (GMM'ler) kullanarak dikey bileşen için OSTA'yı gerçekleştirilir, ikinci yaklaşımda ise yatay bileşen için OSTA hesaplamaları sırasında veya sonrasında yatay spektrumu ölçeklendirmek için V/H oranı GMM'lerini kullanılır. Bu çalışma, Türkiye için OSTA icerisinde hem dikey hem de V/H oranı tahmin denklemlerini birleştiren bir dikey yer hareketi mantık ağacını oluşturmayı amaçlamaktadır. Bu çalışmanın temel hedefleri: (i) Türkiye için güvenilir ve güncel bir kuvvetli yer hareketi veritabanı (TSMD) derlemek, (ii) güncellenmiş TSMD'nin deprem büyüklüğü, mesafesi, derinliği ve zemin büyütme ölçeklemesi ile tutarlı olan V/H oranı ve dikey yer hareketi modellerini seçmek, (iii) Türkiye'de dikey yer hareketi bileşeni için bir yer hareketi karakterizasyonu mantık ağacı oluşturmaktır. Bu amaçla, TSMD, 2008-2015 yılları arasında meydana gelen depremlerin kayıtları ile (Mw = 6.1 Elazığ ve Mw = 7.2 Van depremleri de dahil olmak üzere) güncellenmiştir. Güncellenmiş TSMD, deprem verisi, kayıtlar için kaynak-saha mesafesi ölçümleri, kayıt istasyonları için ölçülen kayma dalgası hızı profilleri ve yatay ve dikey bileşenler için spektral ivmelenmeler ile birlikte 2698 kayıt içermektedir. Dört aday V/H oranı modeli (Gulerce ve

Abrahamson, 2011; Gulerce ve Akyuz, 2013; Akkar ve diğerleri, 2014; Bozorgnia ve Campbell, 2016) ve dört aday dikey yer hareketi modeli (Bozorgnia ve Campbell, 2016; Stewart ve diğerleri, 2016; ve Gulerce ve diğerleri, 2017 ve Çagnan ve diğerleri, 2017 model) seçilmiş ve model tahminleri, artıkların analizi ve veriye dayalı teknikler kullanılarak güncellenmiş TSMD'deki gerçek verilerle karşılaştırılmıştır. V/H oranı modellerinin analiz sonuçlarına göre, Gülerce ve Akyüz (2013), Akkar ve diğ. (2014) ve Bozorgnia ve Campbell (2016) V/H oranı modelleri, güncellenmiş TSMD'deki V/H oranları ile uyumludur. Dikey GMM'lerin analiz sonuçlarına göre, Çagnan ve diğ. (2017) modelinin büyüklük ölçeklendirmesi ve Bozorgnia ve Campbell (2016) modelinin derinlik ölçeklendirilmesi, güncellenmiş TSMD ile tutarsızdır. Bunlara ek olarak, Stewart ve diğ. (2016) ve Gulerce ve diğ. (2017) GMM'lerinin küçük depremler için deprem büyüklüğü (SM) ölçeklendirmesi ,TSMD'ye daha iyi uymalari için değiştirilmelidir. Türkiye için önerilen dikey yer hareketi mantık ağacında, SM-değiştirilmiş Stewart ve diğ. (2016) ve SM-değiştirilmiş Gulerce ve diğ. (2017) dikey yer hareketi modelleri ile seçilmiş V/H oranı modelleri ve bu modeller için belirlenmiş mantık ağacı ağırlıkları yer almaktadır.

Anahtar Kelimeler: Güncellenmiş Türk Kuvvetli Hareket Veri Tabanı, V/H Orani Yer Hareketi Modelleri, Düşey Yer Hareketi Modelleri, Uyumluluk Analizi, Mantık Ağacı Ağırlık Faktörleri

To My Beloved Family

ACKNOWLEDGEMENTS

I would like to express my sincere gratitude to Dr. Gülerce for her incessant support and guidance together with Dr. Sandikkaya for shedding light on my way in the course of my education.

Likewise, I would like to thanks Dr. Norman Abrahamson, for his kind suggestions and guidance in the course of preparation of this study.

Above all else, I would like to thank my family for encouraging and paving the way for me in my tough times through my education.

TABLE OF CONTENTS

LIST OF TABLES

TABLES

LIST OF FIGURES

FIGURES

LIST OF ABBREVIATIONS

ABBREVIATIONS

AFAD: The Disaster and Emergency Management Presidency of Turkey

ASA 2014: Akkar et al., (2014b) Ratio (V/H) GMM

BSSC: Building Seismic Safety Council

BC 2016: Bozorgnia and Campbell, 2016 Ratio (V/H) GMM

BC 2016: Bozorgnia and Campbell, 2016 Vertical (V) GMM

CAKS 2017: Çagnan et al., 2017 Vertical (V) GMM

D: Distance

EDR: Euclidean Distance-Based Ranking Method

FAS: Fourier Amplitude Spectrum

GMM: Ground Motion Model

GA 2011: Gülerce and Abrahamson, 2011 Ratio (V/H) GMM

GA 2013: Gülerce and Akyüz, 2013 Ratio (V/H) GMM

GKAS 2017: Gulerce et al., 2017 Vertical (V) GMM

LH: Likelihood Ranking Method

LLH: Log-Likelihood Ranking Method

M_w: Moment Magnitude

NEHRP: National Earthquake Hazards Reduction Program

NGA: Next Generation of Ground-Motion Attenuation Models

PSHA: Probabilistic Seismic Hazard Analysis

PEER: The Pacific Earthquake Engineering Research Center

PGA: Peak Ground Acceleration

RESORCE: Reference Database for Seismic Ground-Motion in Europe

R_{jb}: Joyner-Boore Distance

R_{rup}: Rupture Distance

SBSA 2016: Stewart et al., 2016 Vertical (V) GMM

SIGMA: Seismic Ground Motion Assessment Project

SA: Spectral Acceleration

SMM or SM-Modified: Small Magnitude Modified

TSMD: Turkish Strong Ground Motion Database

TR-Adj: TURKEY Adjusted

V_{s30}: The Average Shear-Wave Velocity (between 0 and 30-meters depth)

Z_{tor}: Depth to Top of Rupture

CHAPTER 1

INTRODUCTION

Ground motion characterization efforts in Turkey and across the globe, have generally included horizontal component of strong ground motion and paid less attention to vertical component due to less damaging nature of it. However, in recent years, multiple studies (Bozorgnia et al., 2016) have been issued and shed light on importance of vertical ground motion in seismic design of: (i) critical structures like nuclear power plant and dams, (ii) tall and base-isolated buildings and long-span bridges and (iii) short period ordinary structures with short source-to-site distance on soil sites. The ground motion models (GMMs) for the horizontal component for Turkey have been developed since 1990s (Douglas, 2011) and detailed discussions related to previous horizontal predictive models can be found in Kale et al. (2015). Recent studies by Gülerce et al. (2016), Sandıkkaya (2017), and Kale (2019) discussed the compatibility of the strong motions recorded in Turkey with the global horizontal GMMs, using the initial or re-visited versions of Turkish Strong Ground Motion Database (TSMD) by Akkar et al. (2014a). Incompatibilities between the global GMMs and Turkish strong motion dataset in small-to-moderate magnitude scaling, large distance scaling, and site amplification scaling were encountered during the evaluation of the residuals, indicating that the GMMs for the vertical ground motions or vertical to horizontal (V/H) ratio should be compared to the Turkish dataset for building a ground motion characterization logic tree for the vertical ground motion component.

To obtain the dependable results, having reliable strong ground motion database is a necessity in order to utilize it for testing the compatibility of V/H ratio and vertical GMMs in terms of magnitude, distance, site amplification, and depth scaling. Strong ground motions recorded during the earthquakes that occurred between years 1976

and 2007 in Turkey were gathered and compiled together with the relevant earthquake and site metadata as the Turkish Strong Ground Motion Database (TSMD) by Akkar et al. (2010) and Sandıkkaya et al. (2010). During the compilation of the Reference Database for Seismic Ground-Motion in Europe (the RESORCE database), Akkar et al. (2014a) revisited the earthquake metadata provided in TSMD (re-visited TSMD). Between years 2008 and 2018, a considerable amount of strong motion accelerograms from low-to-moderate magnitude events have been recorded and these recordings are available in AFAD's website (The Republic of Turkey Ministry of Interior Disaster and Emergency Management, last accessed in August 2018). However, provided waveforms are not processed nor are the earthquake metadata compiled for these recordings. A preliminary effort to add these recordings to the re-visited TSMD was presented in Sandıkkaya (2017) and horizontal components of the recordings from $3.5<M_w< 6$ shallow crustal (depth < 30 km) earthquakes that occurred between 2008 and 2015 were compiled to investigate the magnitude scaling of Turkish GMMs for the horizontal component. One of the main goals of this study is to finalize what Sandıkkaya (2017) has started: to update the TSMD for covering the recordings until the end of 2015, both for the vertical and horizontal ground motion components in a consistent manner with the re-visited TSMD.

Two approaches have been used commonly by developers for creating vertical models; developing model independently for prediction of the vertical component of ground motion or by using existing V/H ratio GMM to scale horizontal GMM. Therefore, this study intends to develop a framework for building the vertical ground motion logic tree that properly captures the epistemic uncertainty considering the center and the range of the model predictions by evaluating the differences in the median predictions of the candidate vertical and V/H ratio GMMs with the regional ground motion datasets using analysis of model residuals and data-driven approaches. We have chosen the updated TSMD for data-driven evaluation of the candidate GMMs mainly because it is an independent dataset (as defined by Mak et al., 2017) for most of the candidate models and it includes sufficient amount of data from small-

to-moderate magnitude earthquakes for a range of source-to-site distances and site conditions.

1.1 Research Statement and Problem Significance

Several up-to-date vertical and V/H ratio ground motion models (GMMs) for different shallow crustal and active tectonic regions were proposed in the last recent years. These efforts considerably increased the number of available models and may lead to a change in the ground motion characterization logic trees utilized in the probabilistic seismic hazard analysis (PSHA) for the vertical ground motion component. When sets of vertical and V/H ratio GMMs are combined in PSHA, differences in the median predictions of selected models might have a substantial impact on the ground motion estimates, depending on the horizontal GMMs utilized in the PSHA. Because the up-to-date vertical GMMs are only recently proposed, median vertical spectra based on recent vertical GMMs and V/H ratio models multiplied by horizontal GMMs were not compared and the differences were not discussed elsewhere. Also, ongoing feasibility and site licensing studies for the Akkuyu and Sinop Nuclear Power Plant sites clearly underlined the need for the guidelines of estimating the vertical design spectrum in the Probabilistic Seismic Hazard Assessment (PSHA) studies conducted in Turkey. Overall objective of this study is to propose a ground motion characterization framework to be used in the PSHA studies in Turkey for the vertical ground motion component. There are four main components of the proposed framework: (i) the updated strong motion dataset for Turkey, (ii) selection of the V/H ratio GMMs that are consistent with the Turkish strong motion dataset (iii) choosing the vertical GMMs that are compatible with the Turkish strong motion dataset and selected V/H ratio model predictions and (iv) providing a complete logic tree with weights at different period bands.

1.2 Limitation of Previous Studies

Several alternative vertical and V/H ratio GMMs were developed for shallow crustal and active tectonic regions in the last decade. Table 1.1 (Çagnan et al., 2017 and

Douglas, 2018) lists, in brief, the name of vertical and ratio GMMs which have been published so far. However, the number of up-to-date vertical and V/H ratio GMMs for shallow crustal and active tectonic regions is rather limited, especially when compared to the number of horizontal GMMs for the same tectonic regime. Therefore, to finalize the selection of candidate GMMs, emphasis put on most recent global models with available predictive variables and period range up to ten seconds. Also, GMM selection criteria proposed by Cotton et al. (2006), Bommer et al. (2010), and Stewart et al. (2016) for horizontal GMMs are utilized to select candidate models for this study. Only one of early-stage GMMs developed for Turkey, the Gülkan and Kalkan (2002) model, predicts for the vertical ground motion component. The accompanying V/H ratio model (Kalkan and Gülkan, 2004) was developed using the V/H ratios from 100 ground motions recorded during 47 events that occurred in Turkey between the years of 1976 and 2002. Kalkan and Gülkan models was eliminated because (i) model coefficients were provided only up to 2s, (ii) generic site classification (site dummies) were utilized for the site amplification scaling.

1.3 Scope of the Thesis

Figure 1.1 shows the scope of thesis as a flowchart. First Chapter is dedicated to general overview of current study. Second Chapter explains the compilation process of updated TSMD, filtration of raw strong motions and statistical information of metadata. In Chapter 3, candidate V/H ratio ground motion models are selected and their consistency with updated TSMD, regarding the magnitude, distance, depth, and site amplification scaling are tested using the analysis of the residuals and other data-driven techniques. In Chapter 4, candidate vertical ground motion models are selected and their consistency with updated TSMD, regarding the magnitude, distance, depth, and site amplification scaling are tested using analysis of the residuals. Also, small magnitude correction of selected vertical models are presented in this chapter. In Chapter 5, final selected V/H ratio and vertical GMMs are combined to provide the ground motion characterization logic tree for vertical ground motion component in Turkey to be implemented in the PSHA studies.

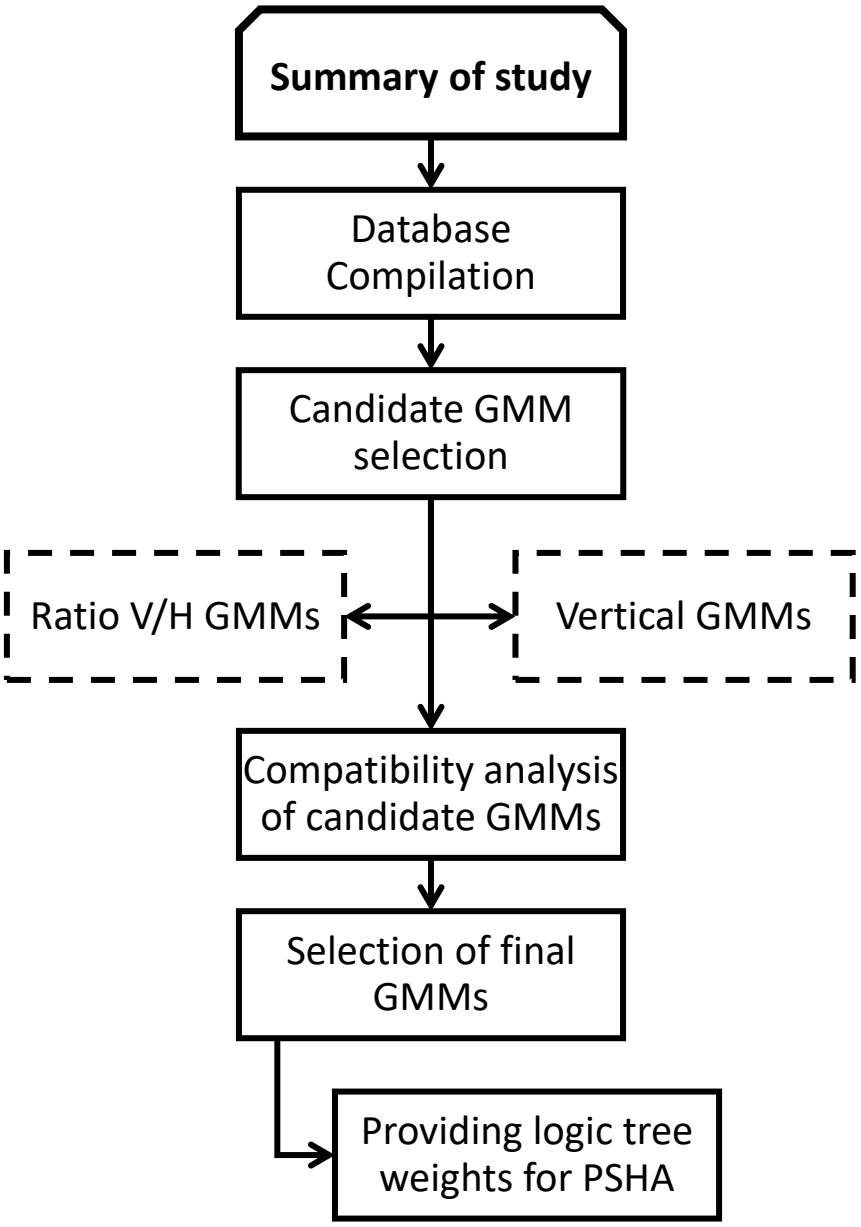

Figure 1.1 Summary of study in shape of flowchart.

Table 1.1 Published Vertical and V/H ratio GMMs

Vertical Ground Motion Models		
Year	Publishers	Data Source
1982	Campbell, K.W.	W.U.S. & Global
1989	Abrahamson, N. A., & Litehiser, J. J.	W.U.S. & Global
1989	Trifunac, M.D., Lee, V.W.	W.U.S. & Global
1993	Bozognia, Y., Niazi, M.	W.U.S.
1996	Sabetta, F.	Italy
1997	Abrahamson, N. A., & Silva, W. J.	W.U.S. & Global
1998	Ansary, M. A., Yamazaki, F.	Japan
2003	Campbell, K. W., & Bozorgnia, Y.	W.U.S. & Global
2003	Berge-Thierry, C., Cotton, F., et al.	Europe & California
2003	Ambraseys, N. ., & Douglas, J.	W.U.S. & Global
2004	Kalkan, E., & Gülkan, P.	Turkey
2005	Ambraseys, N. N., Douglas, J., Sarma, S. K., & Smit, P. M.	Europe & M.E
2008	Cauzzi, C., & Faccioli, E.	Japan
2016	Bozorgnia, Y., & Campbell, K. W.	Global
2016	Stewart, J. P., Boore, D. M., Seyhan, E., & Atkinson, G. M.	Global
2017	Gülerce, Z., Kamai, R., Abrahamson, N. A., & Silva, W. J.	Global
2017	Çağnan, Z., Akkar, S., Kale, Ö., & Sandıkkaya, A.	Global
Vertical to Horizontal Ground Motion Models		
Year	Publishers	Data Source
1996	AMBRASEYS, N. N., SIMPSON, K. A., & BOMMER, J. J.	Europe & M.E
2003	Ambraseys, N. ., & Douglas, J.	W.U.S. & Global
2004	Bozorgnia, Y., & Campbell, K. W.	W.U.S. & Global
2004	Kalkan, E., & Gülkan, P.	Turkey
2011	Gülerce, Z., & Abrahamson, N. A. (GA2011)	Global
2011	Edwards, B., Poggi, V., & Fäh, D.	Japan & Switzerland
2011	Bommer, J. J., Akkar, S., & Kale, Ö.	Europe & M.E
2013	Gulerce, Z., & Akyuz, E. (Turkey-Adjusted GA2011)	Global
2014	Akkar, S., Sandıkkaya, M. A., & Ay, B.	Europe & M.E
2016	Bozorgnia, Y., & Campbell, K. W.	Global
*W.U.S= Western United States, M.E= Middle East		

CHAPTER 2

EXTENDING THE TURKISH STRONG GROUND MOTION DATABASE (TSMD)

Strong ground motions recorded during the earthquakes occurred between 1976 and 2007 were gathered and compiled together with the relevant earthquake and site metadata as the Turkish Strong Ground Motion Database (TSMD) by Akkar et al. (2010) and Sandıkkaya et al. (2010). In 2014, Akkar et al. (2014) revisited the earthquake metadata of TSMD and added only the moderate-to-high magnitude earthquakes occurred after 2008 (e.g. 2010 Elazığ (M_w=6.2), 2011 Simav (M_w=5.9), 2011 Van (M_w=7.1) and Edremit (M_w=5.9) earthquakes) to TSMD within the context of Reference Database for Seismic Ground-Motion in Europe (RESORCE) which is a product of Seismic Ground Motion Assessment project (SIGMA). Between years 2008 and 2015, a considerable amount of strong motions recorded during low-to-moderate magnitude earthquakes in Turkey were accumulated. These recordings are available in AFAD's (The Disaster and Emergency Management Presidency of Turkey) website but the provided waveforms are not processed nor are the earthquake metadata compiled for these recordings. In this chapter, the data compilation procedure is explained in step by step manner, mostly focusing on the efforts for extending the TSMD.

2.1 Compilation of Strong Ground Motion Database

AFAD's Strong Motion Database of Turkey contains 479 earthquakes $M_w > 3$ that occurred between years of 2008 and 2015 with the spatial distribution given in Figure 2.1. All recordings from these earthquakes are gathered; however, events or records with following characteristics are eliminated: (i) events with focal depths more than 30 km, (ii) events with $M_w < 3.5$, (iii) events with unknown style-of-faulting, (iv) records with source to site distance greater than 200 km, (v) stations with unknown

average shear wave velocity profile of the top 30m (V_{S30}) and (vi) events with less than three recordings. After this preliminary elimination, 1189 recordings from 162 earthquakes are compiled and added to TSMD. Additionally, 268 recordings from the recent Ayvacık earthquake swarm (between 2015 and 2017) that satisfies the conditions above are included, leading to 1457 strong motion recordings from 184 events. The event location information (epicentral coordinates and focal depth) is obtained from AFAD's database. Magnitude values and the fault plane solutions are retrieved from Global CMT (http://www.globalcmt.org/CMTsearch.html), Regional Centroid Moment Tensor (http://rcmt2.bo.ingv.it/) and GFZ Moment Tensor (http://gfzpublic.gfz-potsdam.de) databases. The style-of-faulting is determined by applying of P- and T-axes definitions provided by Boore and Atkinson (2007, Table 2.1). Source to site distance metrics calculated from the fault plane solutions based on methodology offered by Akkar et al. (2014): (i) finite-fault distance metrics computed by double couple solutions, (ii) nucleation point assumed at the center of the fault, (iii) fault dimensions determined by Wells and Coppersmith (1994) equations, (iv) Joyner-Boore and Rupture distances calculated by Kaklamanos et al. (2011) procedure proposed for two planes, (v) arithmetic average of the distances computed from 2 planes calculated. Figure 2.2 shows the distribution of the earthquakes and records attributed to the normal, reverse and strike-slip earthquake mechanisms. Majority of the earthquakes were found to have normal and strike-slip mechanisms; whereas, only a few reverse events were determined, consistent with the spatial distribution of events.

Table 2.1 Boore and Atkinson (2007) Procedure

Fault Type	P-axis Plunge	T-axis Plunge
Normal	$P_{pl}^{*}>40$	$T_{pl}^{*}<40$
Reverse	$P_{pl}<40$	$T_{pl}>40$
Strike-slip	$P_{pl}<40$	$T_{pl}<40$
*: plunge of the P- and T-axes of the double-couple fault-plane solution		

When the recording stations are classified into NEHRP site classes (BSSC, 2015); it is observed that more than 90% of the records and stations belong to Class D ($180<V_{S30}<360$) and Class C ($360< V_{S30}<760$) (Figure 2.3).

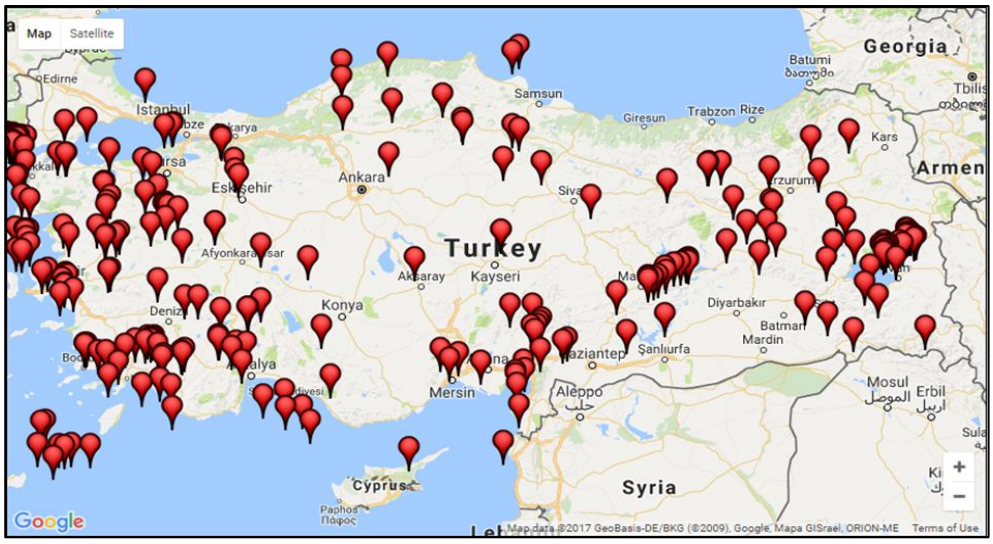

Figure 2.1 Spatial distribution of compiled earthquakes (2008-2015) (http://kyhdata.deprem.gov.tr).

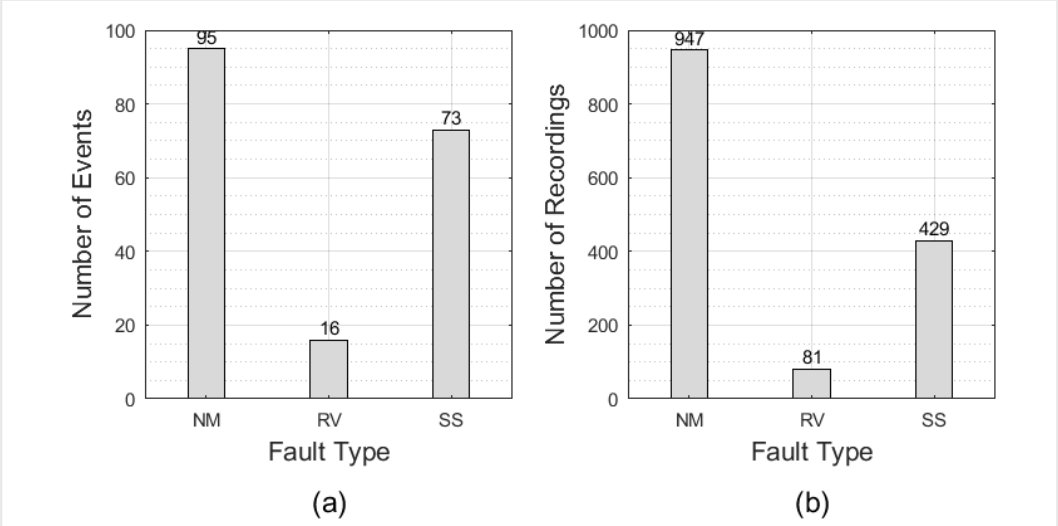

Figure 2.2 Distribution of (a) number of events vs. style-of-faulting, (b) number of recordings vs. style-of-faulting (compiled dataset).

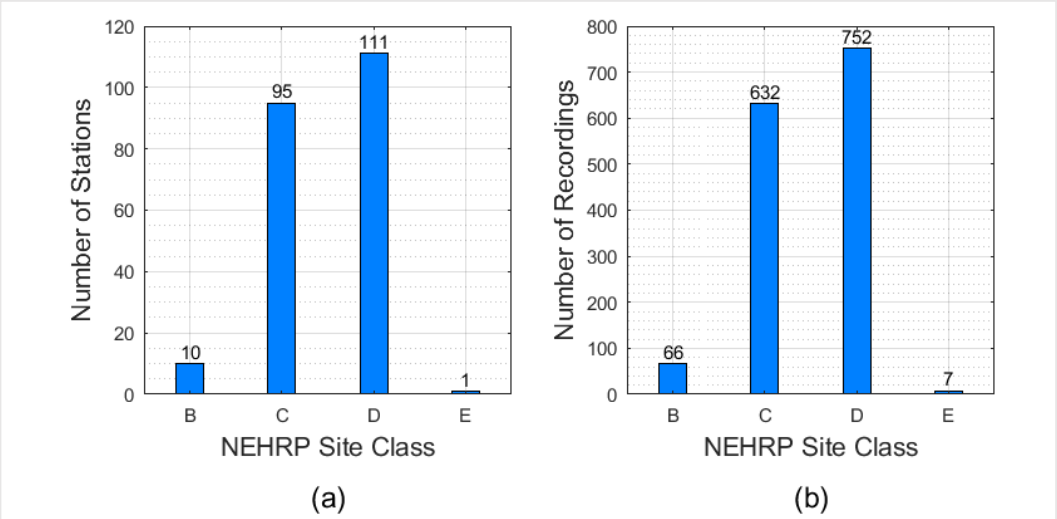

Figure 2.3 Distribution of (a) number of stations (b) number of recordings, within NEHRP (BSSC, 2015) site classes (compiled dataset).

2.2 Strong-Motion Data Processing

Raw strong ground motion recordings contain a certain amount of noise due to multiple reasons. These noise-contaminated recordings must be evaluated and corrected before using it in any earthquake engineering application. It is impossible to eliminate the noise completely in order to recover the original signal, but the noise-inclusion can be reduced to an acceptable amount. Douglas (2003) mentioned that the noise has two separate origins; non-standard and standard errors. Noise related to non-standard errors could not be cured by common processing techniques and must be analyzed by visual inspecting of each time history. Non-standard records include signals from multiple shocks (MS), high-frequency spikes (SP), S-wave trigger (SWT) issues, insufficient digitizer resolution (IDR), insufficient sampling rate, early termination of coda, and clipping of accelerograms (Douglas, 2003). MS, SP and IDR were the most encountered errors during the visual inspection of the recordings added to TSDM. MS-related errors were fixed by visually selecting and separating the main shock signal from the afteshock signal. SP-related errors were treated by replacing the acceleration ordinate of the spike with the average of the accelerations on either side of the spike. 25 recordings were eliminated from the compiled dataset because of

insufficient digitizer resolution. Figure 2.4 shows an example of the recordings eliminated from the database due to insufficient digitizer resolution.

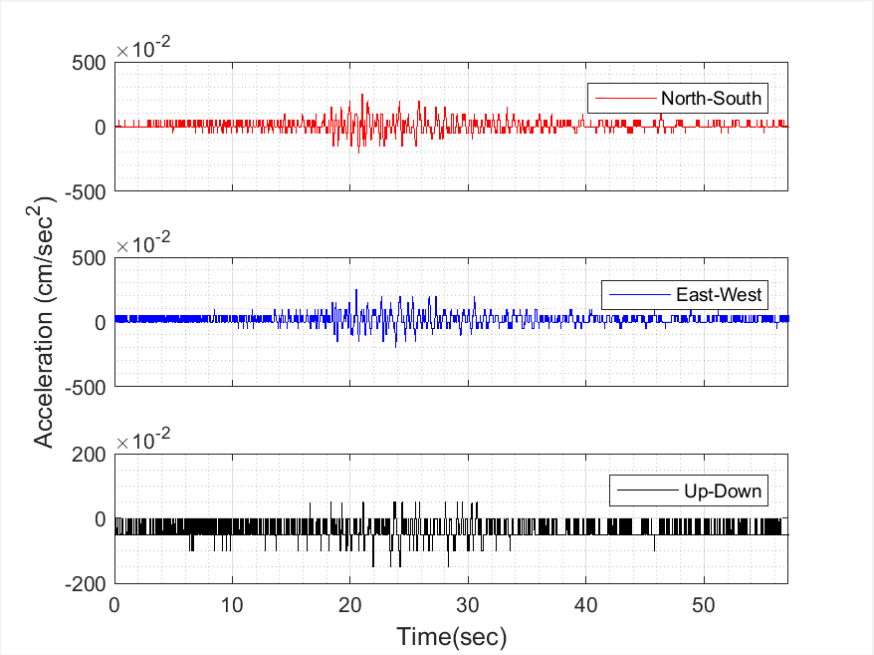

Figure 2.4 Example of the recordings eliminated from the database due to insufficient digitizer resolution (Raw Record# 20111029222-4902; N-S: north-south, E-W: east-west, U-D: up-down).

Same procedure which was employed for processing of TSMD (Akkar et al., 2010) is also followed in the processing of the compiled dataset for consistency. After the visual inspection of each recording for non-standard errors, zeroth-order correction is applied to each recording. The low-cut (high pass) and high-cut (low-pass) filter values are determined by an iterative procedure that monitors the behavior of the Fourier amplitude spectrum as well as the velocity and displacement time series (Boore and Bommer 2005; Akkar and Bommer 2006; Douglas and Boore 2011). Figure (2.5) displays the acceleration, velocity and displacement time series for an example recording (east-west component of Record# 20080112150644-1005). The unphysical appearance of velocity and displacement time series is a sign of the existence of standard errors in the recording. Low-cut and high-cut filter values were

chosen as 0.15s and 40s, respectively. Figure (2.6) presents raw and processed (band-pass filtered by chosen filter values) FAS for the same record and Figure (2.7) depicts the band-passed time series of the same record based on chosen filter corners. Low-cut filter values are selected carefully because they directly affect the usable spectral range and inappropriate low-cut filter values may lead to the loss of the major part of the accelerometric information. Theoretical corner frequency line (AS00 line) proposed by Atkinson and Silva (2000) is used to check the selected low-cut filter values. Figure (2.8a) shows that all points are located below the AS00 line and the preferred low-cut filter values are in expected correlation with magnitude. Please note that the majority of recorders are modern digital instruments which provide a significantly good match with the theoretical line.

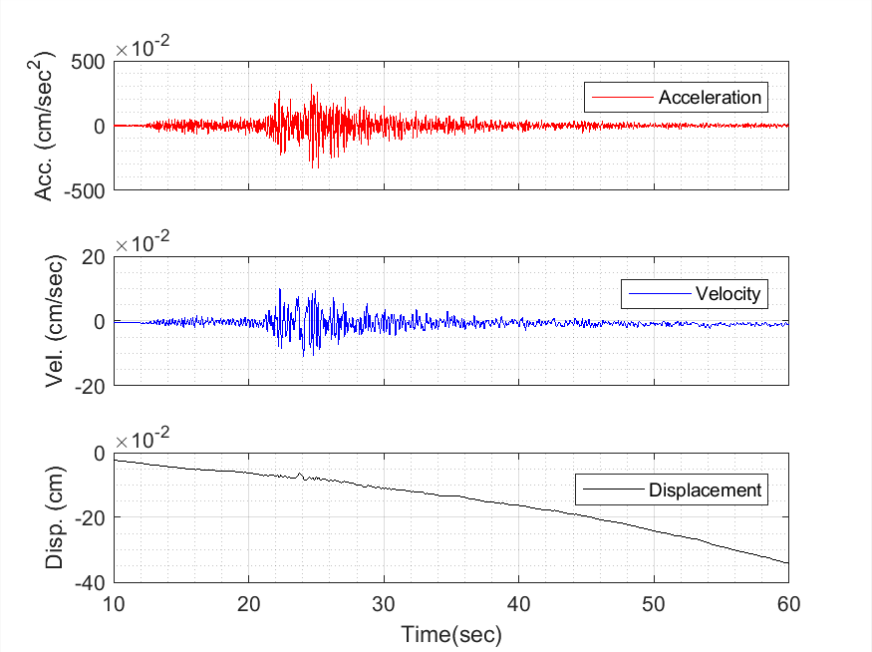

Figure 2.5 Time Series for an East-West Component of Raw Record 20080112150644-1005.

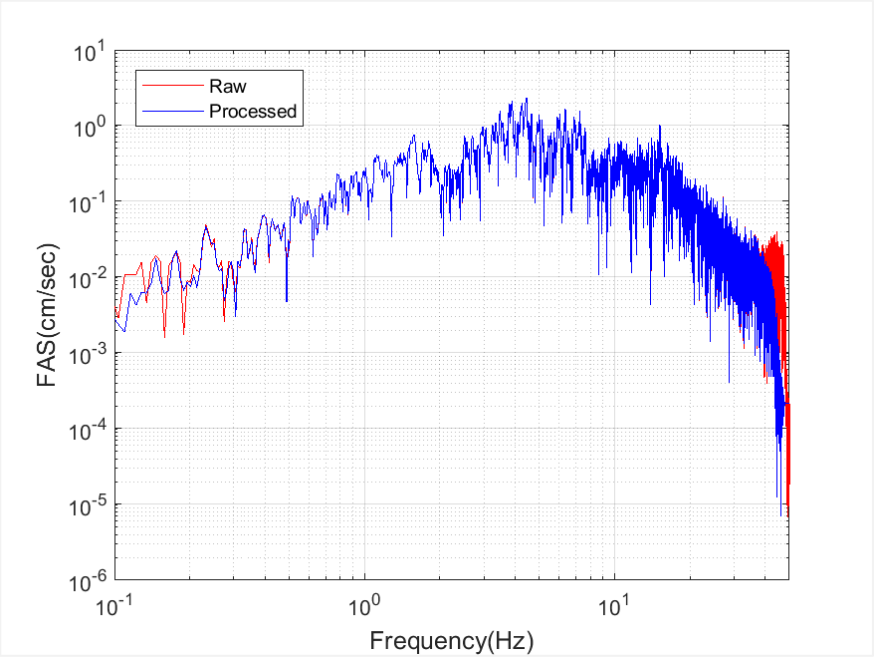

Figure 2.6 Raw and processed FAS for the East-West component of Record# 20080112150644-1005.

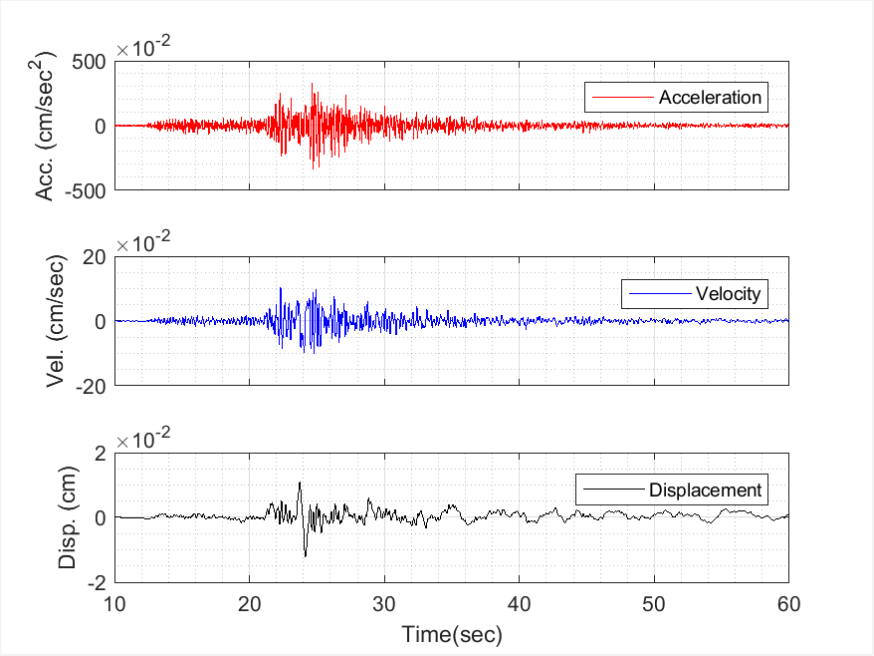

Figure 2.7 Processed (band-pass filtered) East-West component of Record# 20080112150644-1005.

The maximum usable period for each recording is calculated by taking the inverse of 1.25 times the low-cut filter value. Figure (2.8b) presents the number of recordings as a function of maximum usable period. It is observed that the number of records reduces significantly for periods larger than 3s. The response spectra of vertical and two horizontal components are calculated and the geometric average of horizontal components are used in calculations (Akkar et al., 2006, Boore et al., 2005, Douglas et al., 2011).

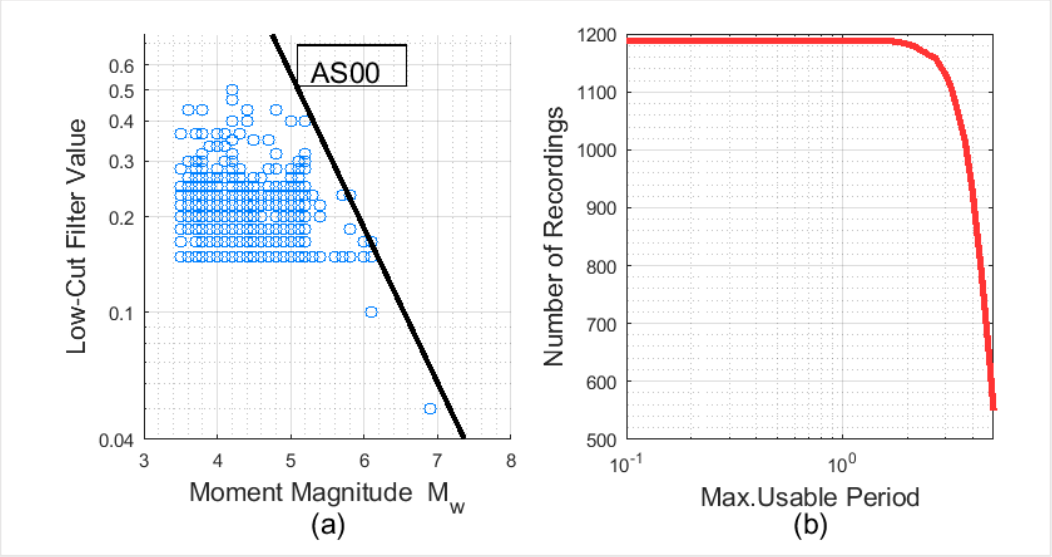

Figure 2.8 (a) Distribution of low cut filter values with magnitude and comparison with the theoretical corner frequency line, (b) period dependence of number of ground motions based on the lowest useable frequency (compiled dataset).

2.3 Discussion of the Updated TSDM (Merged Database)

When the TSMD is updated with the additional recordings summarized above, the final updated database contains 2698 recordings from 672 earthquakes. The magnitude-distance distribution of the updated TSMD for peak ground acceleration (PGA) is given in Figure 2.9. Figure 2.9 shows that the majority of strong ground motion recordings in the original TSMD belonged to $5<M_w<6.5$ events recorded at distances more than 30 kilometers; therefore, near-field recordings of large magnitude events which are critical from engineering design point of view were limited. Also, the number of recordings for $M_w<5$ earthquakes, which play an important role in defining the regional magnitude

scaling were not sufficient (Gülerce et al., 2016; Sandıkkaya, 2017). Updated TSMD includes substantially more recordings from small magnitude events and the number of near-field recordings is improved in the moderate magnitude range. Figure (2.10a) and (2.10b), show the number of recordings in each magnitude and distance bin for the post- and pre-2008 recordings and the merged database. These figures confirm that there is a significant enhancement in distribution of data in moderate magnitude range together with an increase in near-source recordings which is suitable for testing the applicability of V/H ratio and vertical GMMs in Turkey.

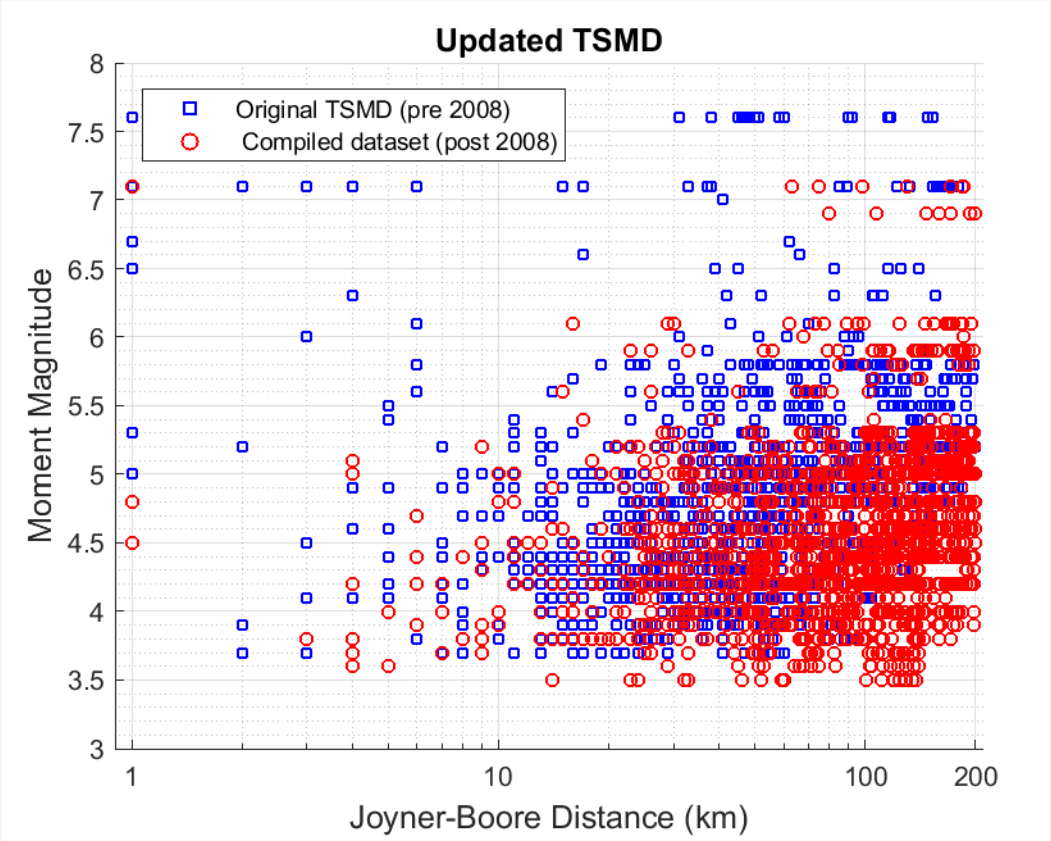

Figure 2.9 Distribution of magnitude-distance pairs for PGA (original TSMD and new recordings are represented by blue triangles and red circles, respectively).

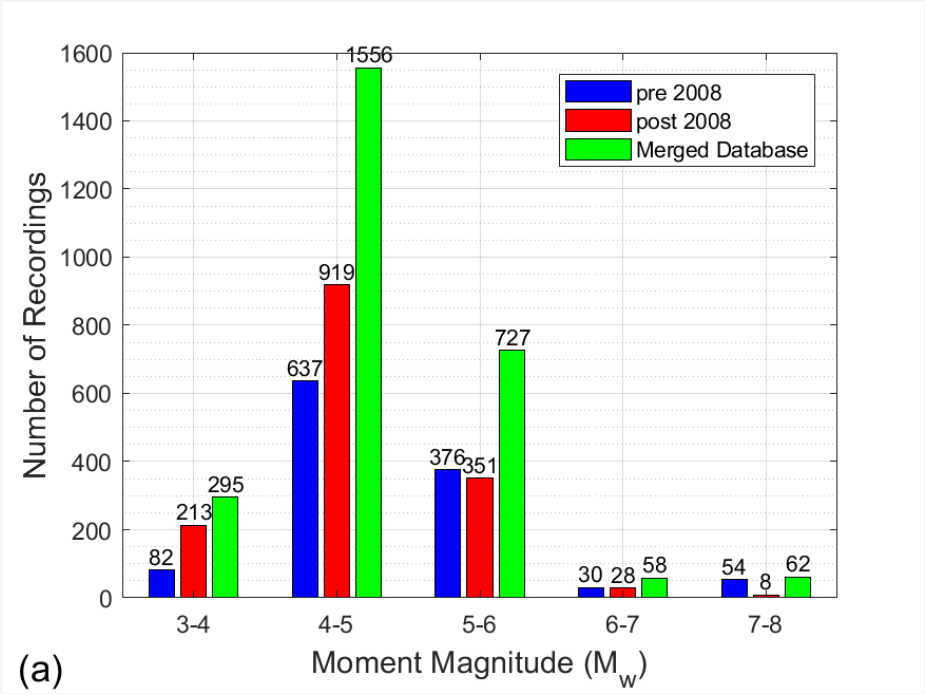

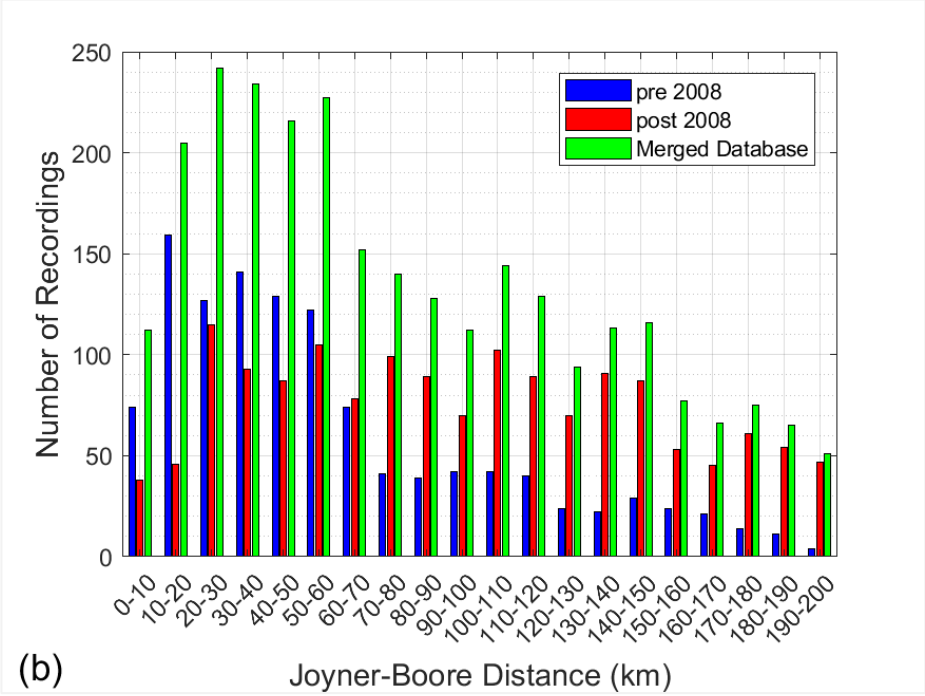

Figure 2.10 (a) Number of Recordings with respect to Moment Magnitude Bins (b) Number of Recordings with respect to Distance Bins.

Figure 2.11 displays the number of recordings as a function of maximum usable period for the updated TSMD, pre-2008 recordings (original TSDM), and compiled dataset (2008-2017). It is observed that the maximum usable period for original TSDM has a significant drop at around 2 seconds spectral period. This drop is observed at 3 seconds in the compiled dataset and at 4 seconds for updated TSMD. Therefore, the maximum usable period range is significantly improved resulting in almost 117 percent increase in the number of recording.

Figure 2.12 shows that more than 90% of events and relevant recordings in the updated TSMD belong to strike-slip and normal style of faulting classes and only less than 5% of the events can be classified as reverse events, in correlation with the major tectonic structure of Turkey. According to Figure 2.13, majority of recordings, events or stations are classified as Class D ($180<V_{S30}<360$) and Class C ($360< V_{S30}<760$).

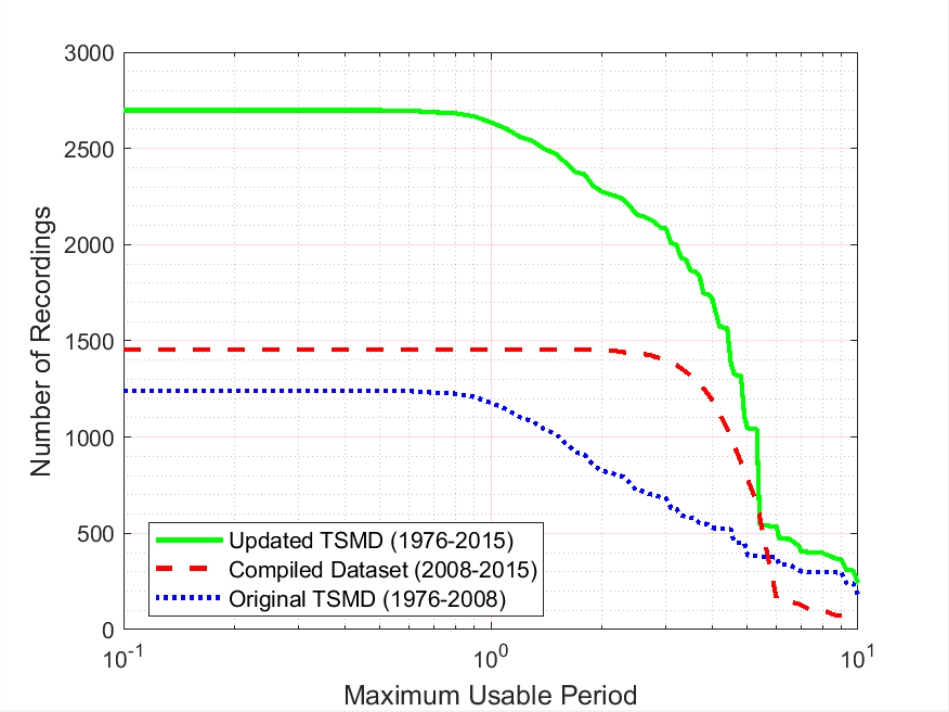

Figure 2.11 Number of recordings as a function of maximum usable period for updated TSMD (Merged Database), original TSMD and compiled dataset.

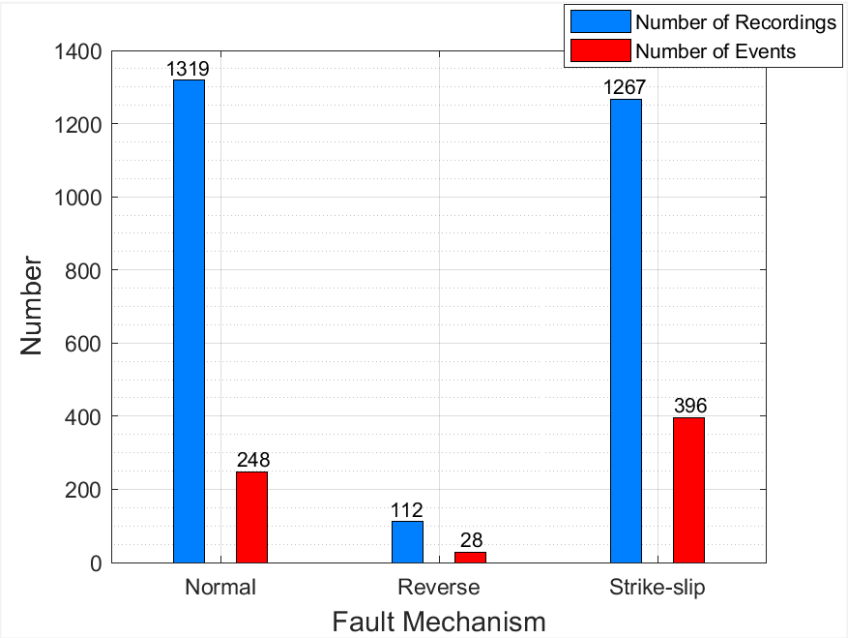

Figure 2.12 Distribution of (a) number of recordings vs. style-of-faulting, (b) number of events vs. style-of-faulting (updated TSMD).

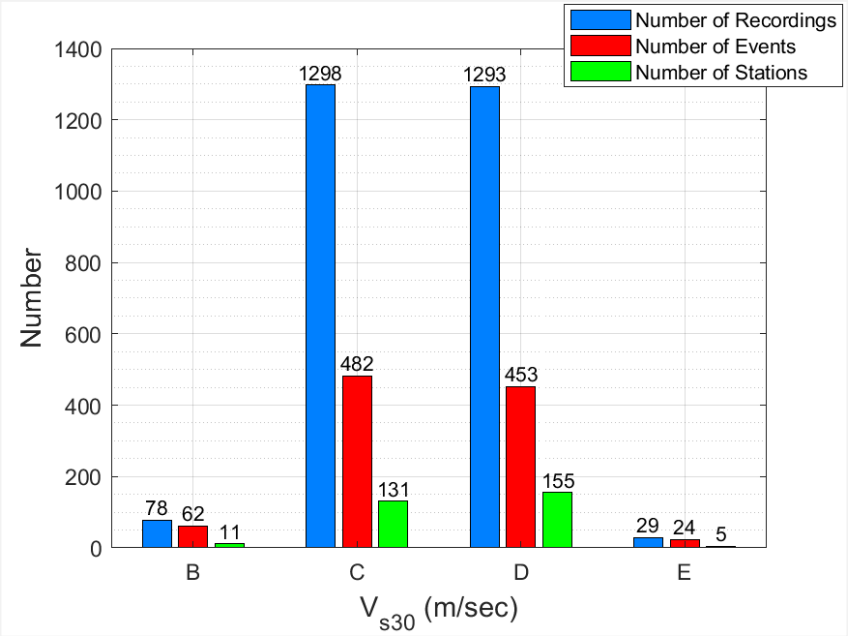

Figure 2.13 Distribution of (a) number of stations, (b) number of recordings within NEHRP site classes (updated TSMD).

CHAPTER 3

EVALUATION OF VERTICAL TO HORIZONTAL RATIO GROUND MOTION MODELS

The ground motion models (GMMs) for the horizontal component ground motions for Turkey have been developed since 1990s (Douglas, 2011) and detailed discussions related to previous horizontal predictive models can be found in Kale et al. (2015). Recent studies by Gülerce et al. (2016), Sandıkkaya (2017), and Kale (2017) discussed the compatibility of the strong motions recorded in Turkey with the global horizontal GMMs, using the initial or re-visited versions of TSDM. Incompatibilities between the global GMMs and Turkish strong motion dataset in small-to-moderate magnitude scaling, large distance scaling, and site amplification scaling were encountered during the evaluation of the residuals, indicating that the GMMs for the vertical ground motions or vertical to horizontal (V/H) ratio should be compared to the Turkish dataset for building a ground motion characterization logic tree for the vertical ground motion component. Therefore, four candidate vertical GMMs proposed by (Gülerce and Abrahamson, 2011; Gülerce and Akyüz, 2013; Akkar et al., (2014b) and Bozorgnia and Campbell, 2016) are selected and their compatibility are tested utilizing the updated TSDM in terms of above mentioned scalings. Different data testing procedures based on the analysis of model residuals are employed to evaluate the performance of the selected candidate models.

3.1 Selection of Candidate Ground Motion Models

Only one of early-stage GMMs developed for Turkey, the Gülkan and Kalkan (2002) model, predicts for the vertical ground motion component. The accompanying V/H ratio model (Kalkan and Gülkan, 2004) was developed using the V/H ratios from 100 ground motions recorded during 47 events that occurred in Turkey between the years

of 1976 and 2002. On the other hand, several alternative V/H ratio GMMs were developed for shallow crustal and active tectonic regions in the last decade. Table 1.1 lists, in brief, the name of vertical and ratio GMMs which have been published so far. The GMM selection criteria proposed by Cotton et al. (2006), Bommer et al. (2010), and Stewart et al. (2016) for horizontal GMMs are utilized to select four candidate V/H ratio models for this study. Global V/H ratio models proposed by Gülerce and Abrahamson (2011; GA2011) and Bozorgnia and Campbell (2016; BC2016, superseding the Bozorgnia and Campbell, 2004 model) were built using the NGA-West 1 (Chiou et al., 2008) and NGA-West 2 (Ancheta et al., 2014) databases, respectively. The pan-European model proposed by Bommer et al. (2011) was updated by Akkar et al. (2014b; ASA2014) using the RESORCE database. Gülerce and Akyüz (2013; GA2013) proposed the Turkey-adjusted version of the GA2011 V/H ratio model; the functional form of the model is the same as that of GA2011 model but some of the coefficients were adjusted using the original version of TSDM. Models proposed by Edwards et al. (2011) and Poggi et al. (2012) do not cover the full range of site conditions: they are developed only for rock and soft sites, respectively. Therefore, these models are not included in the candidate model list. Kalkan and Gülkan (2004) V/H ratio model was also eliminated because: (i) model coefficients were provided only up to 2s, (ii) generic site classification (site dummies) were utilized for the site amplification scaling. Eventually, four candidate GMMs (GA2011, GA2013, ASA2014, and BC2016) are selected for testing within the scope of this study. Tables 3.2 and 3.3 summarize and compare the main features of the candidate models; e.g. datasets used for development, applicability ranges, independent parameters, etc. The spectral shapes for the median estimates of the candidate GMMs for M6 and M7 earthquakes at 30 km for generic rock (V_{S30}=800 m/s) and soft (V_{S30}=180 m/s) sites are compared in Figures 3.1 and 3.2, respectively (the other descriptor parameters are given in the figure captions). According to Figures 3.1 and 3.2, the variability in the median predictions of the models is more pronounced for rock sites, especially for the short periods. In the middle period band (0.1-1 sec), the median estimates of each model are closer to each other.

Table 3.1 Functional Forms of the Candidate V/H Models

Candidate GMM	General Functional Form (for median)	Development Method
GA 2011	$\ln\left(\frac{V}{H}\right) = f_{Mag,Rrup} + f_{flt} + f_{site}$	Regression on V/H ratio values
GA 2013	$\ln\left(\frac{V}{H}\right) = f^{*}_{Mag,Rrup} + f_{flt} + f^{*}_{Site}$	Only the adjustment coefficients are regressed for
ASA 2014	$\ln\left(\frac{V}{H}\right) = f_{Mag,Rjb} + f_{flt} + f_{site}$	Regression on V/H ratio values
BC 2016	$\ln\left(\frac{V}{H}\right) = f_{Mag} + f_{Rrup} + f_{flt} + f_{HW} + f_{site} + f_{sed} + f_{hyp} + f_{dip} + f_{atn}$	Vertical and horizontal models were developed individually, ratio was calculated and regressed

Notes: Abbreviations used in the table are: Mag: moment magnitude, Site: site amplification, flt: faulting mechanism, R_{rup}: rupture distance, R_{jb}: Joyner-Boore distance, HW: hanging wall effect**, sed: basin response effects, hyp: hypocentral depth, dip: dip angle, atn: large distance attenuation.

*Same functional form but some of the coefficients are TR-adjusted (TR.Adj).
**Hanging-wall effects included in this model are neglected in our study.

Table 3.2 Properties and Applicability Ranges of the V/H Models

General Information				Applicability Range		
Candidate GMM	**Database**	**Number of recordings**	**Number of events**	**M_w range**	**Distance range (km)**	**Spectral period range (sec)**
GA 2011	PEER-NGA W1	2684	127	5-8	0-200	0-10
GA 2013	Built by PEER-NGA W1, (Modified by TSMD)	2684 (1142)	127 (288)	5-8 (4-8)	0-200	0-10
ASA 2014	RESORCE	1041	221	4-8	0-200	0.01-4
BC 2016	PEER-NGA W2	6989	282	3-8	0-300	0-10

* Numbers in parenthesis represents the number of events and recordings that were used to modify GA2011

For rock sites, the amplitudes of GA2011 and ASA2014 models are pretty similar and the GA2013 and BC2016 models give the highest and the lowest estimates, respectively (Figure 3.1). The GA2013 model represents the upper bound because the constant term of the GA2011 model was modified with a positive shift in the short periods due to the trends observed in the original TSMD (Gülerce and Akyüz, 2013). Figure 3.2 shows that the median estimates of GA2011 GMM, which includes a significant non-linearity in the site amplification model, is lower than the median estimates of GA2013 and BC2016 models. An interesting observation is related to the peaks of the spectral shapes: the peaks are observed at 0.06-0.07s spectral periods for GA2011 and GA2013 models, while the peak is shifted to higher periods in ASA2014 model, especially in soft soil conditions. The tendency of the peak of BC2016 model is completely opposite, the peak is around 0.1s for hard rock sites but it shifts to shorter periods (0.07s) for the soft soil sites. Differences in the shape of the V/H ratio at high frequencies and the periods of the peak could be related to the differences observed in the high frequency attenuation parameter (kappa) in the vertical and horizontal components (Ktenidiou et al., 2014). However, the number of studies that provide kappa values for vertical and horizontal components is too limited to draw general conclusions for the tendency of the peak in the V/H ratio models.

3.2 Analysis of the Model Residuals

To evaluate the misfit between the model predictions and the actual ground motion data, median estimations of each candidate model are computed using the predictive parameters in the updated TSMD. The total residual, denoted by $R_{ijk,}$ is the difference between the natural logarithm of the observed ground motion a_{ijk} and the model prediction, p_{ijk} from the i^{th} event at the j^{th} station at period k (Eq. 3.1). Then, using the two-step regression method, the total residuals are decomposed into three components: the mean offset (c_k) representing the average bias of the actual data relative to the model predictions in each period, inter-event ($\emptyset_{jk}$) and intra-event (τ_{jik}) residuals (e.g. Scassera et al. 2009; Al-Atik et al. 2010).

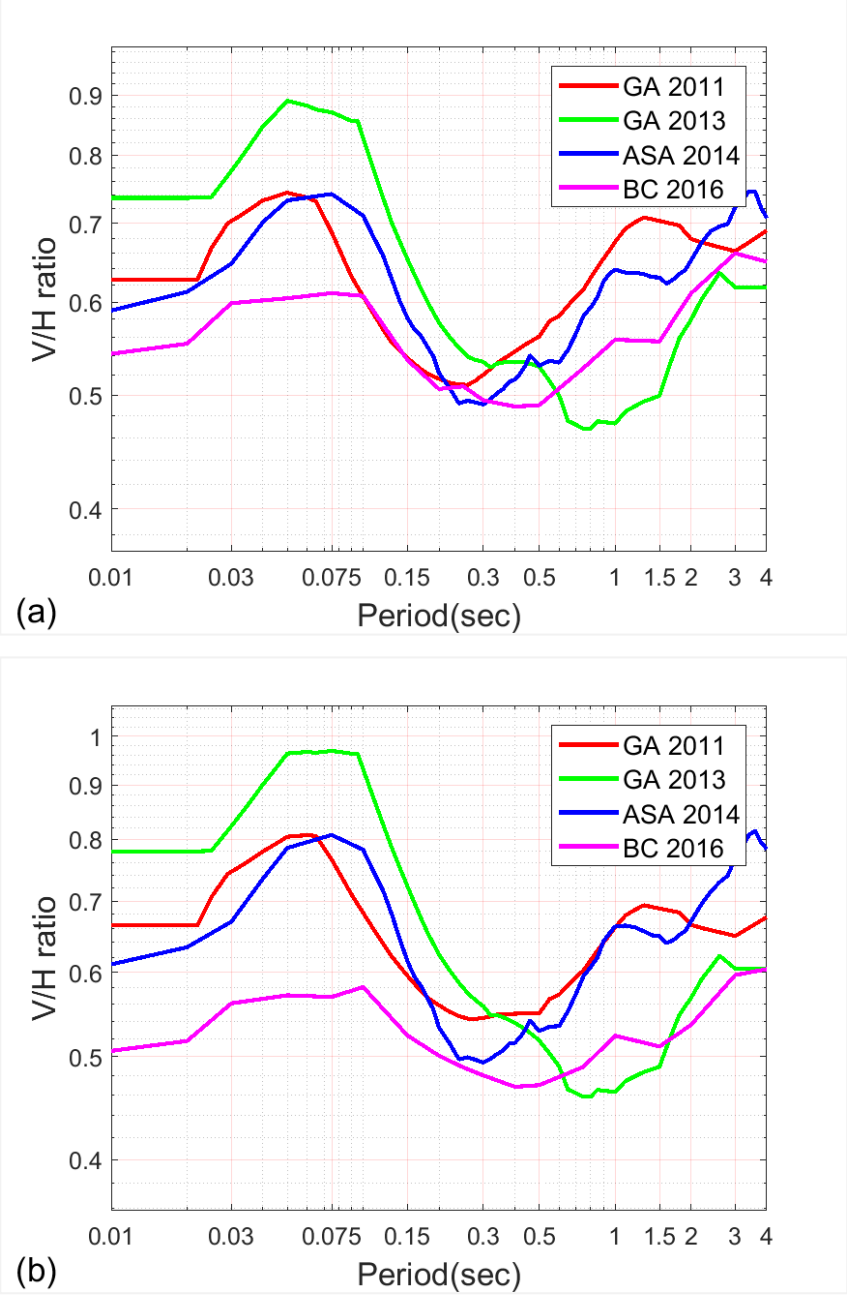

Figure 3.1 Spectral shapes for the median estimates of the candidate V/H ratio GMMs for (a) M_w =6, V_{s30} =800 m/sec, R=30 km, Z_{tor}=5.36 km (b) M_w =7, V_{s30} =800 m/sec, R=30 km, Ztor=2.29 km.

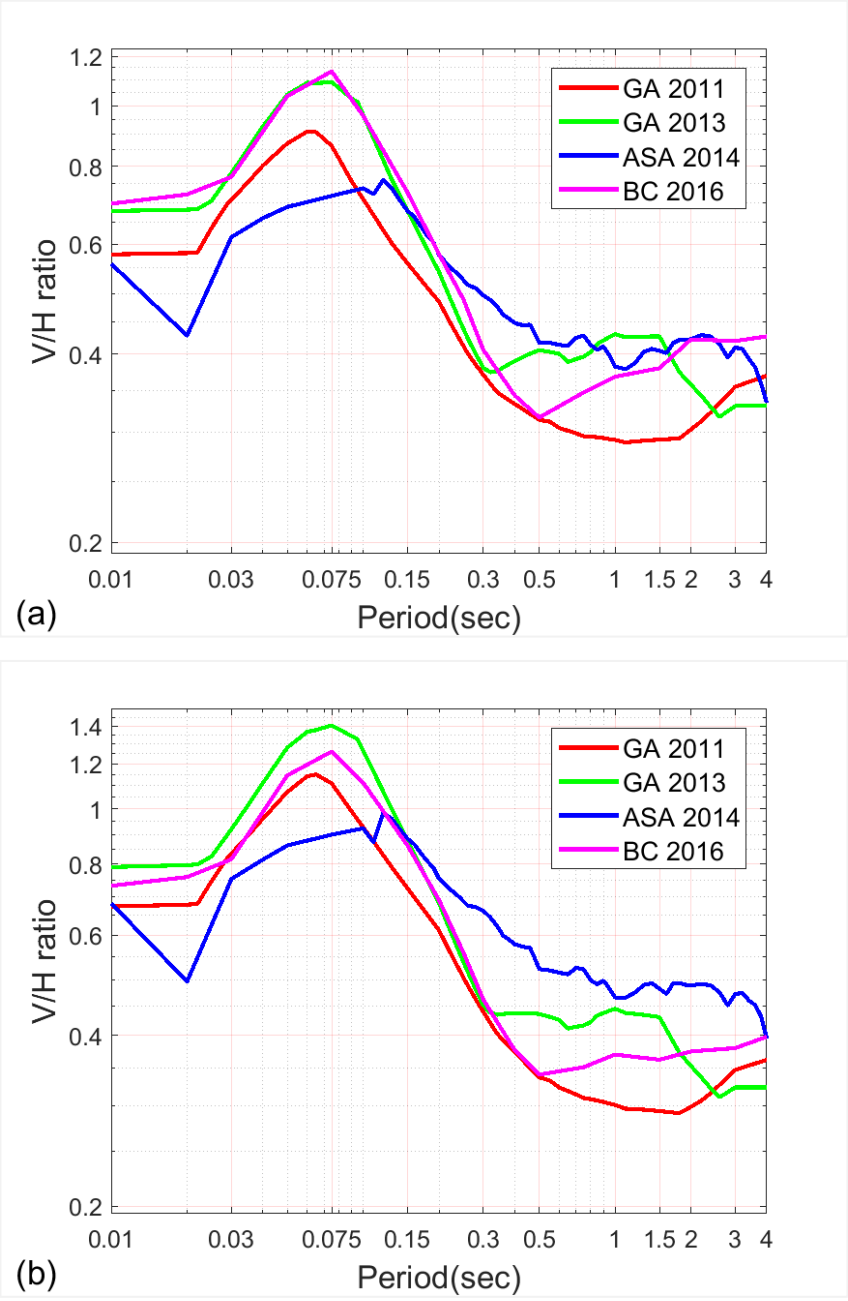

Figure 3.2 Spectral shapes for the median estimates of the candidate V/H ratio GMMs (a) M_w =6, V_{s30} =180 m/sec, R=30 km, Ztor=5.36 km (b) M_w =7, V_{s30} =180 m/sec, R=30 km, Ztor=2.29 km.

$$R_{ijk} = \ln(a_{ijk}) - \ln(p_{ijk}) = c_k + \emptyset_{jk} + \tau_{ijk} \quad (3.1)$$

To check the compatibility of the magnitude and depth to the top of the rupture (Z_{tor}) scaling of the candidate models with the updated TSMD, the inter-event residuals are plotted with respect to M_w and depth to the top of the rupture (Z_{tor}) for PGA, T = 0.07s, 0.3s, and 1.0s spectral accelerations in Figures 3.4-3.11, respectively. The analyses were performed 12 other spectral periods but these periods are selected since they (approximately) represent the positive and negative peaks of the V/H ratio vs. period. In each figure, the inter-event residuals for strike-slip, reverse and normal events are given by red, black and green symbols; whereas, the average of the residuals is shown by pink lines. Similarly, the distribution of the intra-event residuals with the record parameters such as rupture/Joyner-Boore distance and V_{S30} is given in Figures 3.4-3.11. Figures 3.4-3.11 show similar trends in the inter-event residuals vs. magnitude plots for all candidate models except BC2016: negative residuals are observed for $M_w \geq 6.5$ events for periods up to T=0.3s, indicating the overestimation of short period V/H ratios for large magnitude events. A similar trend was observed by Gülerce et al. (2016) for the horizontal ground motion component however, the dataset used by Gülerce et al. (2016) had only a limited number of $M_w \geq 6.5$ events. BC2016 model, representing the lower bound in Figures 3.1-3.2, does not show any systematic negative bias in the large magnitude scaling. Average residuals of the models are generally positive for small magnitudes, especially for $M_w<4$ events. This tendency is less pronounced in BC2016 and ASA2014 models. In general, the inter-event residuals for all models lie very close to the zero line, especially after T=0.3s; however, a slightly positive trend is observed in the residuals of GA2011 model after T=1s for $M_w<6.5$ events. Distribution of the inter-event residuals with Ztor imply that the depth scaling of all models are consistent for Z_{tor} <15km. An insignificant positive trend is visible for Z_{tor} >15km, which could be related to the cut-off values in the Z_{tor} scaling of the models to avoid unconstrained extrapolation. However, the positive trend in the residuals of BC2016 model is very noticeable after T=2s indicating a significant difference in the Z_{tor} scaling of the model from that of the updated TSMD at long periods. Distribution of intra-event residuals with distance suggests no trends within the applicability range of the selected models, except for a small negative trend

in the 0-10 km observed between T=0.05-0.2s. It should be underlined that the data in this distance range is very limited to indicate any systematic bias. The site amplification scaling of all models are consistent; distribution of residuals indicates no systematic bias in the distribution residuals. The residuals are slightly on the positive side for T≤0.75s, then becomes negative in very soft sites (V_{S30}=100-200m/s). Amount of reverse events and recordings from these events in the updated TSMD are limited; however, the distribution of the residuals with any of the model parameters does not show a significant variation with style-of-faulting. The mean offset values (c_k) for the candidate GMMs are compared in Figure 3.3. The mean offset values for GA2013, ASA2014 and BC2016 models are quite small through all spectral periods. The maximum misfit is obtained in the GA2011 model, consistent with the observations from the residual plots. The lower magnitude limit of the GA2011 model (Table 3.2) is higher than all other candidate model, which has a negative effect on the model's performance for predicting the ground motions in updated TSMD that mostly includes small magnitude events. GA2011 model's constant term was modified for GA2013 model based on the mean offsets calculated by using the original TSMD; therefore, the mean offset values of GA2013 model given in Figure 3.3 is smaller than GA2011 and close to that of ASA2014 model.

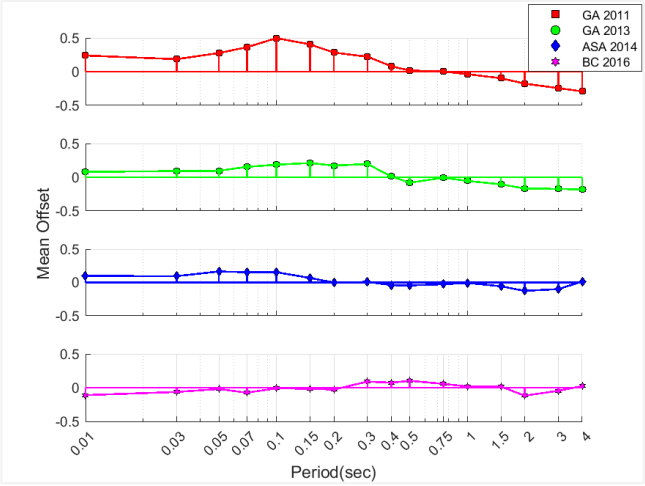

Figure 3.3 Distribution of mean offsets for each candidate model

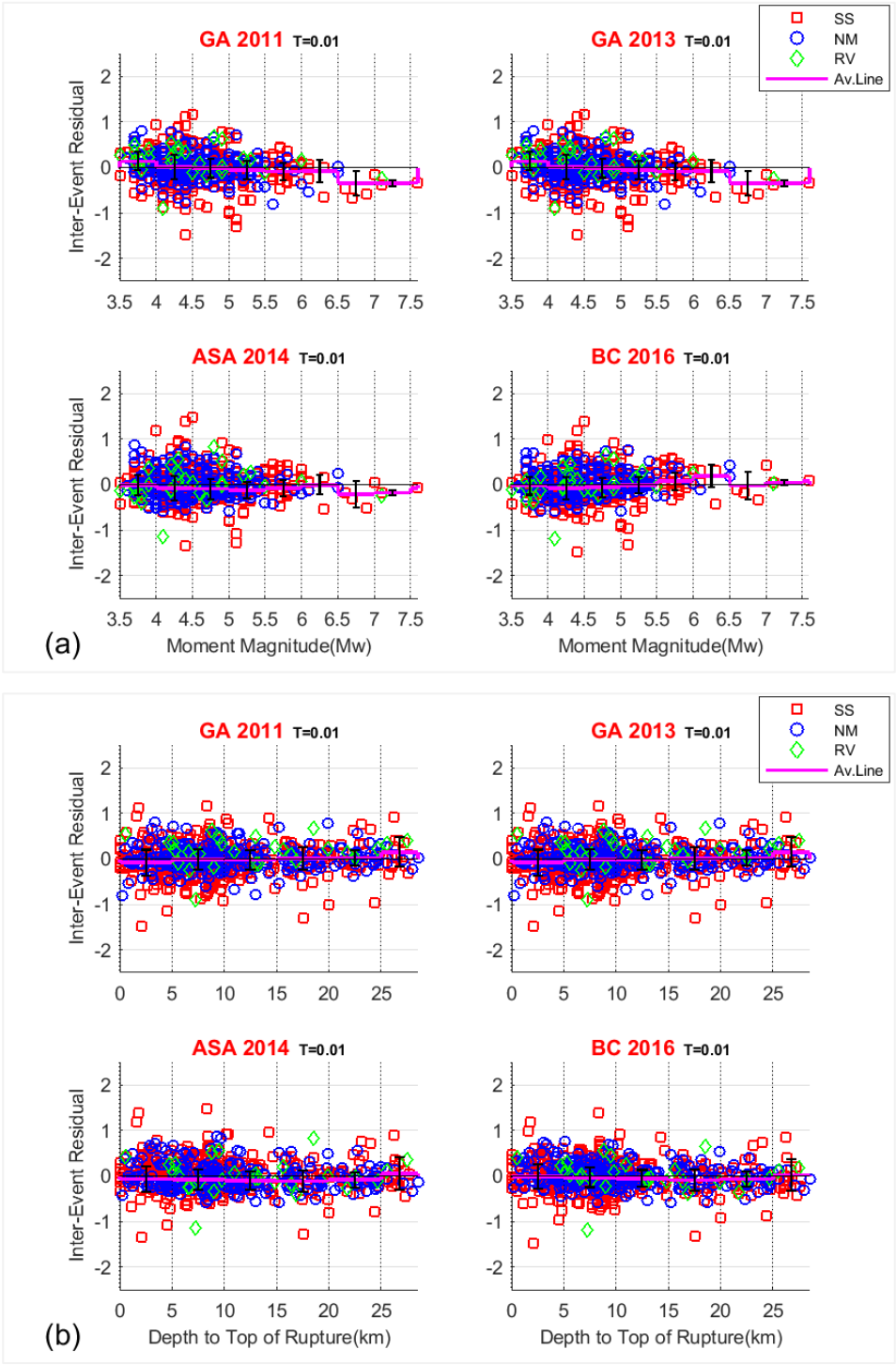

Figure 3.4 Distribution of the inter-event residuals with (a) magnitude, (b) depth to the top of the rupture for Sa at 0.01sec or at PGA depending on the model.

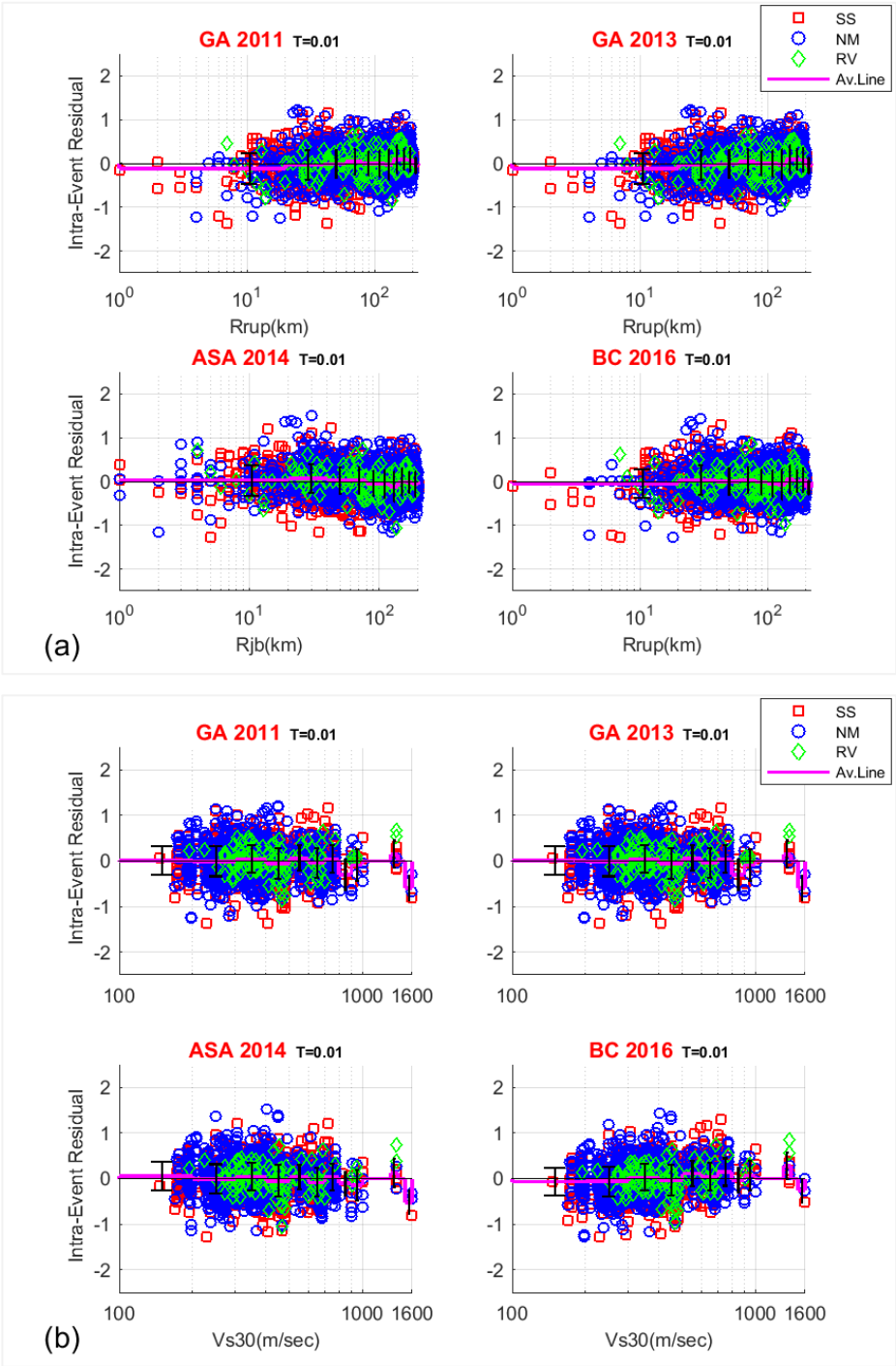

Figure 3.5 Distribution of the intra-event residuals with (a) rupture distance or Joyner-Boore distance depending on the model, (b) V_{S30} for Sa at 0.01sec or at PGA depending on the model.

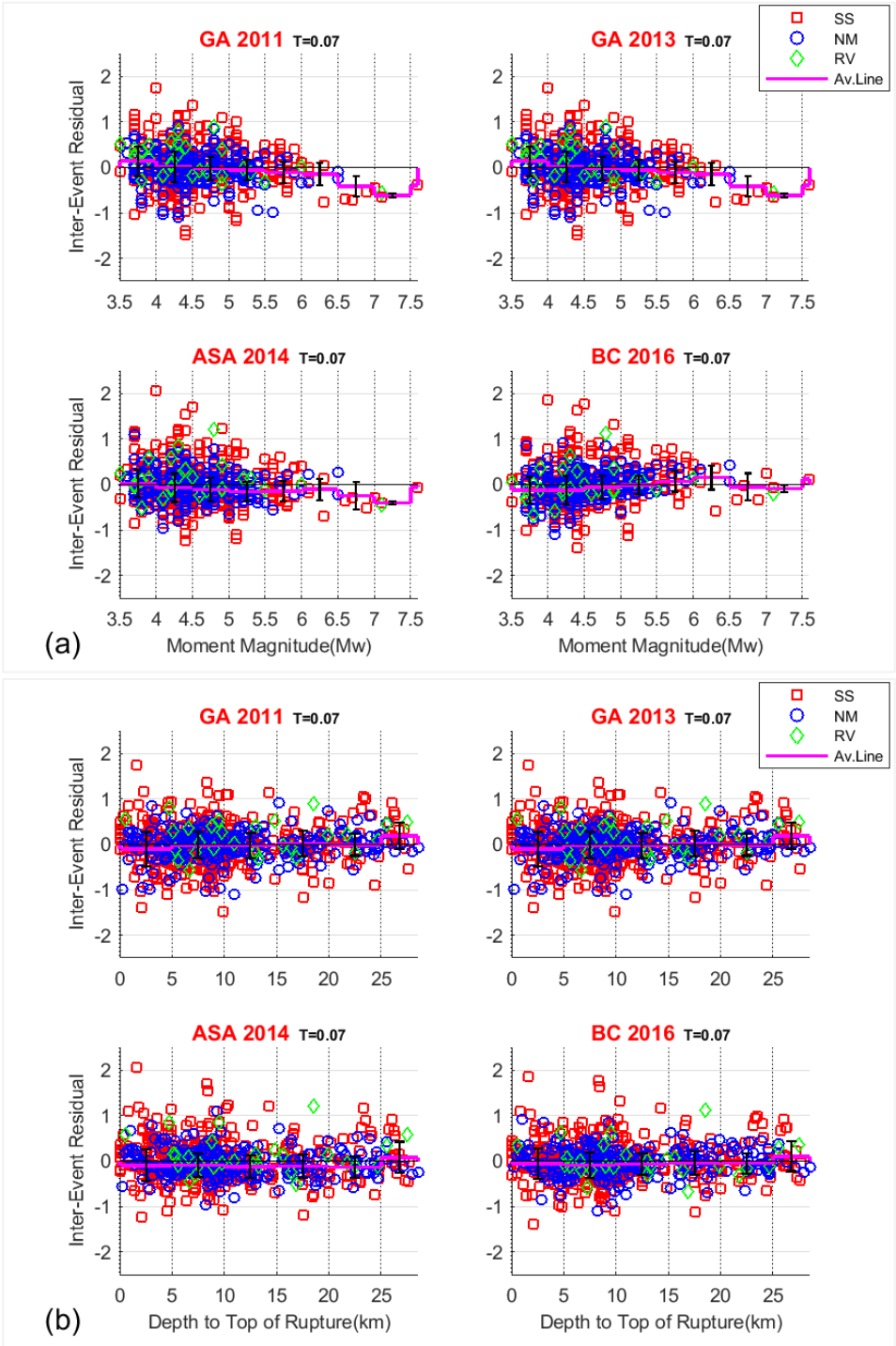

Figure 3.6 Distribution of the inter-event residuals with (a) magnitude, (b) depth to the top of the rupture for Sa at 0.07sec.

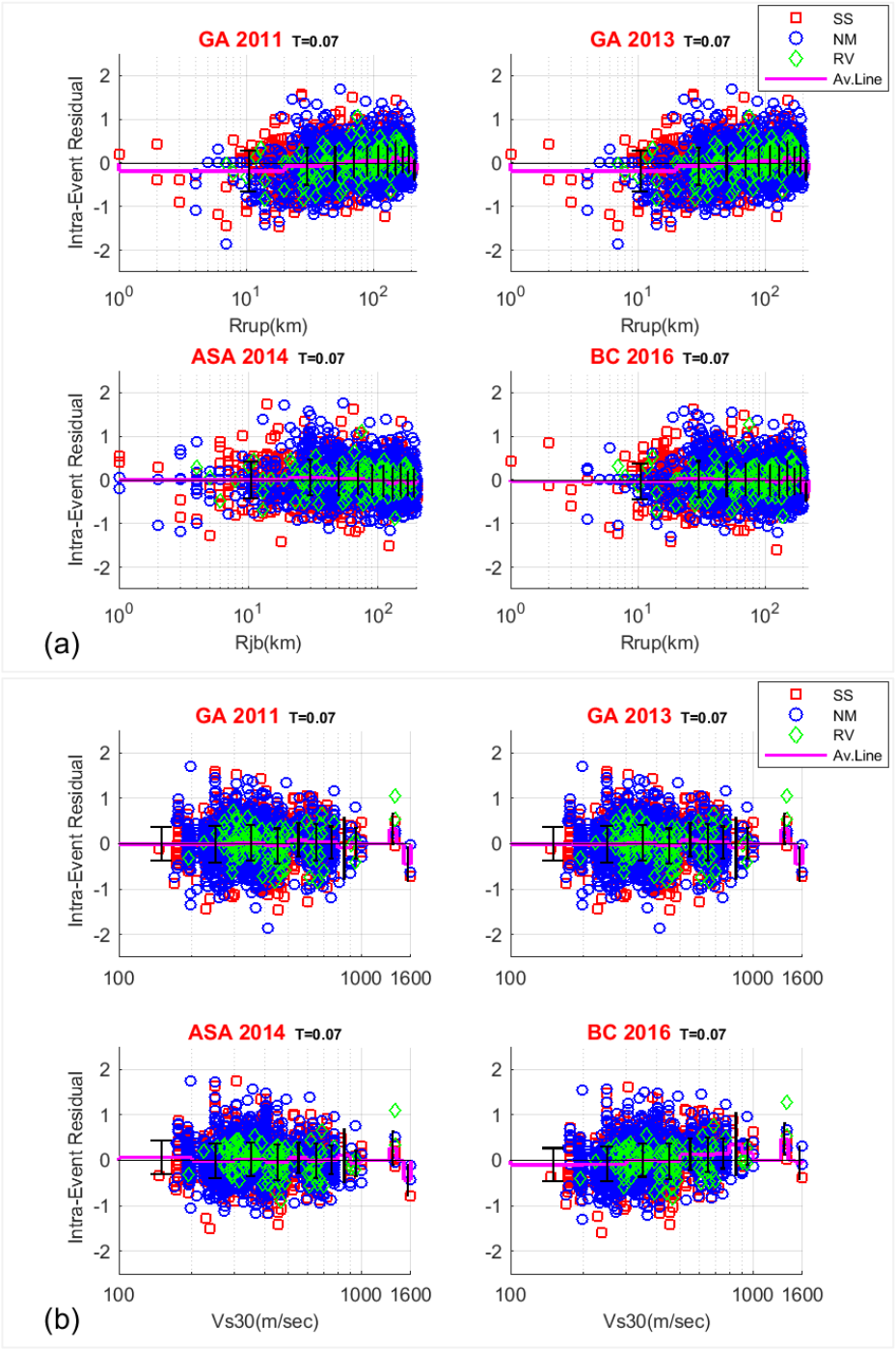

Figure 3.7 Distribution of the intra-event residuals with (a) rupture distance or Joyner-Boore distance depending on the model, (b) V_{S30} for Sa at 0.07sec.

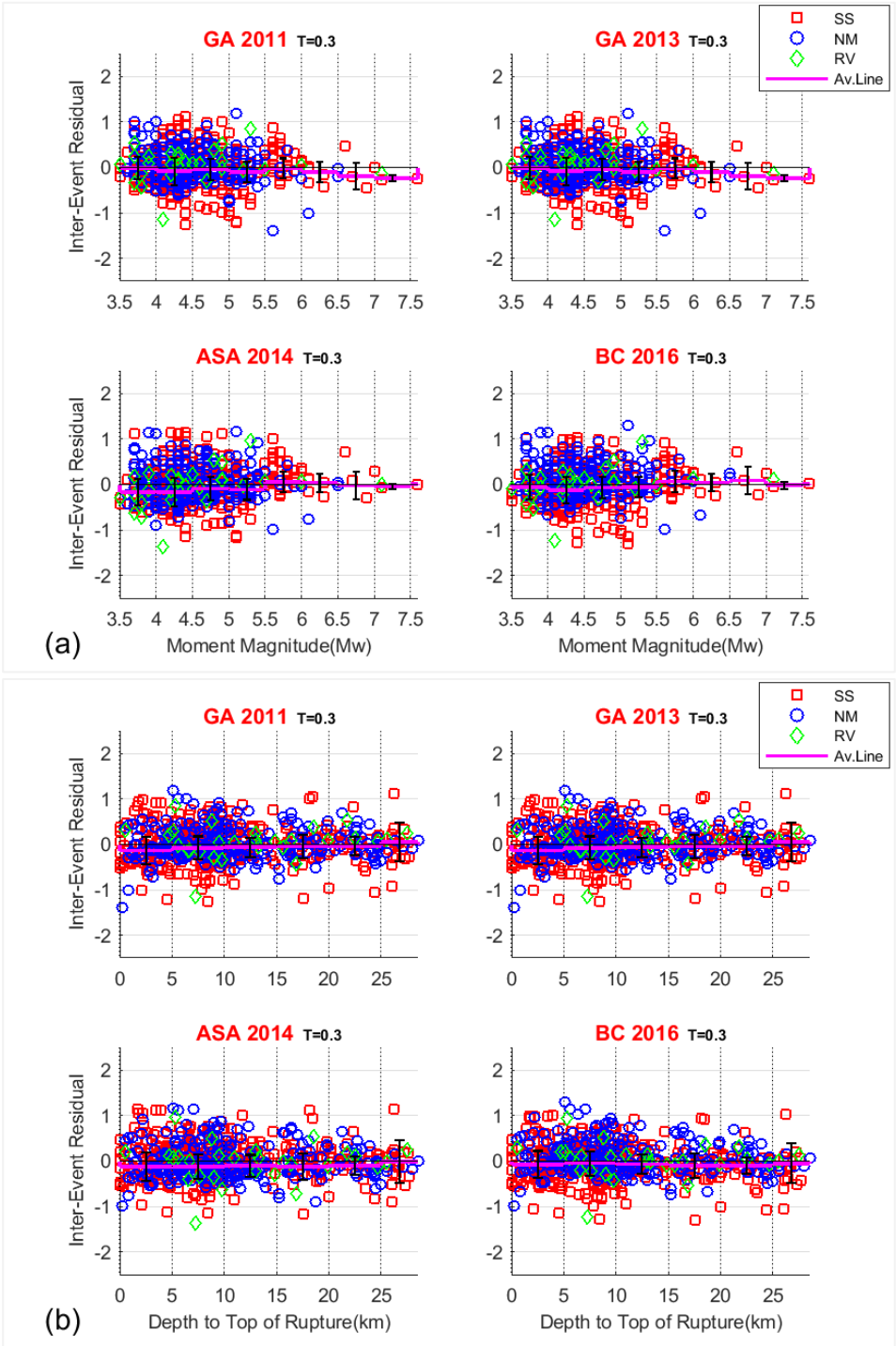

Figure 3.8 Distribution of the inter-event residuals with (a) magnitude, (b) depth to the top of the rupture for Sa at 0.3 sec.

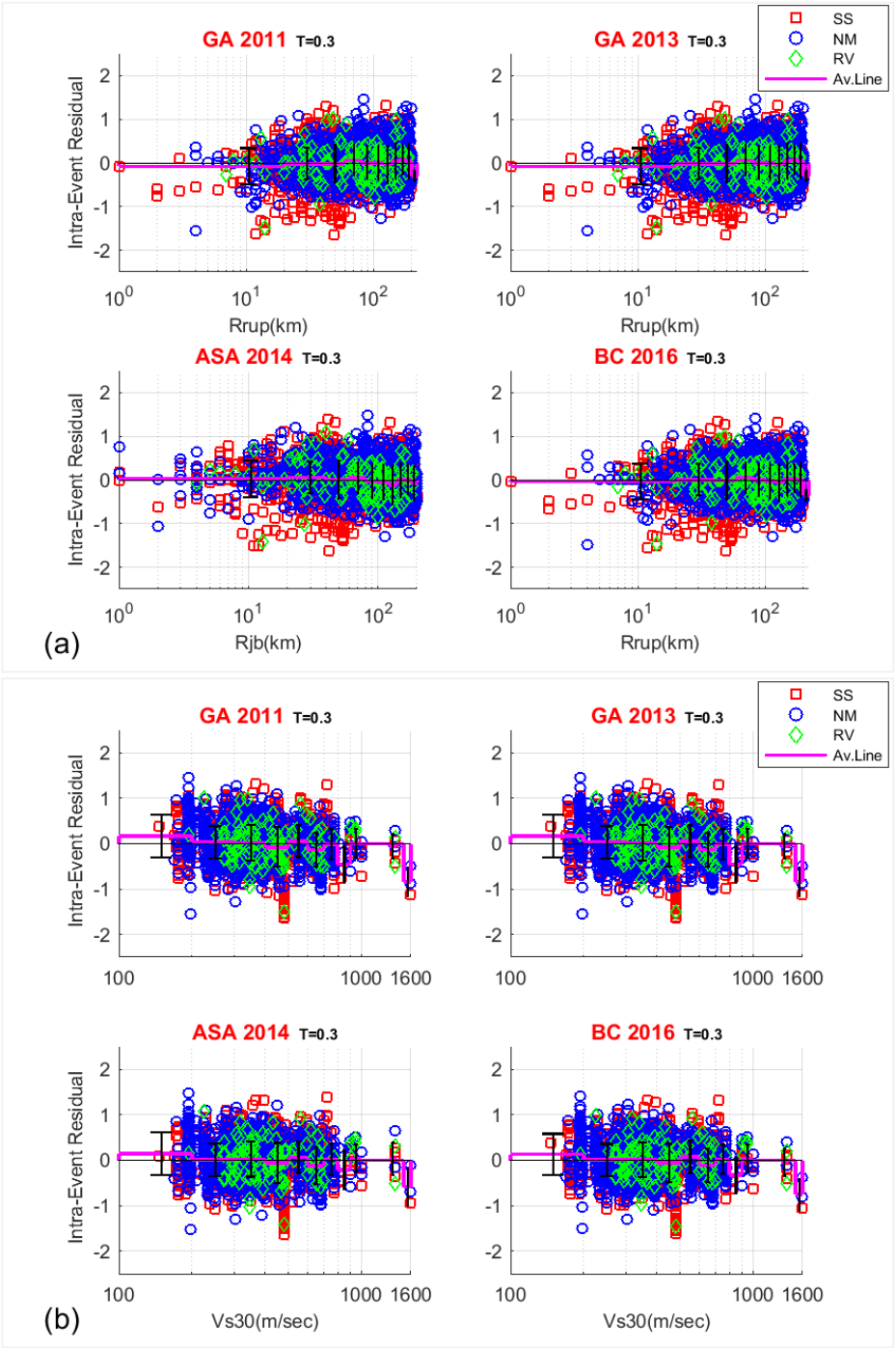

Figure 3.9 Distribution of the intra-event residuals with (a) rupture distance or Joyner-Boore distance depending on the model, (b) V_{S30} for Sa at 0.3 sec.

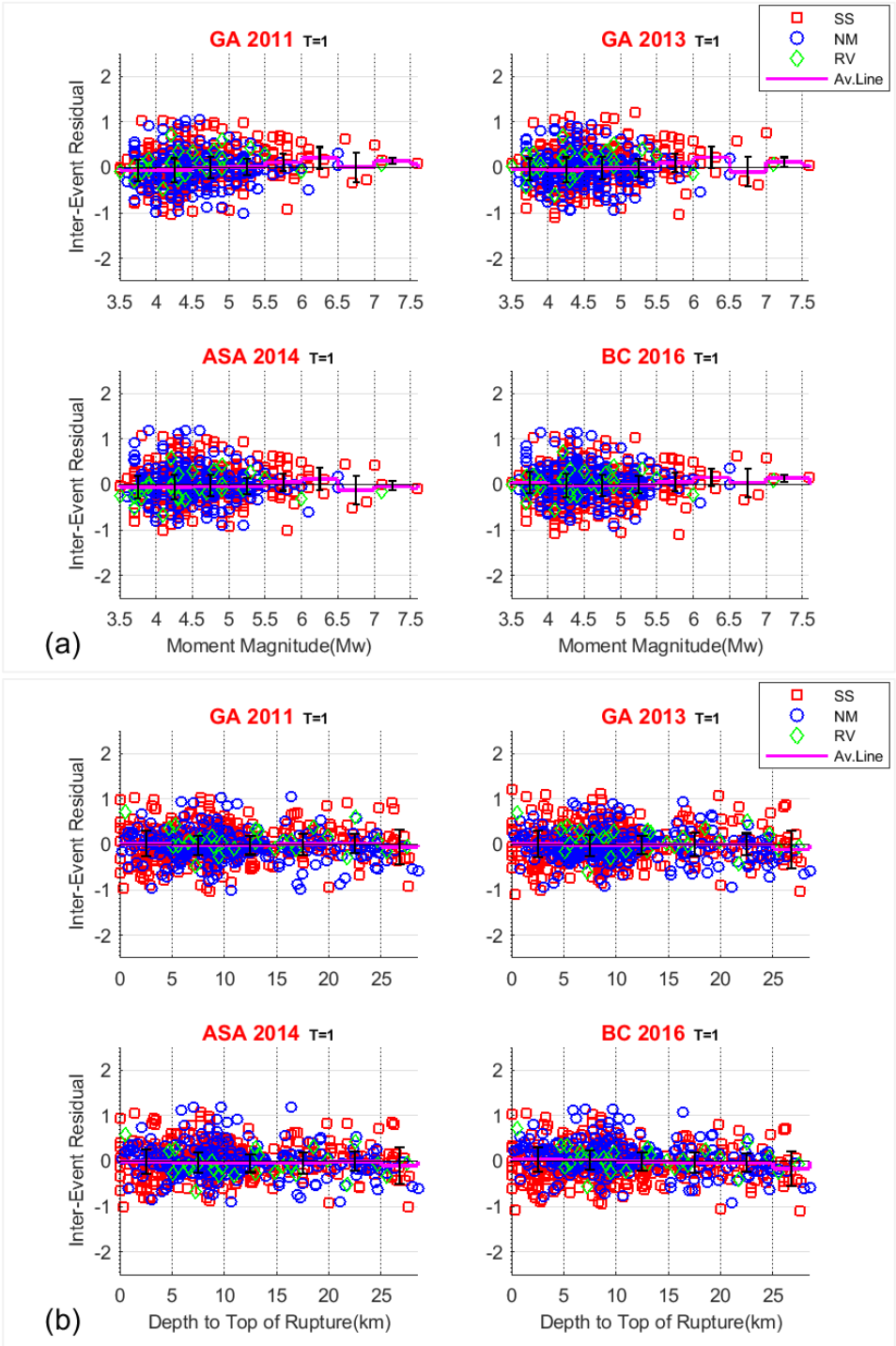

Figure 3.10 Distribution of the inter-event residuals with (a) magnitude, (b) depth to the top of the rupture for Sa at 1 sec.

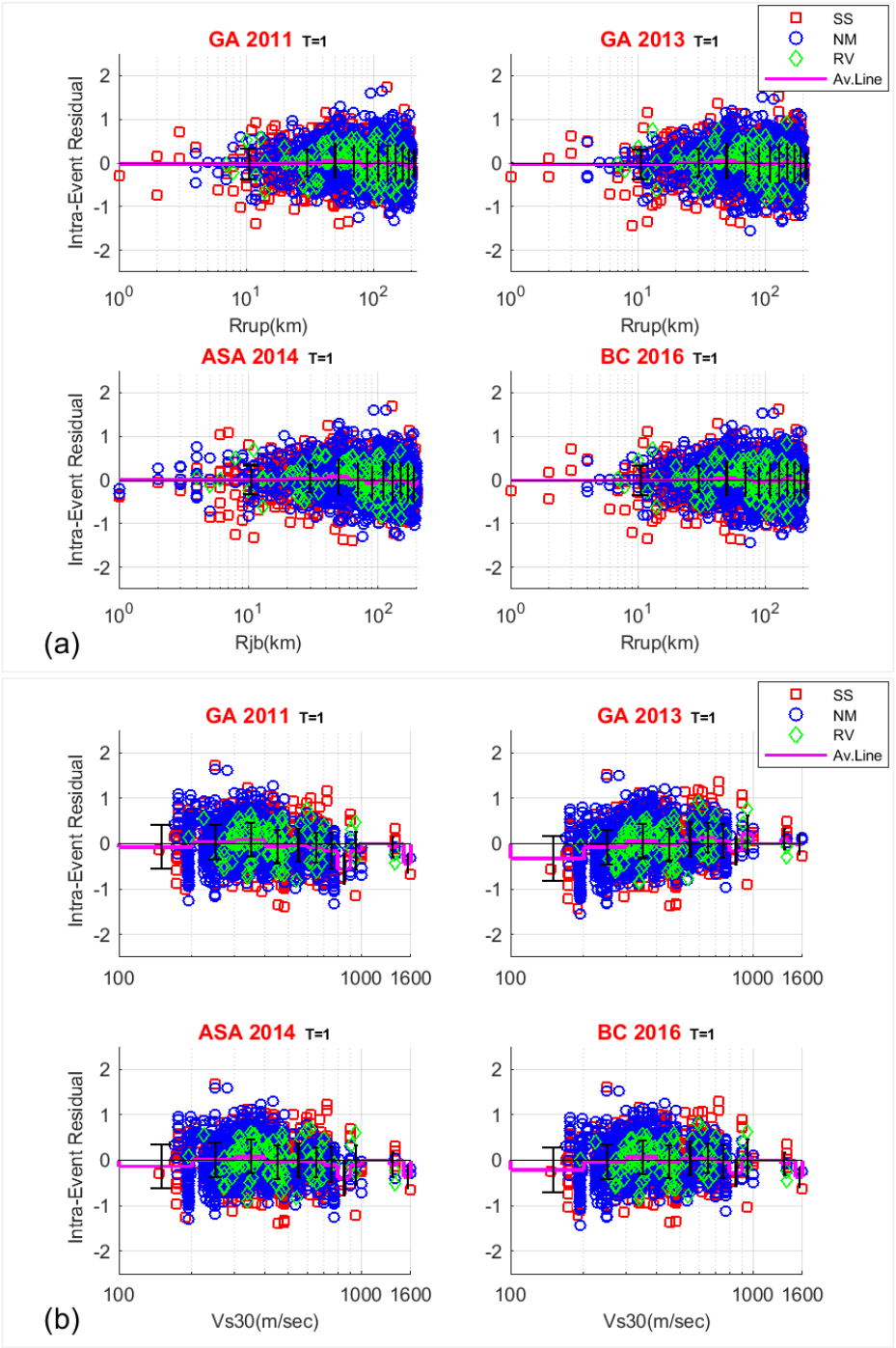

Figure 3.11 Distribution of the intra-event residuals with (a) rupture distance or Joyner-Boore distance depending on the model, (b) V_{S30} for Sa at 1 sec.

3.3 Data Testing and Ranking Approaches

Inaccurate selection and ranking of ground motion models could have a substantial effect on seismic hazard analysis results, especially because ranking scores are generally used for assigning logic-tree weights. For sake of true interpretation of candidate GMM's performance, the residual analysis should be combined by data-driven (ranking) approaches. Among these ranking methods, Likelihood (LH) (Scherbaum et al., 2004), log-likelihood (LLH) (Scherbaum et al., 2009), and Euclidean Distance-Based Ranking (EDR) (Kale and Akkar, 2013) methods have been used in the recent international projects (e.g. the SHARE project).

The LH method was founded on the basis of likelihood concept. Since predictive GMMs are lognormally distributed, the natural logarithm of each prediction made by the candidate GMM and the normalized residuals (calculated by subtracting log of model predictions from the log of the observed data and dividing by the candidate model's standard deviation) follow normal distribution. LH index calculates the exceedance probabilities of residuals at a specific period. Median of the all LH values at specific period, a.k.a. the ranking value or the LH index, is used for comparison purposes. LH index value varies between 0 and 1 and for best case scenario it takes the value of 0.5. The related formula is shown at Equation 3.2: Z_0 is the normalized residual for a particular observation, $u|Z_0|$ is the likelihood of an observation to be equal to or larger than Z_0 and ERF is the error function acronym (Scherbaum et al., 2004). LH method results affected by sample size and personal decision making regarding classes and thresholds and it is unable to quantify the eligibility of standard deviation predicted by candidate GMMs (Scherbaum et al., 2009; Kale et al., 2013).

$$LH(|Z_0|) = 2 \times u(|Z_0|) = ERF\left(\frac{|Z_0|}{\sqrt{2}}, \infty\right) \tag{3.2}$$

LLH method is a modified version of the LH method for overcoming previously mentioned drawbacks. This information-theoretic selection procedure makes use of the log-likelihood method for calculating the Kullback–Leibler distance which represents the amount of information loss between two candidate models (Delavaud

et al., 2009). Therefore, LLH method calculates the average log-likelihood of candidate GMMs together with the occurrence probability of the actual data using GMMs' distribution to produce related LLH index (Scherbaum et al., 2009). Lesser LLH index means that candidate GMM has better prediction ability. Beauval et al. (2012) showed by synthetic data analysis that LLH indexes within a range of 1.5 to 1.6, represent very good model performance, however, indexes greater than 3 to 4 indicate poor model performance. The LLH method might favor candidate GMMs with larger standard deviation which could lead to misjudgment (Kale and Akkar, 2013). The related formula is shown at Equation 3.3 in which N is the number of observed ground motion data, x_i, and $g(x_i)$ is the probability density function of the predictions (assumed as normal distribution).

$$LLH = \frac{1}{N}\sum_{i=1}^{N} \log_2\left(g(x_i)\right) \tag{3.3}$$

EDR method is constructed based on Euclidean distance concept in a way to overcome the drawbacks of previous ranking methods (LH and LLH). For that reason, the standard deviation (aleatory variability) effect is calculated by MDE (modified Euclidean distance) index and model bias effect is determined by ƙ (Kappa) index separately. The optimum value for ƙ is 1 and it means that misfit between observations and predictions of candidate GMM is minimal. The EDR index is computed based on both MDE and Kappa indexes. The separation of aleatory variability and model bias effects from each other is useful for PSHA studies with different objectives (regional or site-specific). Smaller EDR index means that candidate GMM has better performance. Kale et al. (2013) show that the EDR method generally favors candidate GMMs with simpler functional form. The related formula is shown at Equation 3.4, where N is the number of observed ground motion data, ƙ is Kappa parameter and MDE is modified Euclidean distance.

$$EDR^2 = ƙ \times \frac{1}{N} \times \sum_{i=1}^{N} MDE_i^2 \tag{3.4}$$

The LLH method of Scherbaum et al. (2009) and the EDR method of Kale and Akkar (2013) are utilized to test the compatibility of the candidate models with the updated TSMD and to support the findings from the analysis of model residuals. The period dependent variation of the LLH and EDR scores of GA2011, BC2016, ASA2014 and GA2013 models is provided in Figure 3.12. Figure 3.12 shows that the period-dependent variation of the LLH scores of the candidate models are consistent with the mean offset values obtained from the analysis of the residuals. The LLH scores of GA2013, ASA2014 and BC2016 models are quite close to each other and vary between 0.7-1.1, showing that all three models have a significantly good fit with the updated TSMD. The performance of the GA2011 model in terms of LLH score is quite different that the others; similar to the mean offset values, LLH scores also show a bigger difference between the model predictions and observed data. The EDR scores given in Figure 3.12 are not steady, indicating that the predictive performance of the models is not the same for each period range. For example, GA2013 has the lowest scores in period range of 0.01-0.15s whereas it gives the worst performance after 0.4s. The performance of the ASA14 model is generally better than others for periods longer than 0.2s; however, between 0.75s and 1.5s, GA2011 provides slightly better results than ASA2014. In the range of 0.2s-0.5s and 2s-4s period bands, ASA2014 GMM has the first rank. The performance of GA2013 and GA2011 is better than other GMMs at periods shorter than 0.15s and 0.75s-1.5s period band, respectively. In order to select the models with the best prediction performance at different period ranges, the period-dependent EDR scores are divided into three period bands: the short-period band (between 0.01s and the peak of V/H ratio - 0.07s, see Figure 3.1), mid-period band (between the peak and the bottommost point as 0.07s-0.5s) and the long-period band (0.5s-4s). The average EDR scores are computed for each period band and given in Figure 3.13. The EDR scores of GA2013 and ASA2014 are the lowest and the highest at short-period band, respectively. In this period range, BC2016 and GA2011 have similar EDR scores. ASA2014 yields to the lowest EDR scores for mid- and long period bands. Although GA2013 gives the second lower scores for the long-period band, it attains the highest score in the mid-period range.

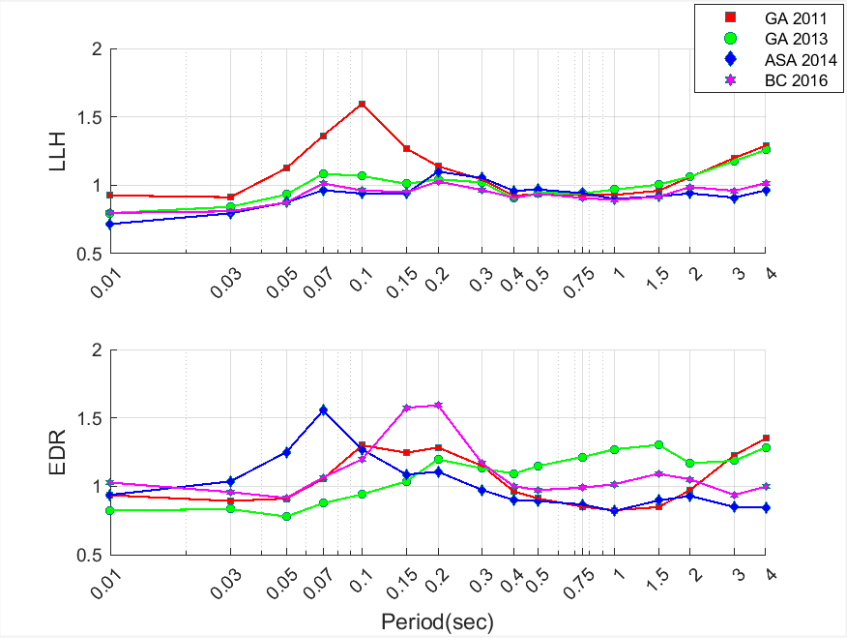

Figure 3.12 Period dependent variation of LLH (a) and EDR (b) scores of the selected models.

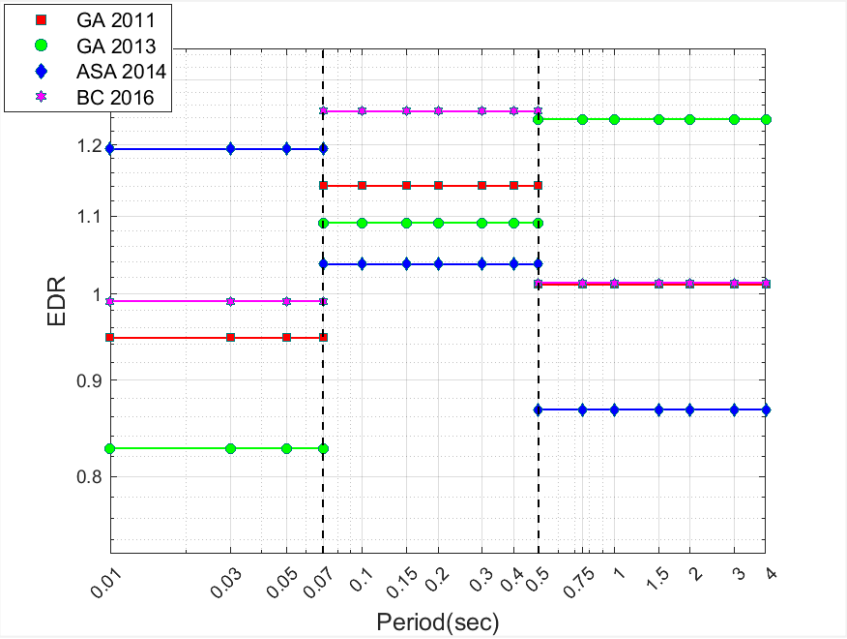

Figure 3.13 Average EDR scores of the candidate models in short-, mid- and long-period band.

CHAPTER 4

EVALUATION OF VERTICAL MODELS

The main objectives of current chapter is to choose the vertical ground motion models (GMMs) that are consistent with the magnitude, distance, depth, and site amplification scaling of the updated Turkish ground motion database. Vertical GMMs going to combine with the previously chosen V/H ratio models in Chapter 5 to provide the ground motion characterization logic tree for vertical ground motion component in Turkey by evaluating the differences in the median predictions of selected vertical and V/H ratio GMMs. Therefore, four vertical GMMs (proposed by Bozorgnia and Campbell, 2016; Stewart et al., 2016; and Gulerce et al., 2017 using the NGA-West 2 database and Çagnan et al., 2017 model based on the RESORCE database) are selected and the model predictions are compared with the actual data in the updated Turkish ground motion dataset using the analysis of the residuals.

4.1 Selection of Candidate Ground Motion Models

Number of up-to-date vertical GMMs for shallow crustal and active tectonic regions is rather limited, especially when compared to the number of horizontal GMMs for the same tectonic regime (Table 1.1). The PEER NGA-West1 project provided improved horizontal GMMs that include recent large magnitude earthquakes, but the models for the vertical component (Bozorgnia and Campbell, 2016, Stewart et al., 2016, and Gülerce et al., 2017) were not developed until the end of NGA-West2 project. The NGA-West2 vertical model developers had used the subsets of the NGA-West2 database and the same approach for developing the models: regressions were performed directly on the vertical spectral accelerations. Çagnan et al. (2017, hereafter CAKS2017), representing the only recent effort in Europe during and after the RESORCE initiation, used the horizontal GMM of Akkar et al. (2014a) and vertical-

to-horizontal ratio GMM of Akkar et al. (2014b) to develop the vertical model. Because these models share the same functional form, the parameters of the vertical GMM were not re-estimated, they were calculated by summing up the parameters of the horizontal and V/H ratio models. Tables 4.1 and 4.2 summarize and compare the main features of these four candidate models; e.g. datasets used for development, applicability ranges, independent parameters, etc. It should be noted that regional anelastic attenuation coefficients provided by Stewart et al. (2016, hereafter SBSA2016) for Turkey and Gülerce et al. (2017, GKAS2017) for Middle East were employed in this study.

Using the data that are independent of the candidate GMMs is the sensible choice to test the predictive performance of the GMM. In this study, the overlap between the updated TSMD and the dataset used by each candidate model is model-specific. Exact amount of Turkish strong motion data that was included in the regression was not specified in the papers of NGA-West 2 vertical models (BC2016, GKAS2017, and SBSA2016). On the other hand, the amount of data from Turkey in the NGA-West 2 database is sparse (only 55 recordings). Consequently, the overlap between the updated TSMD and the dataset used by BC2016, GKAS2017, and SSBA2016 models are negligible. For the case of CAKS2017 model, the overlap between the evaluation dataset and the dataset used in the model is significant.

Two different sets of median predictions of the candidate vertical models are compared in Figures 4.1-4.2. Figure 4.1 shows the median estimates for M5 and M6 earthquakes at 30km for V_{S30}=360 m/s to display how the models compare to each other in the center of the updated Turkish dataset, while Figure 4.2 shows the median estimates for M8-R50km and M7-R100km scenarios for V_{S30}=360 m/s to evaluate how the models extrapolate to large magnitudes and distances. Median estimates of BC2016, SBSA2016, and GKAS2017 models given in Figure 4.1 are quite close to each other with variability lying in the expected range. It is notable that the median estimates of the BC2016 model given in Figure 4.1 are up to 20% smaller than the other two models driven from the same dataset.

On the other hand, median predictions of the CAKS2017 model differ substantially from the others: CAKS2017 model shows approximately a factor-of-2-difference with the other models in the short-to-medium period band (up to 1 sec spectral periods).

Figure 4.2 indicates that the candidate GMMs' median estimates for the scenarios extrapolated to large magnitudes and distances can be divided into two groups in terms of amplitude and spectral shape. For these scenarios, median estimates of SBSA2016 and GKAS2017 models are 40-50% higher than that of BC2016 and CAKS2017 models. The observed difference in the peak of the V/H ratio model of Akkar et al. (2014) in Chapter 3 (Figure 3.2), is also visible in Figure 4.2: peak of the spectral shapes are shifted higher periods in CAKS2017 model.

4.2 Analysis of the Model Residuals and Small Magnitude Correction

As explained in previous Chapter, analysis of residuals is used as the preliminary tool to evaluate the misfit between the model predictions and the actual ground motion data. Median predictions of each candidate model are computed using the predictive parameters in the updated TSMD (Turkish Strong Motion Database, Akkar et al., 2010) and the total residuals, the mean offset ($c_{k)}$ at each period, the inter-event ($\emptyset_{jk}$) and intra-event (τ_{jik}) residuals are calculated using Eq. 3.1 given in Chapter 3. To check the compatibility of the magnitude and depth to the top of the rupture (Z_{tor}) scaling of the candidate models with the updated TSMD, the inter-event residuals are plotted with respect to M_w and Z_{tor} for PGA, T = 0.01s, 0.1s, 0.3s, and 1.0s spectral accelerations in Figures 4.3-4.10, respectively. In each figure, the inter-event residuals for strike-slip, reverse and normal events are given by red, black and green symbols; whereas, the average of the residuals is shown by pink lines. Similarly, the distribution of the intra-event residuals with the record parameters such as rupture /Joyner-Boore distances and V_{S30} is given in Figures 4.3-4.10.

Table 4.1 Functional Forms of the Candidate Vertical Models

Candidate GMM	General Functional Form (for median)
BC 2016	$\ln(V) = f_{Mag} + f_{Rrup} + f_{flt} + f_{HW} + f_{site} + f_{sed} + f_{hyp} + f_{dip} + f_{atn}$
GKAS 2017	$\ln(V) = f_{Mag,Rrup} + f_{flt} + f_{HW} + f_{site} + f_{ztor} + f_{as} + f_{rg}$
SBSA 2016	$\ln(V) = f_{Mag,flt} + f_{Rjb,Mag} + f_{site,Mag,flt,Rjb}$
CAKS 2017	$\ln(V) = f_{Mag,Rjb} + f_{flt} + f_{site}$

Notes: Abbreviations used in the table are: Mag: moment magnitude, Site: site amplification, flt: faulting mechanism, R_{rup}: rupture distance, R_{jb}: Joyner-Boore distance, HW: hanging wall effect*, sed: basin response effects, hyp: hypocentral depth, dip: dip angle, atn: large distance attenuation., z_{ror}: depth-to-top-of-rupture effect, as: aftershock effect, rg: regional effect.

*Hanging-wall effects are neglected in our study.

Table 4.2 Properties and Applicability Ranges of the Vertical Models

General Information				Applicability Range		
Candidate GMM	**Database**	**Number of recordings**	**Number of events**	**M_w range**	**Distance range (km)**	**Spectral period range (sec)**
BC 2016	PEER-NGA W2	15161	321	3-8	0-300	0-10
GKAS 2017	PEER-NGA W2	15597	326	3-8	0-300	0-10
SBSA 2016	PEER-NGA W2	17089	Not provided	3-8	0-300	0.01-10
CAKS 2017	RESORCE	1041	221	4-8	0-200	0.01-4

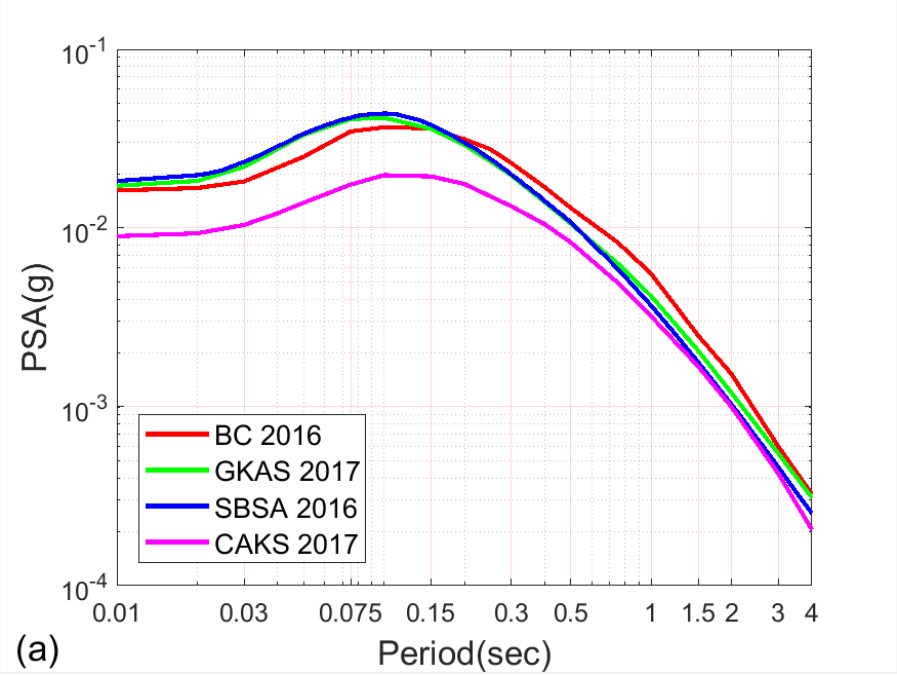

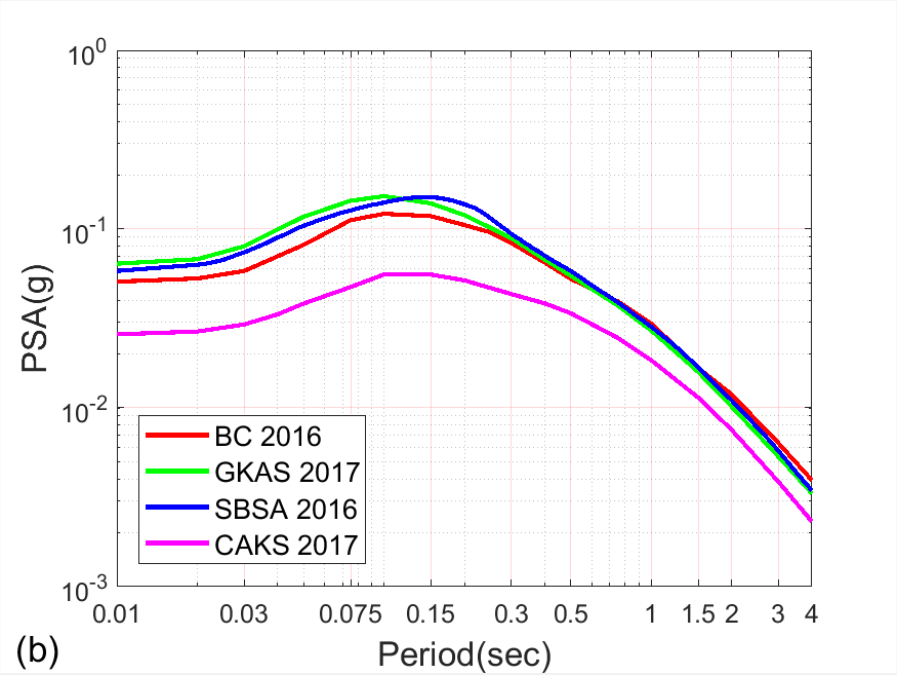

Figure 4.1 Spectral shapes for the median estimates of the candidate GMMs for the center of the data (a) M_w =5, V_{s30} =360, R=30, Z_{tor}=5.36 (b) M_w =6, V_{s30} =360, R=30, Z_{tor}=5.36

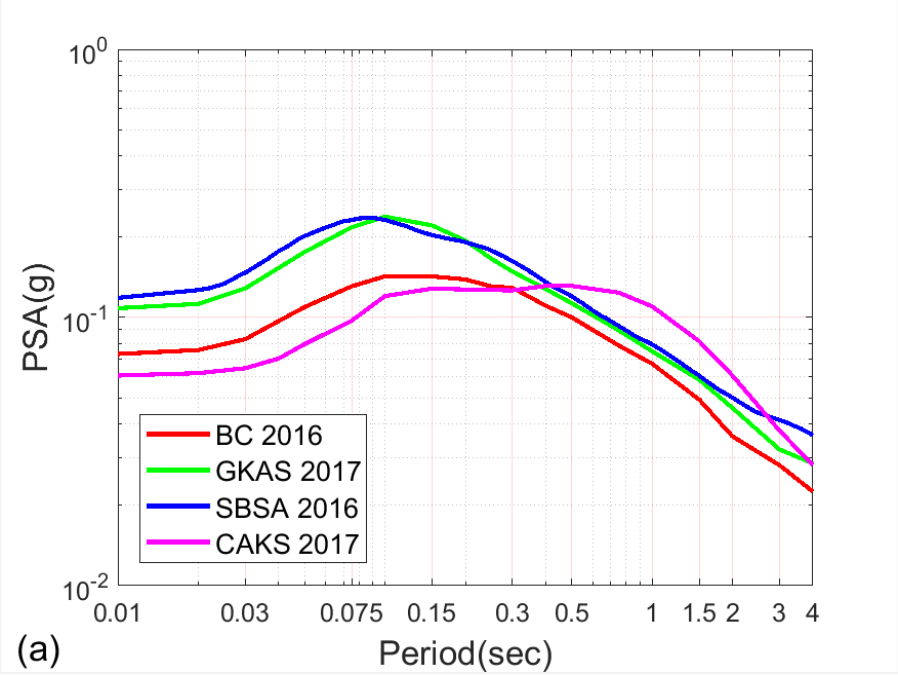

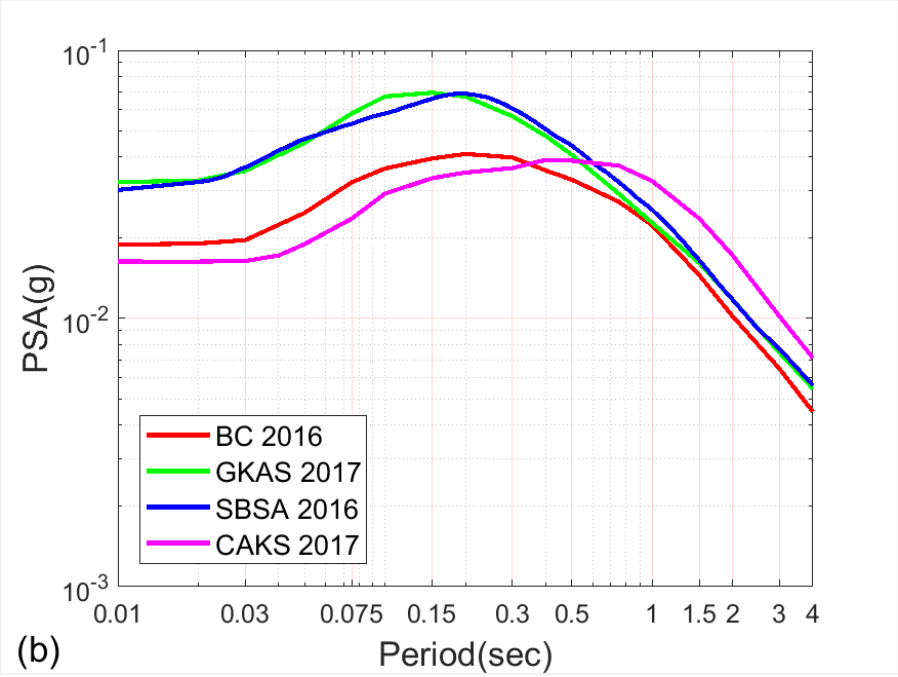

Figure 4.2 Spectral shapes for the median estimates of the candidate GMMs, showing how the models extrapolate to large magnitudes and large distances (a) M_w=8, V_{s30}=360 m/s, R=50km, Z_{tor}=0 (b) M_w =7, V_{s30}=360 m/s, R=100km, Z_{tor}=2.29

Distribution of the intra-event residuals with distance suggests no trends, except for a small negative tendency in the 0-10km range; however, data in this distance range is very limited to indicate any systematic bias. The site amplification scaling of all models are consistent; Figures 4.3-4.10 present no systematic trends in the distribution residuals, except that the intra-event residuals are slightly on the negative side for very soft sites (V_{S30}=100-200m/s) at short spectral periods. Trends observed in the inter-event residuals vs. magnitude plots are different than the findings of Chapter 3: no bias or slightly negative trends were observed in the V/H ratio model predictions, especially for M_w<6.5 events. On the other hand, Figures 4.3-4.10 show that the NGA-West2 vertical GMMs have the tendency to underestimate the small magnitude events (M_w<4.5); however, no systematic bias exist in the model predictions for $M_w \geq 4.5$ earthquakes. Distribution of inter-event residuals of CAKS2017 model with magnitude is different than the NGA-West2 models, showing significant underestimation for $M_w \geq 4.5$ earthquakes in each period. These results are consistent with Figures 4.1 and 4.2: comparison of median curves displayed that the CAKS2017 model predictions are significantly smaller than other candidate models for each scenario. Updated TSDM may be used to apply a small magnitude correction to the NGA-West2 models; however, the number of data points above $M_w \geq 5.5$ is not sufficient for the attempt of modifying the moderate-to-large magnitude scaling of CAKS2017 GMM. Therefore, this GMM is eliminated from the candidate model list. Distribution of the inter-event residuals imply that the Z_{tor} scaling of CAKS2017, GKAS2017, and SBSA2016 models are consistent with the updated TSDM, especially for Z_{tor}<15km. However, inter-event residuals of the BC2016 model are systematically positive in this range, especially for normal earthquakes (blue dots). Similar trends for the V/H ratio model of Bozorgnia and Campbell (2016) were observed at the longer periods in Chapter 3. Gülerce et al. (2017) showed that the style-of-faulting and Z_{tor} parameters interact with each other in the regression analysis; therefore, a modification in the Z_{tor} scaling of BC2016 for Turkey is not proposed. Instead, this model is eliminated from the candidate model list, leaving only two vertical GMMs (GKAS2017 and SBSA2016) in the final logic tree.

The small magnitude scaling of GKAS2017 and SBSA2016 models are modified for Turkey based on the updated TSDM using the function given in Equation 4.1:

$$f(M) = \begin{cases} C_{1-TA} \times (M - 4.5) & for\ (M \leq 4.5) \\ 0 & for\ (M > 4.5) \end{cases} \quad (4.1)$$

Where C_{1_TA} is the adjustment function coefficient determined separately for each GMM by least-square regression. The model fit to the residuals by Eq. 4.1 is presented in Figures 4.11(a) and 4.12(a) by the cyan lines. Note that the selected adjustment function affects the magnitude scaling only for small events; therefore, the well-constrained moderate-to-large magnitude scaling of the GKAS2017 and SBSA2016 models are not modified. To develop a smooth model as a function of the spectral period, C_{1_TA} values are smoothed across periods (Figures 4.11b and 4.12b) and the final set of coefficients are provided in Table 4.3. After the small-magnitude correction, the model residuals are re-calculated using the modified forms of the GKAS2017 and SBSA2016 models. The inter-event residuals after the magnitude adjustment are plotted with respect to M_w in Figures 4.11(c) and 4.12(c) for each model, showing that the inter-event residuals of the adjusted models are evenly distributed along the zero line and the magnitude scaling of the adjusted models are compatible with the magnitude scaling of the updated TSMD.

The mean offset values for GKAS2017 and SBSA2016 models after the small magnitude adjustment are given in Figures 4.13 and 4.14, respectively. In both figures, the trends in the mean offset vs. period distribution are approximately equal: values calculated for the complete dataset lie within 0.5-1 negative unit for the short period range, are smaller than -0.5 in the mid-period band, and increase at longer periods probably due to the reduced number of recordings used for comparison at those periods. On the other hand, the mean offset values decrease significantly when the dataset is limited to Mw≥5 events and almost reduce to zero for Mw≥6 earthquakes, indicating that the biggest contributor of the relative bias between the model predictions and the actual data in the updated TSMD is the small magnitude earthquakes.

Using the mean offset values to modify the constant terms of the GKAS2017 and SBSA2016 models would decrease the moderate-to-large magnitude predictions even through the data does not justify this reduction; therefore, the constant terms of the GMMs are not modified.

Table 4.3 Coefficients for Small-Magnitude Correction Applied to GKAS2017 and SBSA2016 Models for Turkey

$C_{1\text{-}TA}$ coefficient for		
Period	GKAS 2017 GMM	SBSA 2016 GMM
0.01	-0.506	-0.684
0.03	-0.669	-0.852
0.05	-0.772	-0.946
.07	-0.68	-0.88
0.1	-0.601	-0.784
0.15	-0.496	-0.651
0.2	-0.436	-0.56
0.3	-0.374	-0.49
0.4	-0.405	-0.49
0.5	-0.435	-0.49
0.75	-0.502	-0.49
1	-0.557	-0.49
1.5	-0.62	-0.49
2	-0.67	-0.49
3	-0.75	-0.49
4	-0.812	-0.49
5	-0.87	-0.49
6	-0.92	-0.49
7.5	-0.975	-0.49
10	-1.07	-0.49

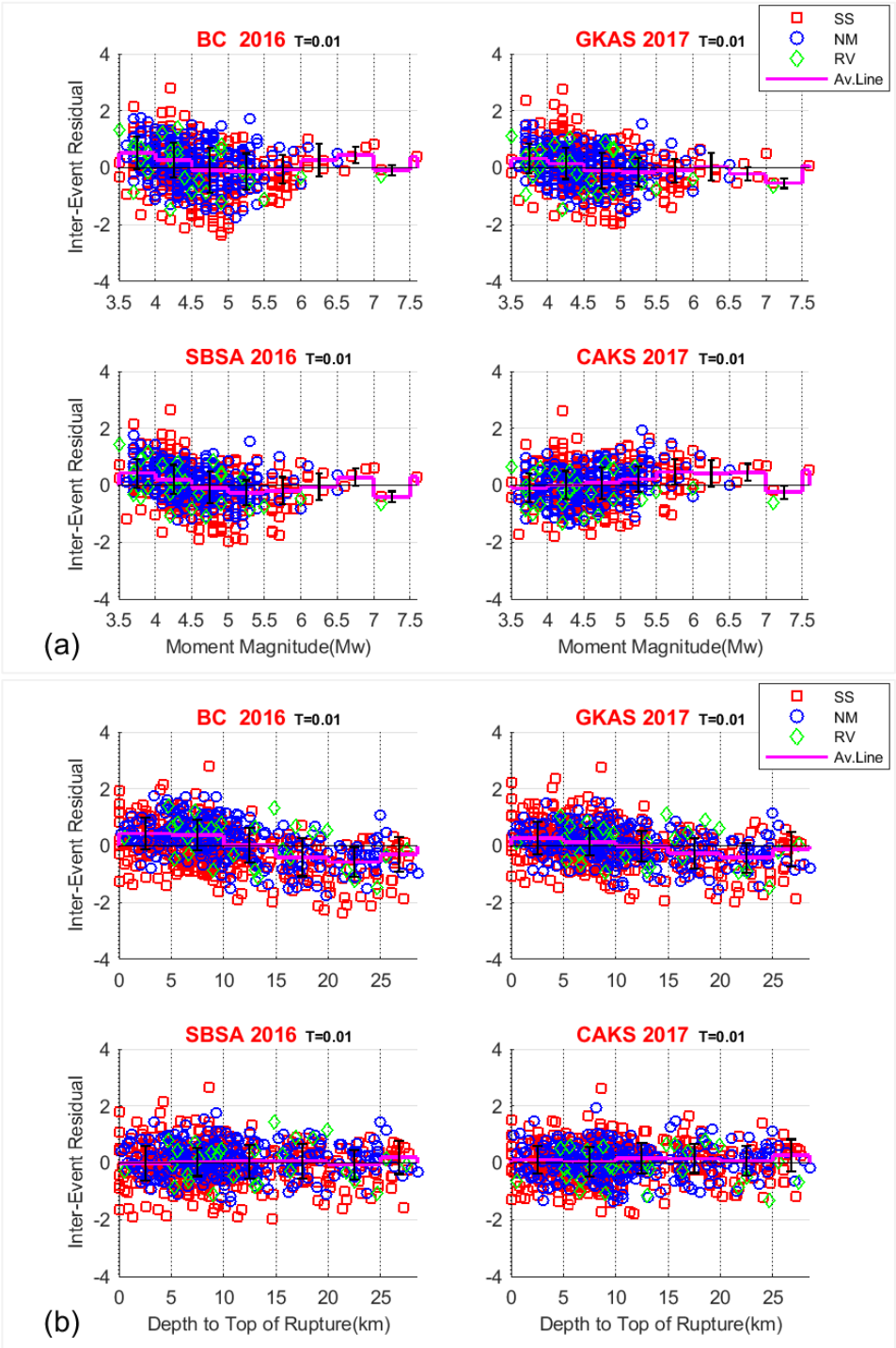

Figure 4.3 Distribution of the inter-event residuals with (a) magnitude, (b) depth to the top of the rupture for Sa at 0.01sec or at PGA depending on the model.

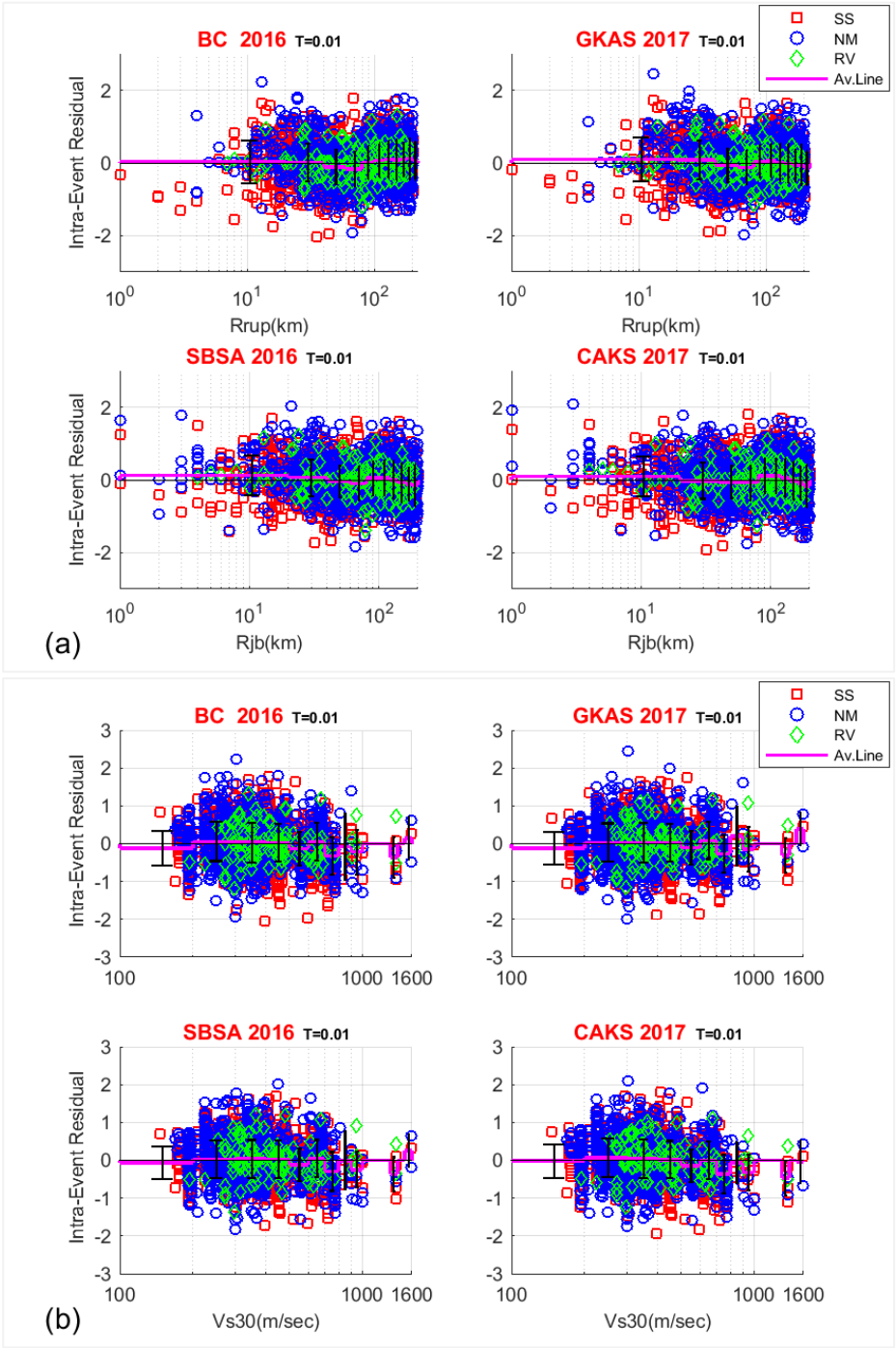

Figure 4.4 Distribution of the intra-event residuals with (a) rupture distance or Joyner-Boore distance depending on the model, (b) V_{S30} for Sa at 0.01sec or at PGA depending on the model.

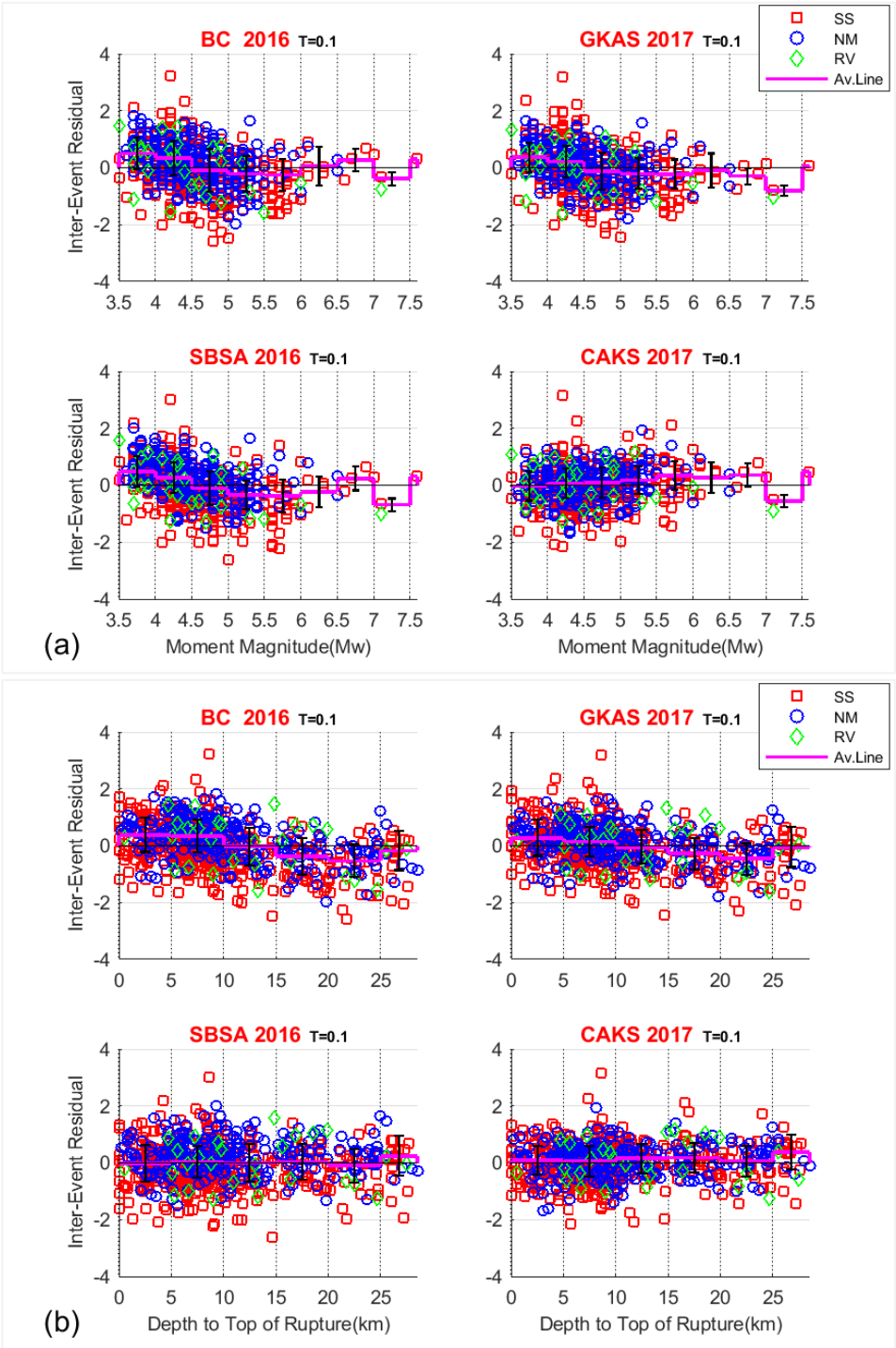

Figure 4.5 Distribution of the inter-event residuals with (a) magnitude, (b) depth to the top of the rupture for Sa at 0.1sec.

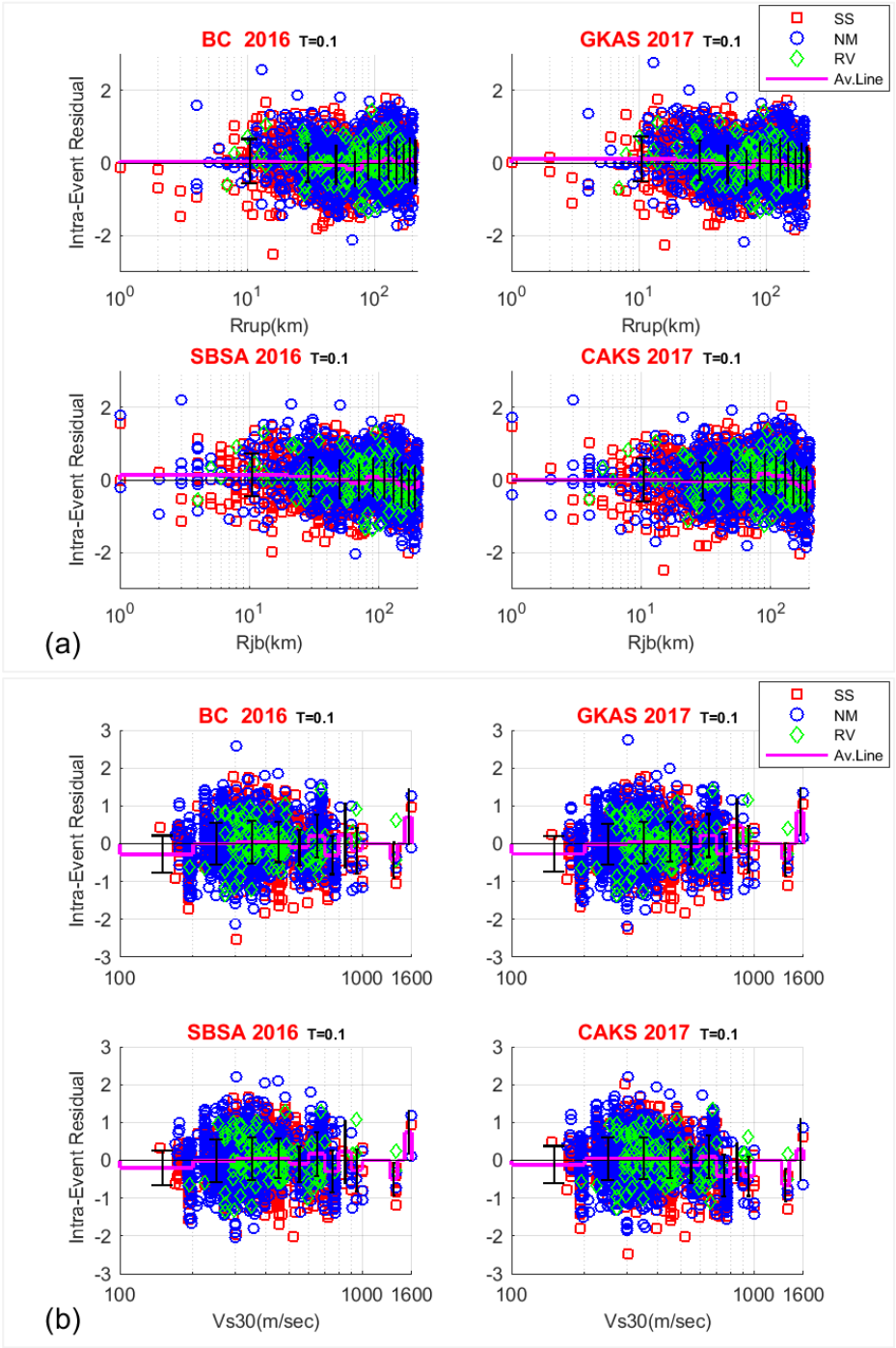

Figure 4.6 Distribution of the intra-event residuals with (a) rupture distance or Joyner-Boore distance depending on the model, (b) V_{S30} for Sa at 0.1sec.

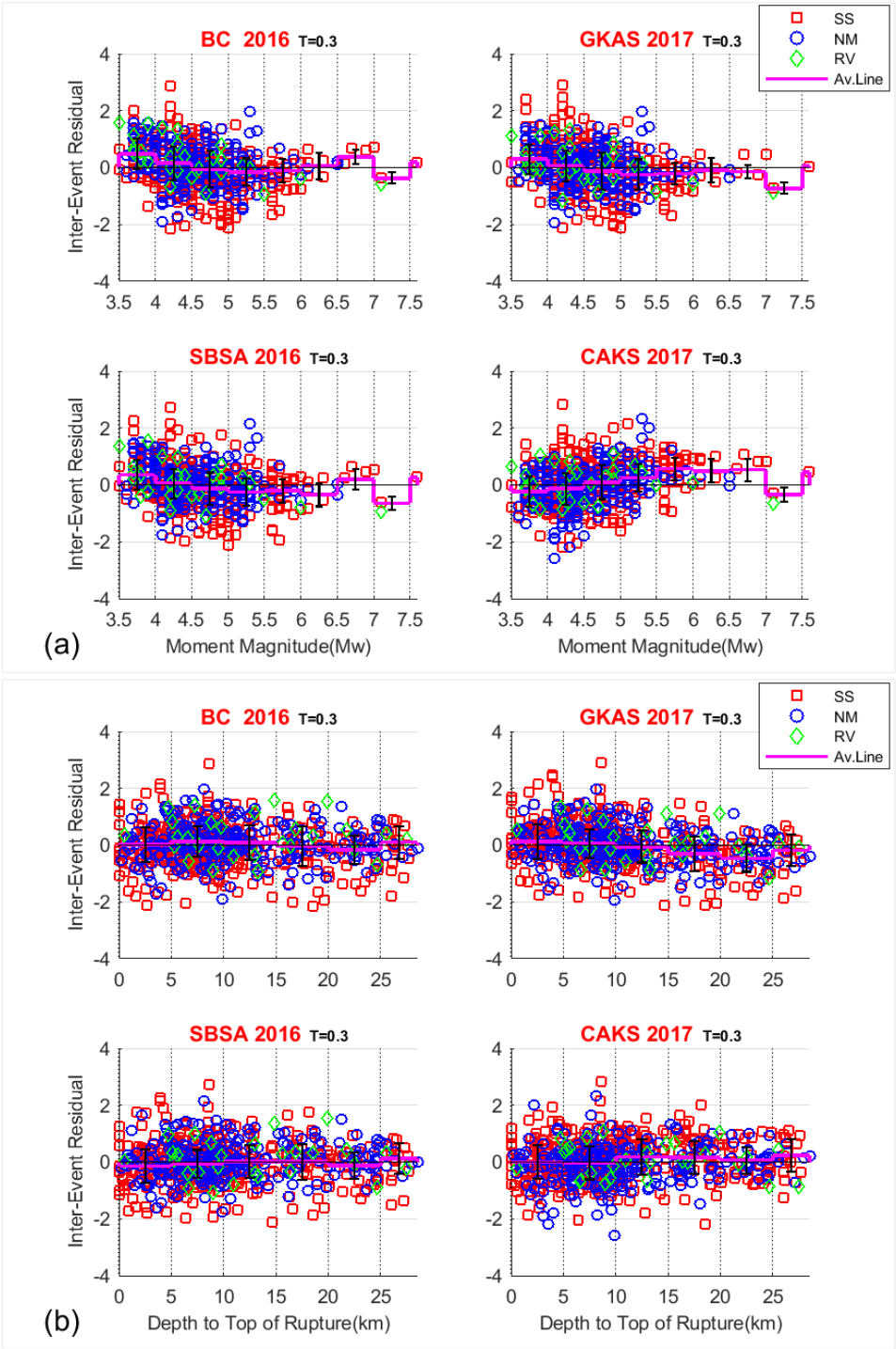

Figure 4.7 Distribution of the inter-event residuals with (a) magnitude, (b) depth to the top of the rupture for Sa at 0.3sec.

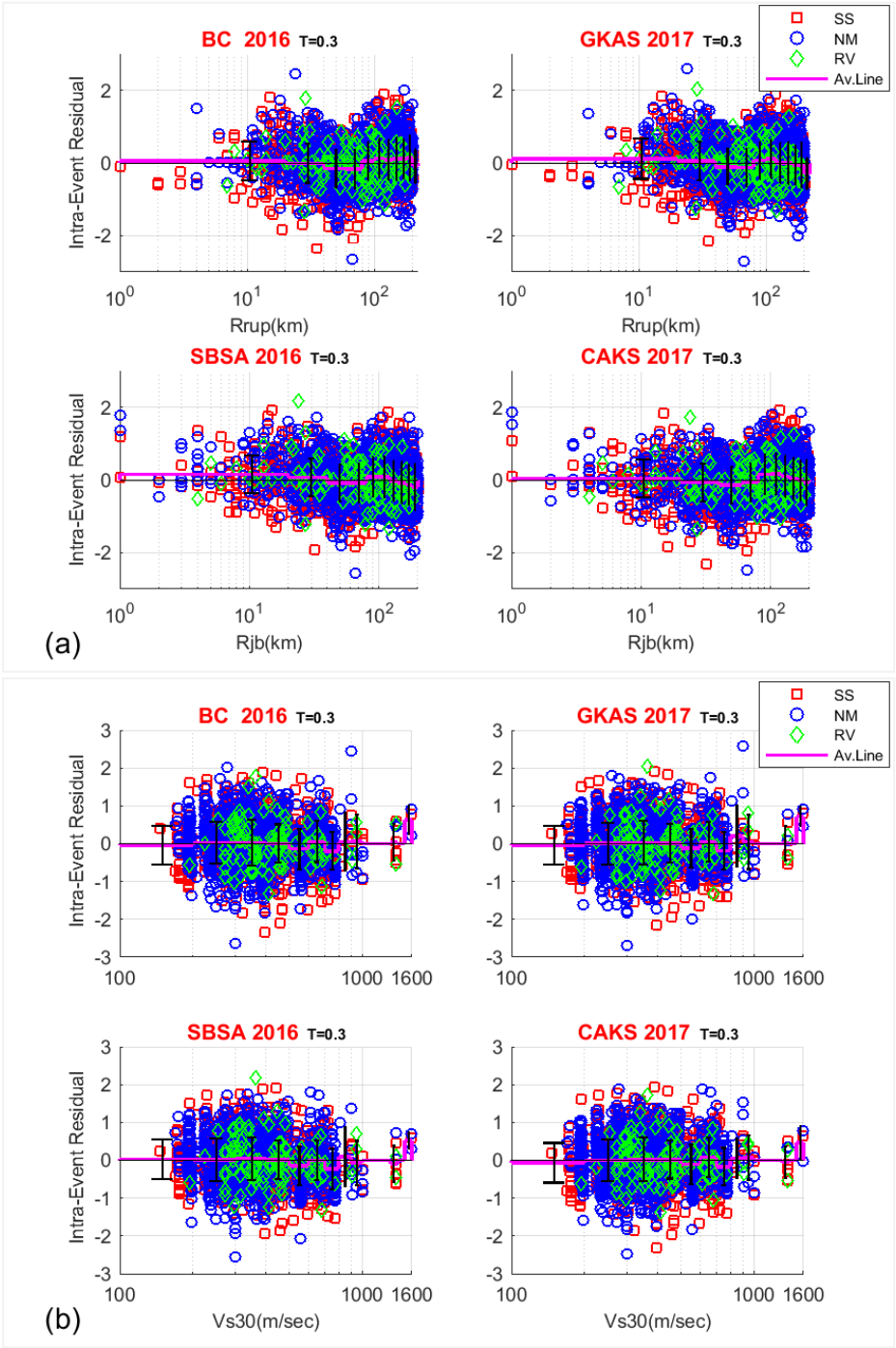

Figure 4.8 Distribution of the intra-event residuals with (a) rupture distance or Joyner-Boore distance depending on the model, (b) V_{S30} for Sa at 0.3sec.

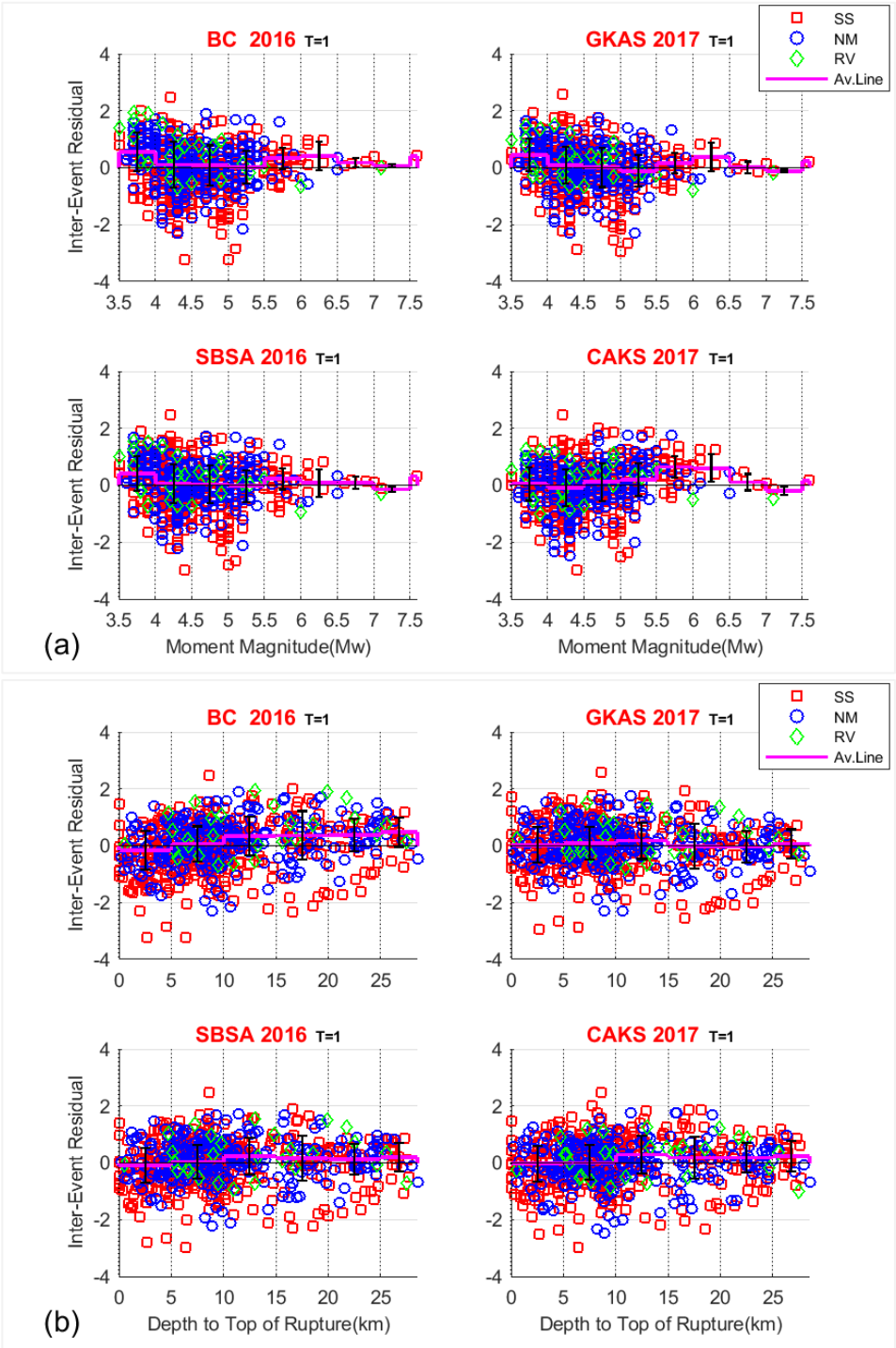

Figure 4.9 Distribution of the inter-event residuals with (a) magnitude, (b) depth to the top of the rupture for Sa at 1sec.

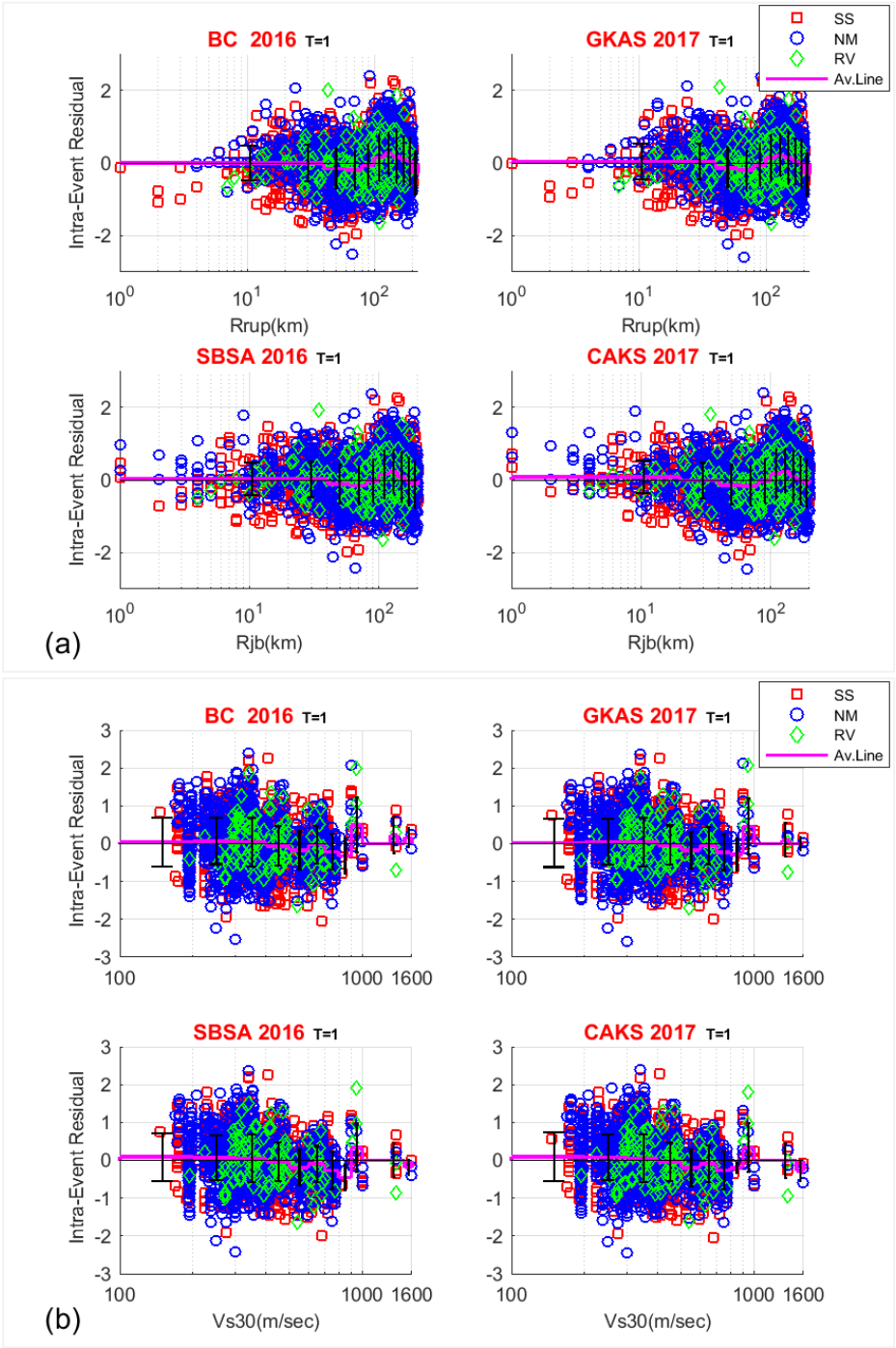

Figure 4.10 Distribution of the intra-event residuals with (a) rupture distance or Joyner-Boore distance depending on the model, (b) V_{S30} for Sa at 1sec.

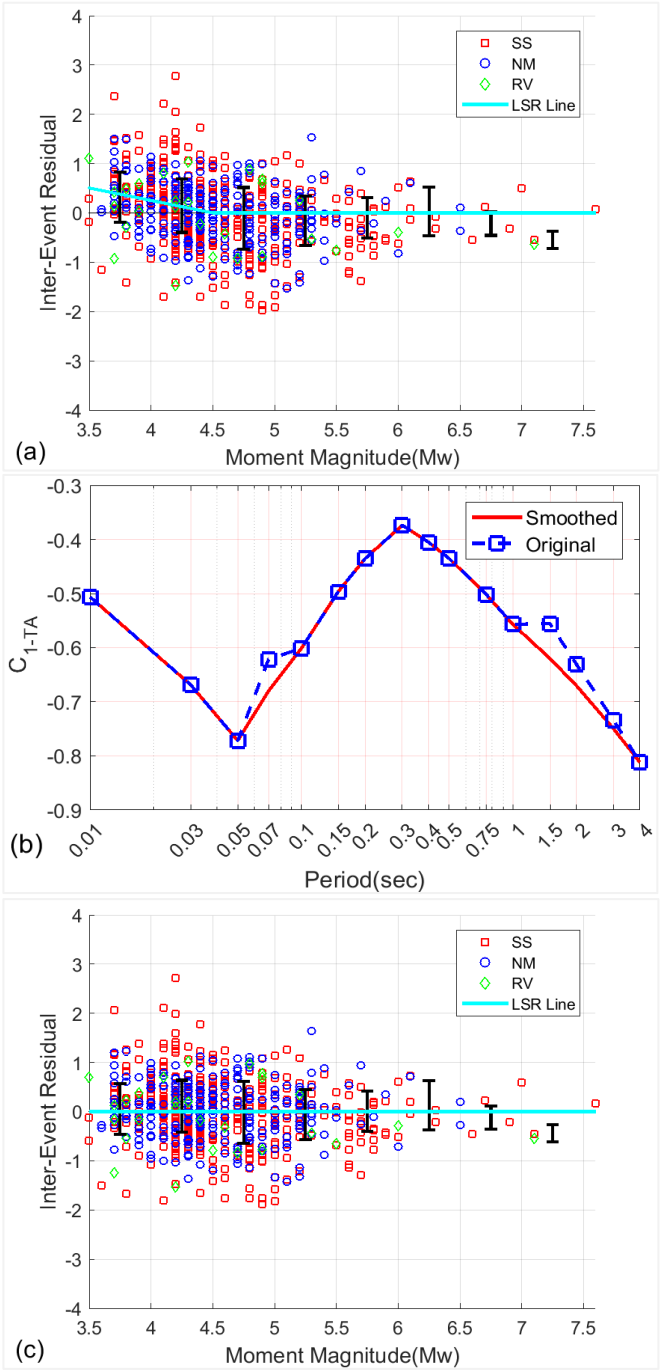

Figure 4.11 GKAS2017 model's (a) Distribution of the inter-event residuals of PGA with magnitude for the unmodified. The adjustment function fitted to the inter-event residuals is shown by green lines, (b) Estimated and smoothed coefficients from regression, (c) Distribution of the inter-event residuals with magnitude after the small magnitude adjustment for PGA.

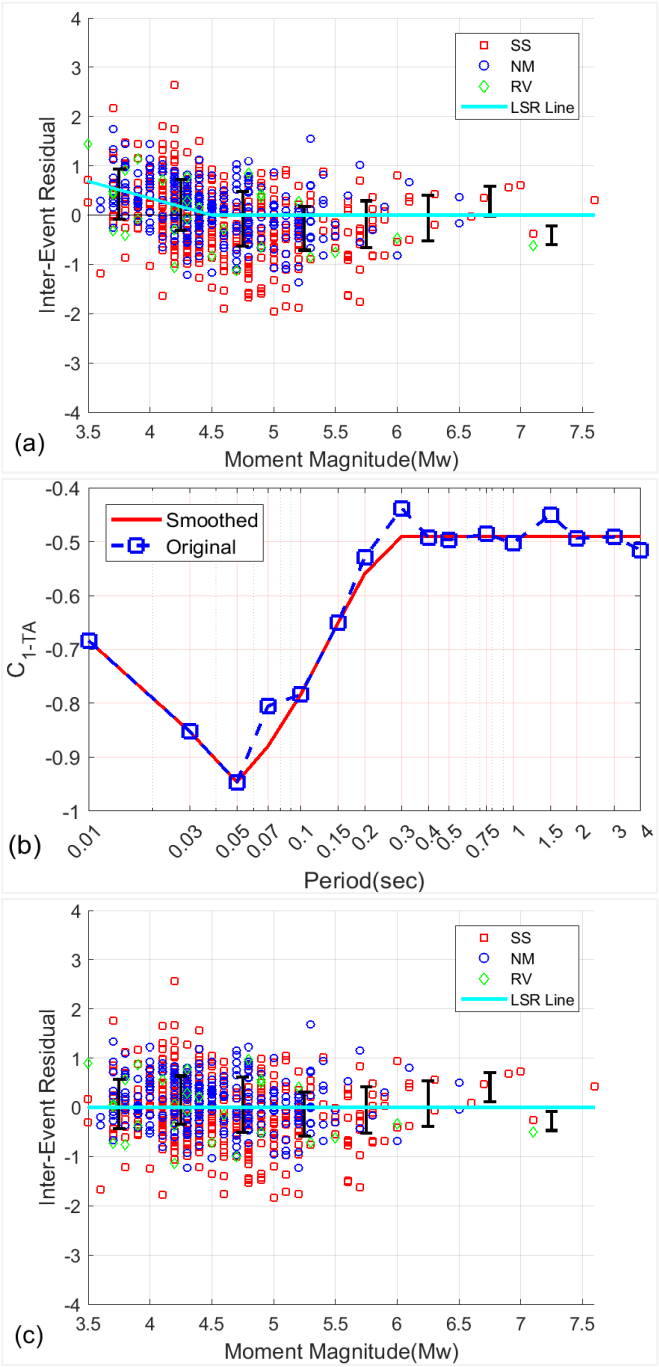

Figure 4.12 SBSA2016 model's (a) Distribution of the inter-event residuals of PGA with magnitude for the unmodified. The adjustment function fitted to the inter-event residuals is shown by green lines, (b) Estimated and smoothed coefficients from regression, (c) Distribution of the inter-event residuals with magnitude after the small magnitude adjustment for PGA.

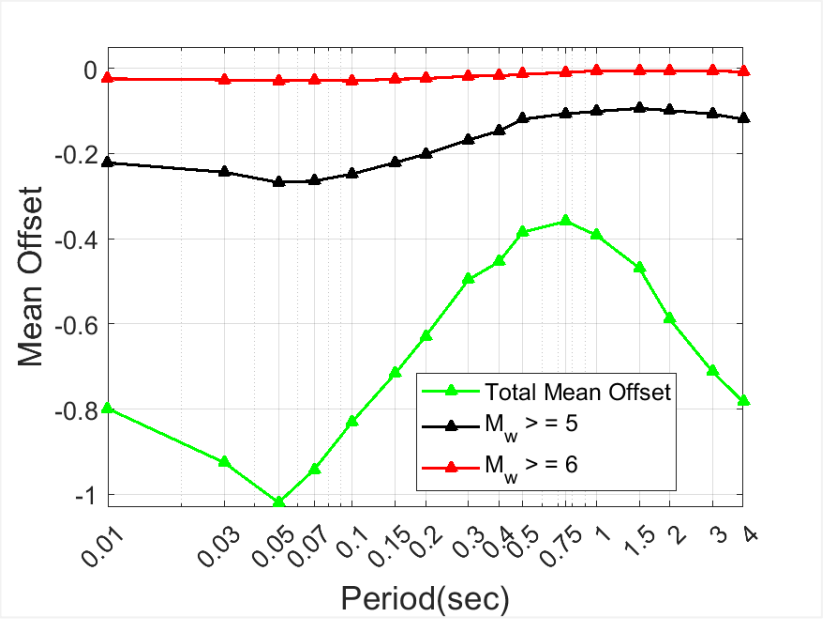

Figure 4.13 The mean offset values calculated for the entire dataset (green line), for $M_w \geq 5$ events (black line), and for $M_w \geq 6$ earthquakes (red line) after the small magnitude adjustment applied to GKAS2017 model.

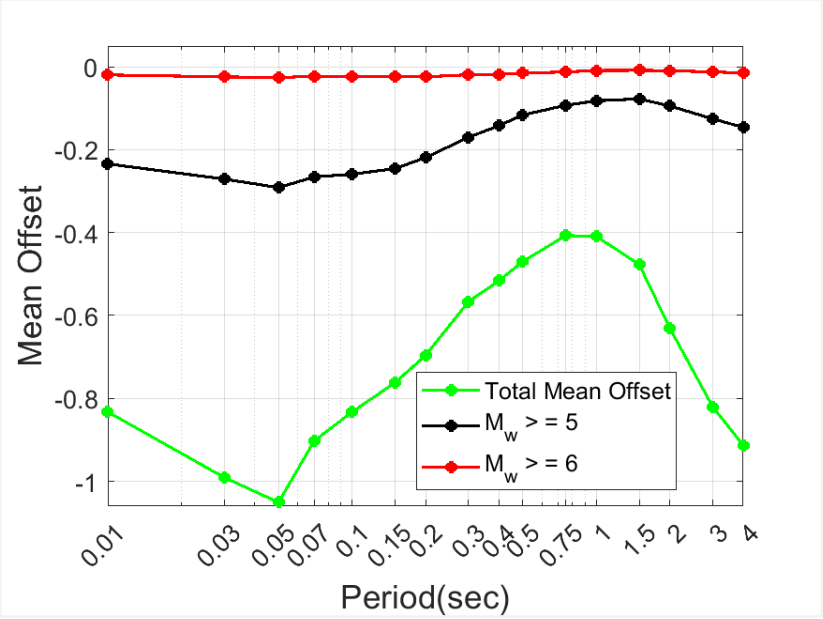

Figure 4.14 The mean offset values calculated for the entire dataset (green line), for $M_w \geq 5$ events (black line), and for $M_w \geq 6$ earthquakes (red line) after the small magnitude adjustment applied to SBSA2016 model.

CHAPTER 5

CONCLUSION

The overall objective of this study is to propose a ground motion characterization framework to be used in the PSHA studies in Turkey for the vertical ground motion component. There are four main components of the proposed framework: (i) the updated strong motion dataset for Turkey (detailed in Chapter 2), (ii) selection of the V/H ratio models that are consistent with the Turkish strong motion dataset (given in Chapter 3), (iii) choosing the vertical GMMs that are compatible with the Turkish strong motion dataset and selected V/H ratio model predictions (summarized in Chapter 4), and (iv) providing a complete logic tree with weights at different period bands to be implemented in the PSHA studies. Updating the original TSMD was a substantial effort and deserved a standalone section because significant amount of data in small-to-moderate magnitude range has been obtained after 2008. Within the contents of this study, 1457 recordings from 184 events occurred after 2008 were selected, analyzed, and added to the original TSMD. This update significantly increased the number of data in the original version, especially in the moderate magnitude range; therefore, the updated TSMD is suitable for testing the applicability of V/H ratio and vertical GMMs in Turkey.

Four candidate V/H ratio models were selected (GA2011, GA2013, ASA2014 and BC2016) and their compatibility with the updated TSMD in terms of magnitude, distance, and site effects scaling were evaluated using the analysis of residuals and data-driven approaches. Analysis of the residuals showed no systematic bias in the median predictions of all candidate models (Figures 3.4-3.11), except for the consistently negative residuals in the large magnitude range ($M_w \geq 6.5$) at the short periods (up to T=0.3s). This underestimation might be related to several factors (e.g. amount of non-linearity in the V/H ratio model, differences in the high frequency

attenuation parameters); however, the shape of the V/H ratio combines these factors as an overall indicator of the difference. Trellis plots (Figures 3.1-3.2) showed that the period of the peak of the candidate V/H ratio models is different than each other, probably due to the regional differences in the high frequency attenuation factor (a.k.a. kappa) in vertical and horizontal ground motions. This conclusion should be tested using the results of the ongoing studies on kappa at different shallow crustal and active tectonic regions. Until more information is available on vertical and horizontal kappa values, the selection of the V/H ratio models had to depend on the data testing methods provided in this thesis. Both the mean offset plot (Figure 3.3) and the LLH scores (Figure 3.12-3.13) showed that the average misfit of the GA2011 model is larger than the other candidate models; therefore, this model is eliminated from the final logic tree. Other candidate models have almost equal mean offset values and LLH scores, indicating that they are suitable for ground motion characterization studies in Turkey. On the other hand, distribution of the EDR (Figure 3.12-3.13) scores suggests different prediction performances for different period bands. To account for this difference, BC2016 and GA2013 models are selected for the short-period band (up to 0.07s), GA2013 and ASA2014 models are selected for the mid-period band (0.07s-0.5s) and finally, ASA2014 and BC2016 models are selected for the long-period band (T>0.5s).

Four candidate Vertical models (BC2016, GKAS2017, SBSA2016 and CAKS2017) were selected and their compatibility with the updated TSMD in terms of magnitude, distance, and site effects scaling were evaluated using the analysis of residuals. Analysis of the residuals illuminated trends in the distribution of inter-event residuals of CAKS2017 and BC2016 models with magnitude (M_w) and depth to top of rupture (Z_{tor}) respectively. Distribution of inter-event residuals of CAKS2017 model with magnitude revealed anomaly with other NGA-West2 models, showing significant underestimation for $M_w \geq 4.5$ earthquakes in each period. These results are consistent with Figures 4.1 and 4.2 which displayed that the CAKS2017 model predictions are significantly smaller than other candidate models for each scenario. Inter-event residuals of the BC2016 model revealed systematically positive trends for Z_{tor}<15km,

especially for normal earthquakes (Figures 4.3-4.10). Similar trends for the V/H ratio model of Bozorgnia and Campbell (2016) observed at the longer periods in Chapter 3 (Figures 3.4-3.11). Therefore, CAKS2017 and BC2016 models eliminated from the candidate model list, leaving only two vertical GMMs (GKAS2017 and SBSA2016) in the final logic tree. The small magnitude scaling of GKAS2017 and SBSA2016 models modified for Turkey based on the updated TSDM.

Based on the findings of this study, two sets of GMMs are selected for the final logic tree: the SM- modified versions of the vertical GKAS2017 and SBSA2016 models will be used for all periods; however, two different V/H ratio GMMs are chosen for short, medium and long period bands. Bozorgnia and Campbell (2016, BC2016) and Gülerce and Akyüz (2013, GA2013) models are selected for Zone 1 (up to 0.07s), GA2013 and Akkar et al. (2014, ASA2014) models are selected for Zone 2 (0.07s-0.5s) and ASA2014 and BC2016 models are selected for Zone 3 (T>0.5s). When both vertical and V/H ratio GMMs are utilized to develop the vertical spectrum for any earthquake scenario, significant differences in the median curves may exist, depending on the horizontal GMMs used to multiply the median V/H ratio curves. Two sets of trellis plots for M_w=6 scenario at 30km away for V_{S30}=360 m/s are presented in Figure 5.1 for demonstration: in Figure 5.1(a), the SM- modified GKAS 2017 and SBSA2016 models are combined with the V/H ratio models multiplied with TR-adjusted horizontal NGA-W1 models (Gülerce et al., 2016), while in Figure 5.1(b), V/H ratio models are multiplied with the NGA-West 2 horizontal models (equally-weighted). Both figures showed that the median predictions of the SM-modified vertical GMMs are higher than the median curves based on the V/H ratio models; however, the difference is less pronounced when the V/H ratio models are multiplied with the NGA-West 2 horizontal GMMs.

5.1 Logic Tree for Vertical Ground Motion Characterization

Akkar et al. (2017) used the trellis plots of candidate horizontal GMMs for Turkey to determine the center, body and the range of median predictions for several scenarios

at rock sites (V_{S30}=760 m/s). For this purpose, the ratio of the median prediction of any candidate GMM divided by the "median" of the median predictions of each candidate model was used to calculate the "distance to the median" for that particular candidate. Eventually, the distance to the median values were combined for all scenarios and the combined values were utilized to select the GMMs that represent the center, upper bound and the lower bound for each period. A similar approach is used in this study to determine the logic tree weights provided in Table 5.1. Trellis plots for 250 scenarios (combinations of M4-M8 events for D10-D100km and V_{S30}=180-800m/s) are used to calculate the "median" of the median predictions (solid red line) as shown in Figures 5.1(a) and 5.1(b) and the "distance to the median" is calculated for each GMM for that scenario. The distance to median values for each particular GMM for all scenarios are averaged to determine the final logic tree weights. The final logic tree weights are utilized to calculate the weighted average of the median predictions for each scenario as shown by the dashed black lines in Figure 5.1 to check the consistency with the "median" of the median predictions. Weighted-average and the median of the median predictions curves are mostly in good agreement as shown in Figures 5.1(a) and 5.1(b); however, small inconsistencies are observed in some scenarios (particularly for V_{S30}=180 m/s) due to the differences in the peak of the spectrum among the selected models.

Figures 5.2 to 5.4 compare the distance to the median values calculated for each GMM for each scenario with the final logic tree weights to see if any persistent trends in the distribution with respect to magnitude, distance or site condition exist. Figure 5.2 shows that the distance to median values for each GMM varies with magnitude because the magnitude scaling of each model is different. BC2016 V/H model predictions for M8 events are generally different than the median in Zone 1 and this fact should be considered in PSHA applications where the dominating scenario has large magnitudes. Figure 5.3 presents the distribution of distance to medians with source to site distance. No systematic trends are observed in these plots, except that the predictions of SM-modified SBSA2016 model seems to be closer to the median

for scenarios up to 30km in Zone 2; therefore, the logic tree weight of this model may be increased for the hazard calculations dominated by near-field seismic sources. Distribution of the distance to median values with V_{S30} (Figure 5.4) shows no systematic trends as well, other than the slightly smaller numbers for SM-modified GKAS2017 model than the average weight factor in Zone 2. In hazard calculations for sites with $V_{S30} \leq 360$ m/s, the weight factor for this model can be decreased and the weight factor for SM-modified SBSA2016 model might be increased to capture the median.

Table 5.1 Logic Tree Weights Proposed in This Study for PSHA Applications in Turkey Whether the V/H Models Multiplied By NGA West2 or TR-Adjusted NGA W1

		Weight Factors to be used if the V/H models multiplied by	
Zone #	GMM	**NGA West2**	**TR-Adjusted NGA W1**
Zone 1	GA2013 (V/H)	0.32	0.31
	BC2016 (V/H)	0.18	0.22
	SMM* GKAS2017 (V)	0.35	0.29
	SMM* SBSA2016 (V)	0.15	0.18
Zone 2	GA2013 (V/H)	0.25	0.27
	ASA2014 (V/H)	0.26	0.25
	SMM* GKAS2017 (V)	0.29	0.29
	SMM* SBSA2016 (V)	0.20	0.19
Zone 3	ASA2014 (V/H)	0.19	0.29
	BC2016 (V/H)	0.30	0.22
	SMM* GKAS2017 (V)	0.23	0.27
	SMM* SBSA2016 (V)	0.28	0.22
*SMM: Small Magnitude Modified			

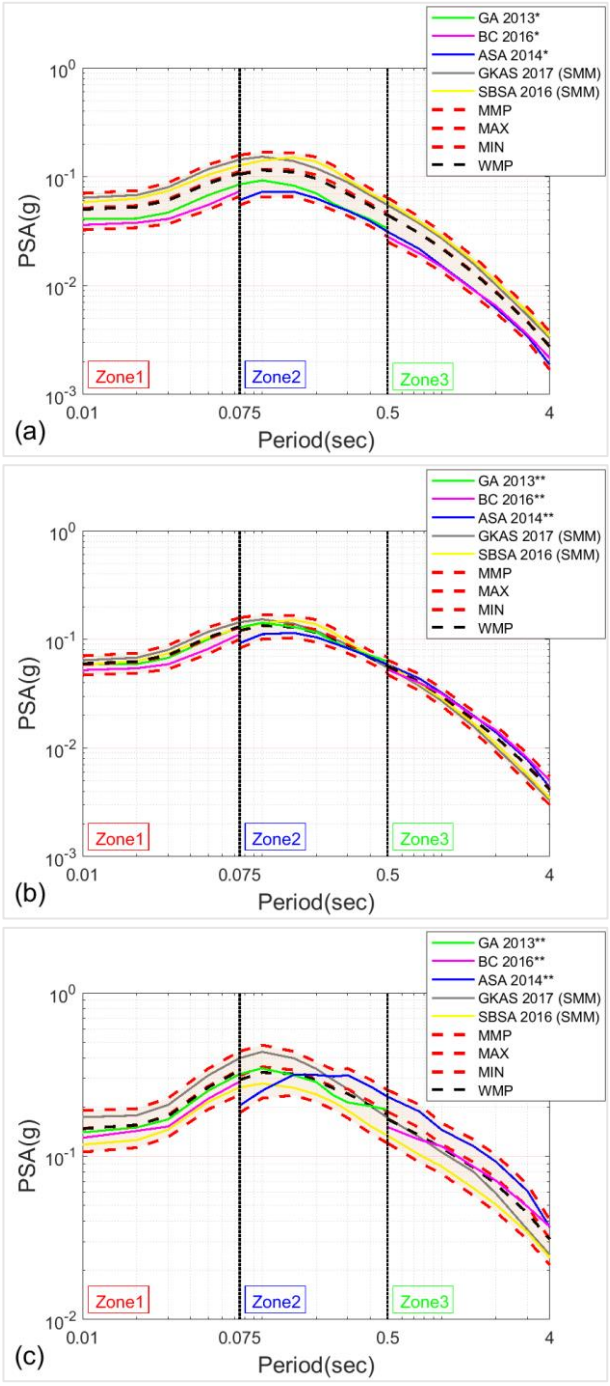

Figure 5.1 Trellis plots of median predictions of selected GMMs for a) Mw=6, V_{S30}=360 m/s, R=30km, (b) M_w=6, V_{S30}=360, R=30km, (c) M_w=7, V_{S30}=180, R=30km. The V/H models, In (b) and (c) multiplied by the NGA-West2 horizontal models specified by (**) and in (a) multiplied by the Tr-adjusted NGA-W1 GMMs specified by (*).

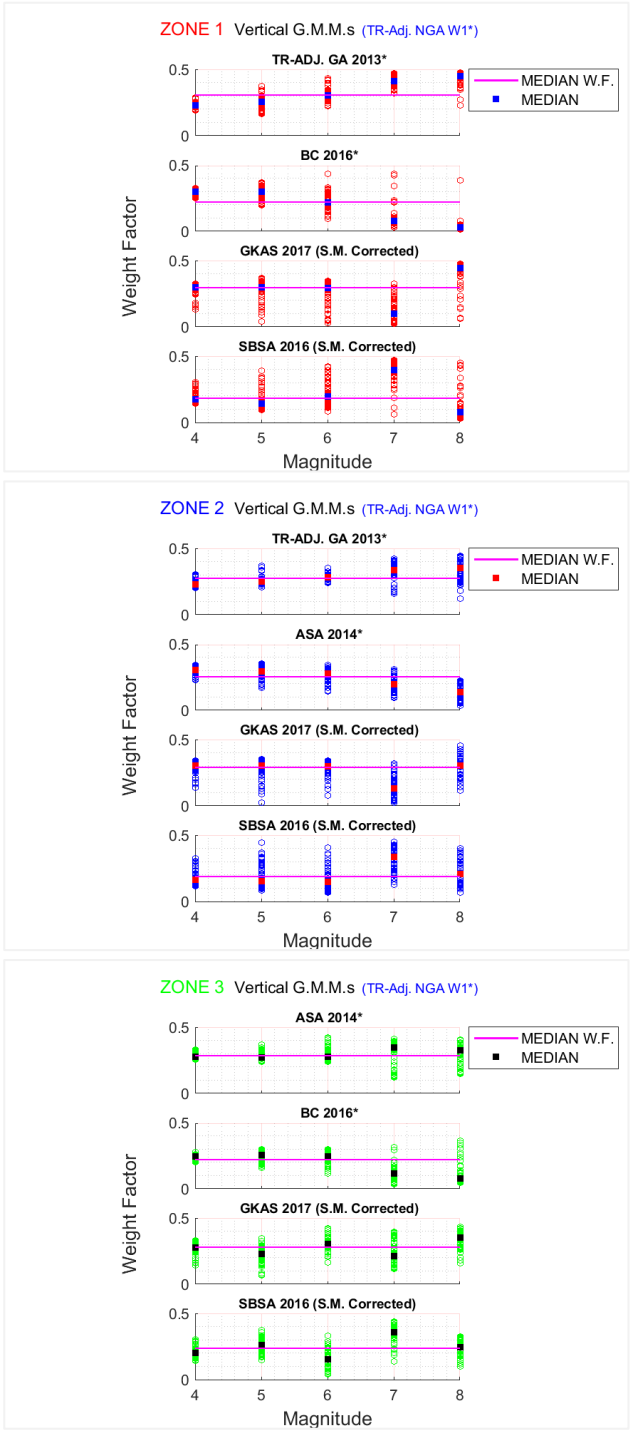

Figure 5.2 Comparison of distance to the median values calculated for each GMM for each scenario with the final logic tree weights with respect to magnitude. GMMs specified by (*) scaled by the Tr-adjusted NGA-W1 horizontal models.

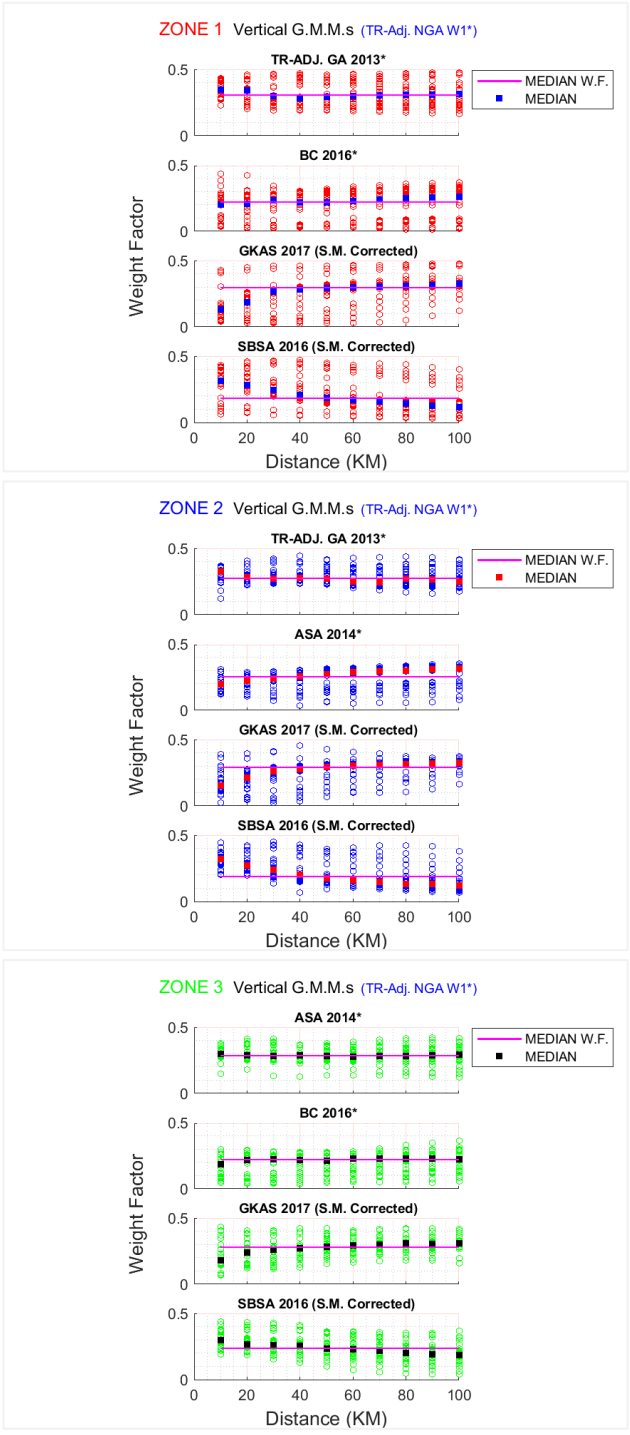

Figure 5.3 Comparison of distance to the median values calculated for each GMM for each scenario with the final logic tree weights with respect to distance. GMMs specified by (*) scaled by Tr-adjusted NGA-W1 horizontal models.

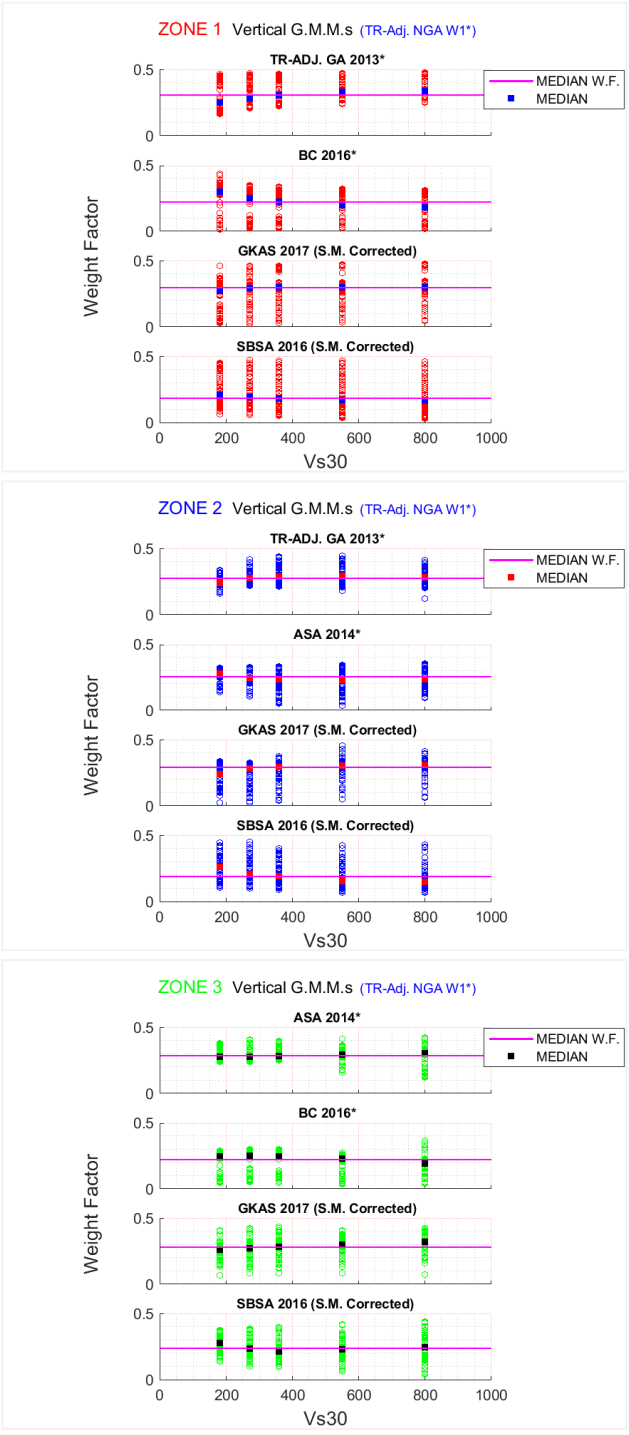

Figure 5.4 Comparison of distance to the median values calculated for each GMM for each scenario with the final logic tree weights with respect to site condition. GMMs specified by (*) scaled by Tr-adjusted NGA-W1 horizontal models.

5.2 Conclusion

The fundamental objective of this study is to provide the guiding principles for selecting and combining the vertical and V/H ratio GMMs in the ground motion characterization logic trees. Recently proposed vertical GMMs pointed out the need for comparing the vertical ground motion estimates based on the vertical and V/H ratio models, indicating that significant differences may occur due to the utilized horizontal ground motion models. Turkey is selected as the region of application because the ongoing licensing activities for two NPP sites in Turkey fueled the discussions on this controversial issue. Differences in the ground motion model development methods, broadness of the range of scenarios to be considered for different PSHA applications, and the limitations of the Turkish ground motion dataset call for the application of different techniques. First, the data-driven approaches such as the analysis of model residuals are applied to both vertical and V/H ratio models. We showed that these data-driven approaches are suitable for selecting and ranking the V/H ratio models; however, the vertical models needed certain modifications (e.g. small magnitude correction) for applicability in Turkey. After choosing, ranking and modifying the selected GMMs, trellis plots are used to check the consistencies in the median vertical ground motion predictions, showing that significant differences exist, especially for "out-of-the-comfort-zone" scenarios. The differences in the trellis plots are also strongly related to the horizontal ground motion models. Standard deviation of the models can be considered in two different ways: (i) standard deviation of inter-event and intra-event residuals of the candidate models may be evaluated and modified based on the evaluation dataset and (ii) the data driven techniques that consider the standard deviation might be utilized. Because the updated TSMD is still limited at large magnitudes and short distances, we prefer not to modify the standard deviation coefficients of the selected models; therefore, two different set of logic tree weights are provided in Table 4. First set should be used if the TR-adjusted GMMs are not incorporated in the employed PSHA software or the software does not allow the user to modify the embedded GMMs. In that case, the original versions of the GKAS2017

and SBSA2017 models may be used instead of the SM-modified versions. The second set of logic tree weights is proposed for the cases where the hazard analyst can utilize the TR-adjusted versions of the NGA-W1 horizontal GMMs in hazard calculations. This general set-up is preferable because it reflects the characteristics of the Turkish dataset by implementing the small magnitude corrections on both horizontal and vertical GMMs.

REFERENCES

Akkar, S., & Bommer, J. J. (2006). Influence of long-period filter cut-off on elastic spectral displacements. *Earthquake Engineering and Structural Dynamics*, *35*(9), 1145–1165. https://doi.org/10.1002/eqe.577

Akkar, S., Çağnan, Z., Yenier, E., Erdoğan, Ö., Sandikkaya, M. A., & Gülkan, P. (2010). The recently compiled Turkish strong motion database: Preliminary investigation for seismological parameters. *Journal of Seismology, 14*(3), 457–479. https://doi.org/10.1007/s10950-009-9176-9

Akkar, S., Sandıkkaya, M. A., & Ay, B. (2014). Compatible ground-motion prediction equations for damping scaling factors and vertical-to-horizontal spectral amplitude ratios for the broader Europe region. *Bulletin of Earthquake Engineering, 12*(1), 517–547. https://doi.org/10.1007/s10518-013-9537-1

Akkar, S., Sandıkkaya, M. A., Şenyurt, M., Sisi, A. A., Ay, B., Traversa, P., … Godey, S. (2014). Reference database for seismic ground-motion in Europe (RESORCE). *Bulletin of Earthquake Engineering*, *12*(1), 311–339. https://doi.org/10.1007/s10518-013-9506-8

Ancheta, T. D., Darragh, R. B., Stewart, J. P., Seyhan, E., Silva, W. J., Chiou, B. S.-J., … Donahue, J. L. (2014). NGA-West2 Database. *Earthquake Spectra*, *30*(3), 989–1005. https://doi.org/10.1193/070913EQS197M

Atik, L. A., Abrahamson, N., Bommer, J. J., Scherbaum, F., Cotton, F., & Kuehn, N. (2010). The Variability of Ground-Motion Prediction Models and Its Components. *Seismological Research Letters*, *81*(5), 794–801. https://doi.org/10.1785/gssrl.81.5.794

Atkinson, G. M., & Silva, W. (2000). Stochastic modeling of California ground motions. *Bulletin of the Seismological Society of America*, *90*(2), 255–274. https://doi.org/10.1785/0119990064

Bommer, J. J., Akkar, S., & Kale, Ö. (2011). A model for vertical-to-horizontal response spectral ratios for Europe and the middle east. *Bulletin of the Seismological Society of America*, *101*(4), 1786–1806. https://doi.org/10.1785/0120100285

Bommer, J. J., Douglas, J., Scherbaum, F., Cotton, F., Bungum, H., & Fah, D. (2010). On the Selection of Ground-Motion Prediction Equations for Seismic Hazard Analysis. *Seismological Research Letters*, *81*(5), 783–793. https://doi.org/10.1785/gssrl.81.5.783

Boore, D. M., & Akkar, S. (2003). Effect of causal and acausal filters on elastic and inelastic response spectra. *Earthquake Engineering and Structural Dynamics*, *32*(11), 1729–1748. https://doi.org/10.1002/eqe.299

Boore, D. M., & Bommer, J. J. (2005). Processing of strong-motion accelerograms: Needs, options and consequences. *Soil Dynamics and Earthquake Engineering*, *25*(2), 93–115. https://doi.org/10.1016/j.soildyn.2004.10.007

Boore, D. M., Douglas, J., Erdik, M., Javanbarg, M., Stafford, P. J., Delavaud, E., … Stewart, J. P. (2013). Selection of Ground Motion Prediction Equations for the Global Earthquake Model. *Earthquake Spectra*, *31*(1), 19–45. https://doi.org/10.1193/013013eqs017m

Boore, D. M., Sisi, A. A., & Akkar, S. (2012). Using pad-stripped acausally filtered strong-motion data. *Bulletin of the Seismological Society of America*, *102*(2), 751–760. https://doi.org/10.1785/0120110222

Bozorgnia, Y., & Campbell, K. W. (2004). The vertical-to-horizontal response spectral ratio and tentative procedures for developing simplified V/H and vertical design spectra. *Journal of Earthquake Engineering*, *8*(2), 175–207. https://doi.org/10.1080/13632460409350486

Bozorgnia, Y., & Campbell, K. W. (2016a). Ground motion model for the vertical-to-horizontal (V/H) ratios of PGA, PGV, and response spectra. *Earthquake Spectra*, *32*(2), 951–978. https://doi.org/10.1193/100614EQS151M

Bozorgnia, Y., & Campbell, K. W. (2016b). Vertical ground motion model for PGA, PGV, and linear response spectra using the NGA-West2 database. *Earthquake Spectra*, *32*(2), 979–1004. https://doi.org/10.1193/072814EQS121M

Çağnan, Z., Akkar, S., Kale, Ö., & Sandıkkaya, A. (2017). Erratum to: A model for predicting vertical component peak ground acceleration (PGA), peak ground velocity (PGV), and 5% damped pseudospectral acceleration (PSA) for Europe and the Middle East (Bulletin of Earthquake Engineering, (2017), 15, 7, (2617-

2643. *Bulletin of Earthquake Engineering*, *15*(12), 5623–5624. https://doi.org/10.1007/s10518-017-0209-4

Campbell, K., & Bozorgnia, Y. (2004). the Vertical-To-Horizontal Response Spectral Ratio and Tentative Procedures for Developing Simplified V/H and Vertical Design Spectra. *Journal of Earthquake Engineering*, *8*(2), 175. Retrieved from http://search.ebscohost.com/login.aspx?direct=true&db=aph&AN=11744655&site=ehost-live

Campbell, K. W., & Bozorgnia, Y. (2007). Campbell-Bozorgnia NGA Ground Motion Relations for the Geometric Mean Horizontal Component of Peak and Spectral Ground Motion Parameters, (May), 1–265. Retrieved from http://peer.berkeley.edu/products/nga_selected_publications/Campbell & Bozorniga_8NCEE-000906.pdf

Campbell, K. W., & Bozorgnia, Y. (2014). NGA-West2 ground motion model for the average horizontal components of PGA, PGV, and 5% damped linear acceleration response spectra. *Earthquake Spectra*, *30*(3), 1087–1114. https://doi.org/10.1193/062913EQS175M

Chiou, B., Darragh, R., Gregor, N., & Silva, W. (2008). NGA project strong-motion database. *Earthquake Spectra*, *24*(1), 23–44. https://doi.org/10.1193/1.2894831

Cotton, F., Scherbaum, F., Bommer, J. J., & Bungum, H. (2006). Criteria for selecting and adjusting ground-motion models for specific target regions: Application to central Europe and rock sites. *Journal of Seismology*, *10*(2), 137–156.

https://doi.org/10.1007/s10950-005-9006-7

Douglas, J. (2003). What is a poor quality strong-motion record? *Bulletin of Earthquake Engineering*, *1*(1), 141–156. https://doi.org/10.1023/A:1024861528201

Edwards, B., Poggi, V., & Fäh, D. (2011). A predictive equation for the vertical-to-horizontal ratio of ground motion at rock sites based on shear-wave velocity profiles from Japan and Switzerland. *Bulletin of the Seismological Society of America*. https://doi.org/10.1785/0120110023

FEMA P-1050-1. (2015). NEHRP Recommended Seismic Provisions for New Buildings and Other Structures. *Fema P-1050-1*, *I*, 555. Retrieved from http://www.fema.gov/media-library-data/20130726-1730-25045-1580/femap_750.pdf

Gülerce, Z., & Abrahamson, N. A. (2011). Site-specific design spectra for vertical ground motion. *Earthquake Spectra*, *27*(4), 1023–1047. https://doi.org/10.1193/1.3651317

Gulerce, Z., & Akyuz, E. (2013). The NGA-W1 Vertical-to-Horizontal Spectral Acceleration Ratio Prediction Equations Adjusted for Turkey. *Seismological Research Letters*, *84*(4), 678–687. https://doi.org/10.1785/0220120190

Gülerce, Z., Kamai, R., Abrahamson, N. A., & Silva, W. J. (2017). Ground motion

prediction equations for the vertical ground motion component based on the NGA-W2 database. *Earthquake Spectra*, *33*(2), 499–528. https://doi.org/10.1193/121814EQS213M

Gülerce, Z., Kargioğlu, B., & Abrahamson, N. A. (2016). Turkey-adjusted NGA-W1 horizontal ground motion prediction models. *Earthquake Spectra*, *32*(1), 75–100. https://doi.org/10.1193/022714EQS034M

Gülkan, P., & Kalkan, E. (2002). Attenuation modeling of recent earthquakes in Turkey. *Journal of Seismology*, *6*(3), 397–409. https://doi.org/10.1023/A:1020087426440

Kale, Ö. (2019). Some Discussions on Data-Driven Testing of Ground-Motion Prediction Equations under the Turkish Ground-Motion Database. *Journal of Earthquake Engineering*, *23*(1), 160–181. https://doi.org/10.1080/13632469.2017.1323047

Kale, Ö., & Akkar, S. (2013). A new procedure for selecting and ranking ground-motion prediction equations (GMPEs): The Euclidean distance-based ranking (EDR) method. *Bulletin of the Seismological Society of America*, *103*(2 A), 1069–1084. https://doi.org/10.1785/0120120134

Kale, Ö., & Akkar, S. (2017). A ground-motion logic-tree scheme for regional seismic hazard studies. *Earthquake Spectra*, *33*(3), 837–856. https://doi.org/10.1193/051316EQS080M

Kale, Ö. (2019). Some Discussions on Data-Driven Testing of Ground-Motion Prediction Equations under the Turkish Ground-Motion Database. *Journal of Earthquake Engineering*, *23*(1), 160–181. https://doi.org/10.1080/13632469.2017.1323047

Kale, Ö., Akkar, S., Ansari, A., & Hamzehloo, H. (2015). A ground-motion predictive model for iran and turkey for horizontal PGA, PGV, and 5% damped response spectrum: Investigation of possible regional effects. *Bulletin of the Seismological Society of America*, *105*(2), 963–980. https://doi.org/10.1785/0120140134

Kalkan, E., & Gülkan, P. (2004). Empirical attenuation equations for vertical ground motion in Turkey. *Earthquake Spectra*, *20*(3), 853–882. https://doi.org/10.1193/1.1774183

Ktenidou, O., Cotton, F., Abrahamson, N. A., & Anderson, J. G. (2017). Erratum to Taxonomy of κ : A Review of Definitions and Estimation Approaches Targeted to Applications . *Seismological Research Letters*, *88*(3), 875–876. https://doi.org/10.1785/0220170058

Kuk, K., Krmpotic, S., Gulerce, Z., Kovacevic, V., Mihaljevic, J., Milutinovic, Z., … Salic, R. (2016). BSHAP project strong ground motion database and selection of suitable ground motion models for the Western Balkan Region. *Bulletin of Earthquake Engineering*, *15*(4), 1319–1343. https://doi.org/10.1007/s10518-016-9950-3

Mak, S., Clements, R. A., & Schorlemmer, D. (2017). Empirical evaluation of

hierarchical ground-motion models: Score uncertainty and model weighting. *Bulletin of the Seismological Society of America*, *107*(2), 949–965. https://doi.org/10.1785/0120160232

Musson, R. W., Valensise, G., Rovida, A. N., Woessner, J., Cotton, F., Hiemer, S., … Crowley, H. (2015). The 2013 European Seismic Hazard Model: key components and results. *Bulletin of Earthquake Engineering*, *13*(12), 3553–3596. https://doi.org/10.1007/s10518-015-9795-1

Poggi, V., Edwards, B., & Fäh, D. (2012). Characterizing the vertical-to-horizontal ratio of ground motion at soft-sediment sites. *Bulletin of the Seismological Society of America*, *102*(6), 2741–2756. https://doi.org/10.1785/0120120039

Sandikkaya, M. A. (2016). Düşük Magnitüdlü Kayıtların Yer Hareketi Tahmin Denklemleri Üzerindeki Etkisi : Türkiye için Bir Ön Çalışma Effects of Low Magnitude Records on Ground-Motion Prediction Equations : A Preliminary Study for Turkey, *37*(3), 237–252.

Sandikkaya, M. A., Yilmaz, M. T., Bakir, B. S., & Yilmaz, Ö. (2010). Site classification of Turkish national strong-motion stations. *Journal of Seismology*, *14*(3), 543–563. https://doi.org/10.1007/s10950-009-9182-y

Scasserra, G., Stewart, J. P., Bazzurro, P., Lanzo, G., & Mollaioli, F. (2009). A comparison of nga ground-motion prediction equations to italian data. *Bulletin of the Seismological Society of America*, *99*(5), 2961–2978. https://doi.org/10.1785/0120080133

Scherbaum, F., Delavaud, E., & Riggelsen, C. (2009). Model selection in seismic hazard analysis: An information-theoretic perspective. *Bulletin of the Seismological Society of America*, *99*(6), 3234–3247. https://doi.org/10.1785/0120080347

Stewart, J. P., Boore, D. M., Seyhan, E., & Atkinson, G. M. (2016). NGA-West2 equations for predicting vertical-component PGA, PGV, and 5%-damped PSA from shallow crustal earthquakes. *Earthquake Spectra*, *32*(2), 1005–1031. https://doi.org/10.1193/072114EQS116M

APPENDICES

All complementary results are provided in attached electronic appendix in form of 1030 high quality photos as bellow:

A. V/H ratio models residual analysis results

B. Vertical ratio models residual analysis results

C. Scenarios used to obtain logic tree weights (Turkey adjusted NGA west1)

D. Scenarios used to obtain logic tree weights (NGA west2)

E. Comparison of distance to the median values